TOTAL ELECTRON CONTENT ESTIMATION AND ANALYSIS OVER THE NIGERIAN GLOBAL NAVIGATION SATELLITE SYSTEM PERMANENT REFERENCE NETWORK

BY

MOSES MEFE

DEPARTMENT OF GEOMATICS,
AHMADU BELLO UNIVERSITY, ZARIA
NIGERIA

OCTOBER, 2015

TOTAL ELECTRON CONTENT ESTIMATION AND ANALYSIS OVER THE NIGERIAN GLOBAL NAVIGATION SATELLITE SYSTEM PERMANENT REFERENCE NETWORK

BY

MOSES MEFE
MSc/ENV-DES/41018/2012-13

A DISSERTATION SUBMITTED TO THE SCHOOL OF POSTGRADUATE STUDIES, AHMADU BELLO UNIVERSITY, ZARIA

IN PARTIAL FULFILMENT OF THE REQUIREMENTS FOR THE AWARD OF
MASTERS DEGREE IN GEOMATICS.

DEPARTMENT OF GEOMATICS,
FACULTY OF ENVIRONMENTAL DESIGN
AHMADU BELLO UNIVERSITY, ZARIA
NIGERIA

OCTOBER, 2015

DECLARATION

I declare that the work in this project Dissertation entitled Total Electron Content Estimation and Analysis over the Nigerian Global Navigation Satellite System Permanent Reference Network has been performed by me in the Department of Geomatics. The information derived from the literature has been duly acknowledged in the text and a list of references provided. No part of this Dissertation was previously presented for another degree or diploma at this or any other Institution.

Mefe MOSES _____ _____

Signature Date

CERTIFICATION

This Dissertation entitled TOTAL ELECTRON CONTENT ESTIMATION AND ANALYSIS OVER THE NIGERIAN GLOBAL NAVIGATION SATELLITE SYSTEM PERMANENT REFERENCE NETWORK by MOSES MEFE meets the regulations governing the award of the degree of MASTERS DEGREE IN GEOMATICS of the Ahmadu Bello University, and is approved for its' contribution to knowledge and literary presentation.

Dr. J. D. Dodo	_____	_____
(Chairman, Supervisory Committee)	(Signature)	(Date)
Dr. L. M. Ojigi	_____	_____
(Member, Supervisory Committee)	(Signature)	(Date)
O. A. Isioye	_____	_____
(Head of Department)	(Signature)	(Date)
Prof. K. Bala	_____	_____
(Dean, School of Postgraduate Studies)	(Signature)	(Date)

DEDICATION

I dedicate this Dissertation to my mother for her constant, unconditional love, care, prayers and support. I also dedicate it to the loving memory of my beloved sister, Josephine Oghenefejiro Esther Oyewole (May 5, 1972 - June 03, 2013).

ACKNOWLEDGMENT

My earnest gratitude to God who gave me all the grace and strength to successfully complete my course work and this Dissertation.

First, I would like to thank my main supervisor, Dr. J. D. Dodo for his complete and constructive scientific guidance, valuable discussions, corrections and suggestions during the course of this Dissertation.

I express my deepest thanks to my co-supervisor, Dr. L. M. Ojigi for his great guidance comments during the period of this Dissertation.

The H.O.D. of the Department of Geomatics, Ahmadu Bello University, Zaria, O. A. Isioye, is sincerely acknowledged for his help and support to me throughout the period of my study. I do acknowledge the following lecturers; Prof. I. J. Nwadialor, Prof. A. A. Musa, Dr. T. O. Adewuyi, Prof. Kola Lawal of the Department of Physics, Dr. S. P. Olaleye, and all academic, non academic and technical staff of the Department of Geomatics, Ahmadu Bello University, Zaria.

I am grateful to the Office of the Surveyor General of the Federation (OSGOF) for the GNSS data from the NIGNET CORS. I am grateful to thank the International GNSS Service (IGS) and the Centre for Orbit Determination in Europe, University of Berne (CODE) who made the DCB files, precise ephemeris data, and the Global Ionospheric Maps IONEX files available. I acknowledge the use of the GPS-TEC software developed by Gopi Seemala of the Institute for Science Research, Boston College, U.S.A.

I wish to acknowledge my course mates; Aliyu A. Onotu, Ebenezer A. Akomolafe, Usman I. Sai', and Ahmadu Ali Abubarkar

I am eternally grateful to my family, my mother Felicia Koko Moses, and all my siblings. Thank you for your support, encouragement and making me realise that I should never let nothing hold me back from my dream. This Masc. is a testament to your faith in me. Words cannot express my gratitude for everything you have.

I in a very special way acknowledge my beloved sister Josephine Esther Oghenefegero Oyewale of blessed memory, who until her death was of enormous support and encouragement to me.

ABSTRACT

In the last decades, knowledge about the ionosphere has grown considerably thanks to the use of GNSS measurements, and in turn the GNSS have highly benefited from this improved knowledge. This Dissertation studied the TEC value for the Nigerian GNSS Permanent Reference Network (NIGNET) over a period of four and a half years (January 2010 to June 2014). The TEC over the NIGNET stations were estimated using two prominent data sources viz. NIGNET CORS observed data in RINEX format, and Global Ionospheric Maps (GIMs) in IONEX format. Annual TEC time series were generated using TEC values from both data sources. The NIGNET CORS-derived TEC results were validated with the GIM-derived TEC (GTEC). Various effects on TEC values were studied such as (diurnal, season, spatial, magnetic storms and solar eclipse, and solar activity). In general the TEC reveals higher values in day time with peak occurring between 13:00 and 14:00 hours. The TEC is lower in the early hours of the day and at night times with minimum diurnal TEC occurring between the hours of 03:00 and 04:00. The TEC increase gradually in the March equinox from a mean value of 23 TECU in January to 27 TECU in February and then 33 TECU in March. The TEC series attains a maximum in the March equinox between March and April with a 43-45% increment from its mean value in January and 5-7% increment from its value at February. There is less than 2% rise in the mean TEC value between the month of March and April, as the TEC remains at its peak within these months. The TEC gradually declines after the month of April and attaining a mean minimum value of 20-22 TECU within the June solstice, corresponding to 33-35% decrease from the TEC peak that occurred in the March equinox. After June solstice, the TEC once again begin a gradual increment in August, attaining another maximum value of 30-32 TECU between the end of September equinox and the beginning of December solstice (between October and November) after which it once again declines gradually at the end of the December solstice. The TEC varies spatially with both longitudes and latitudes, having higher values for the southern stations which are closer to the equator compared to the northern stations farther away from the equator. It was found that the effect of geomagnetic storms on TEC results in increased values during days of storms and the TEC values are proportional to the strength of geomagnetic storm type. A comparison of the TEC values estimated from the NIGNET CORS data and GIM over each NIGNET station for these flares and solar indices show evidence of geomagnetic and solar activity dependence of ionospheric GNSS-derived TEC. Improvement to the study will be to consider the TEC estimation in near or real time and for a longer time period of 11 years corresponding to the solar cycle in order to ascertain the long time correlation of TEC with the solar cycle variation.

TABLE OF CONTENTS

Title Page		III
Declaration page		IV
Certification page		V
Dedication		VI
Acknowledgement		VII
Abstract		VIII
Table of Contents		IX
List of Figures		XIII
List of Tables		XV
List of Appendices		XVI
Abbreviations, Definitions, Glossary and Symbols		XVII
CHAPTER ONE: INTRODUCTION		
1.1	**BACKGROUND TO THE STUDY**	1
1.2	**Statement of Research Problem**	5
1.3	**Aims and Objectives**	7
1.4	**Justification of the Study**	7
1.5	**Scope of Study**	9
1.6	**Research Contributions**	9
CHAPTER TWO: LITERATURE REVIEW		
2.1	**Global Navigation Satellite System**	11
2.1.1	GNSS signals	12
2.2	**GNSS Error Sources**	13
2.2.1	Orbital errors	13
2.2.2	Satellite clock error	15

2.2.3 Receiver noise 15

2.2.4 Multipath error 16

2.2.5 Tropospheric error 17

2.2.6 Ionospheric error 18

2.3 Structure of the Ionosphere 22

2.3.1 Ionospheric variation 27

2.3.5 Major Geographic Regions of the Ionosphere 28

2.4 Ionospheric Disturbances 30

2.4.1 Ionospheric sub storms 30

2.4.2 Geomagnetic storms 31

2.5 Solar-Terrestrial Indices 32

2.5.1 Disturbance storm time index (Dst) 32

2.5.2 Kp-index (Kp) 34

2.5.3 Ap-index (Ap) 34

2.5.4 Sunspot Number (SSN) 35

2.6 Ionospheric Modeling 36

2.6.1 Klobuchar model 37

2.6.2 NeQuick model 38

2.6.3 International Reference Ionosphere 39

2.6.4 NTCM model 40

2.6.5 Global Ionosphere Maps 40

2.7 Total Electron Content (TEC) 41

2.7.1 Slant and vertical TEC 45

2.8 Review of Related Works 47

CHAPTER THREE: MATERIALS AND METHODS

3.1 Study Area 53

3.2 Materials 54

3.2.1 NIGNET CORS Data 54

3.2.2 Differential Code Biases (DCBs) for satellites and receivers 56

3.2.3 Global Ionospheric Maps (GIMs) 56

3.2.4 Solar indices 57

3.2.5 Software 58

3.3 Methodology 58

3.3.1 Data Acquisition 58

3.3.2 TEC evaluation from NIGNET CORS data 59

3.3.3 TEC from IGS GIMs over Nigeria, interpolation and visualisation 59

3.3.4 Seasonal grouping 61

3.3.5 TEC validation and analyses 62

CHAPTER FOUR: RESULTS AND DISCUSSION

4.1 Diurnal, Seasonal and Spatial Variations of TEC over the NIGNET 64

4.1.1 Diurnal TEC Variation over NIGNET 64

4.1.2 Annual TEC Time Series and Seasonal TEC Variation over NIGNET 67

4.1.3 Spatial Variation TEC over NIGNET 70

4.2 Effect of Geomagnetic Storms and Solar Activities on TEC over NIGNET 81

4.2.1 Relation to Geomagnetic storms (Solar Flares) 81

4.2.2 Solar Eclipse of November 03, 2013 86

4.2.3 TEC Correlation with Solar Activity 90

4.3 Validation of NIGNET – Derived TEC with GIM TEC 97

CHAPTER FIVE: CONCLUSION AND RECOMMENDATIONS

5.1 **Conclusion** 101

5.2 **Recommendations** 103

REFERENCES 105

APPENDICES 119

LIST OF FIGURES

Figure 1-1: International GNSS Service Tracking Network 4

Figure 2-1: Radio-Navigation Satellite Systems (RNSS) frequency spectrum 13

Figure 2-2: Multipath effect 16

Figure 2-3: Worldwide distribution of TEC, 13:00 UT on September 27, 2001 20

Figure 2-4: The various layers of the ionosphere 23

Figure 2-5: Major geographic regions of the ionosphere 28

Figure 2-6: The monthly sunspot numbers for the latest five cycles 36

Figure 2-7: Example of actual monthly average time-delay data, along with cosine model fit to data 38

Figure 2-8: Geometry of satellite-receiver link 46

Figure 3-1: Spatial distribution of the NIGNET receiver stations in Nigeria 53

Figure 3-2: GIM grid points covering the NIGNET CORS 61

Figure 3-3: Flow chart of the TEC Evaluation and Analyses methodology 62

Figure 4-1: Mean diurnal TEC profile over the NIGNET 64

Figure 4-2: Diurnal TEC variation over NIGNET deduced from the NIGNET CORS data 65

Figure 4-3: Diurnal TEC variation over NIGNET deduced from the Global Ionospheric Maps for March 06 2012, DoY: 066 66

Figure 4-4: Annual TEC Time Series at ABUZ station 2010-2013 68

Figure 4-5: NIGNET annual TEC time series for 2010-2014 69

Figure 4-6: Mean annual TEC time series for the NIGNET 69

Figure 4-7: Spatial Variation of Monthly Mean TEC over NIGNET Jan – Jun 2010 71

Figure 4-8: Spatial Variation of Monthly Mean TEC over NIGNET
Jul – Dec 2010 72
Figure 4-9: Spatial Variation of Monthly Mean TEC over NIGNET
Jan – Jun 2011 73
Figure 4-10: Spatial Variation of Monthly Mean TEC over NIGNET
Jul – Dec 2011 74
Figure 4-11: Spatial Variation of Monthly Mean TEC over NIGNET
Jan – Jun 2012 75
Figure 4-12: Spatial Variation of Monthly Mean TEC over NIGNET
Jul – Dec 2012 76
Figure 4-13: Spatial Variation of Monthly Mean TEC over NIGNET
Jan – Jun 2013 77
Figure 4-14: Spatial Variation of Monthly Mean TEC over NIGNET
Jul – Dec 2013 78
Figure 4-15: Spatial Variation of Monthly Mean TEC over NIGNET
Jan - Jun 2014 79
Figure 4-16: TEC Behaviour over the NIGNET stations during the 'Valentine's Day' 2011 X2.2-class G1 minor solar flare of February 15 2011 83
Figure 4-17: TEC Behaviour over the NIGNET stations during the M7.9-class G2 moderate solar flare of March 13 2012 84
Figure 4-18: TEC Behaviour over the NIGNET stations during the X5.4-class G3 strong solar flare of March 07 2012 85
Figure 4-19: TEC Behaviour over the NIGNET stations before, during and after the solar eclipse of 03 November 2013 88

Figure 4-20: NIGNET TEC Correlation with Sunspot Number and f.10_index at ABUZ, BKFP and UNEC for 2011 epoch 90

Figure 4-21: Comparative plots of NIGNET TEC and Sunspot Number at ABUZ, BKFP and UNEC for 2011 epoch 91

Figure 4-22: Comparative plots of NIGNET TEC and f.10_index at ABUZ, BKFP and UNEC for 2011 epoch 92

Figure 4-23: GTEC Correlation with Sunspot Number and f.10_index at the NIGNET stations for the period of January 2010 to June 2014 93

Figure 4-24: Comparative plots of GTEC and Sunspot Number at the NIGNET stations for January 2010 to June 2014 94

Figure 4-25: Comparative plots of GTEC and f.10_index at the NIGNET stations for January 2010 to June 2014 95

Figure 4-26: Correlation coefficient between the NIGNET CORS derived TEC (NIGNET_TEC) and the GIM derived TEC (GTEC) 97

Figure 4-27: Comparative plots of equivalent vertical TECs obtained from NIGNET and vertical TECs obtained from GIMs 98

LIST OF TABLES

Table 2.1: Potential effects of the ionosphere on GNSS signals 27

Table 2.2: Geomagnetic storm classification 33

Table 2.3: The sudden storm scale according to Kp- index 33

Table 3.1: NIGNET GNSS CORS stations in Nigeria used in the study 54

Table 3.2: Summary of NIGNET CORS RINEX observation data used in the study 55

Table 3.3: Summary of Differential Code Bias (DCBs) used in the Dissertation 56

Table 3.4: Summary of IGS Global Ionospheric Maps used in the study 57

Table 3.5: Local Circumstances of the solar eclipse of November, 03, 2013 63

Table 4.1: Solar Flares of Solar Cycle 24 examined in the study 82

LIST OF APPENDICES

Appendix I: Annual TEC Time Series for the NIGNET CORS 119

Appendix II: Monthly Mean TEC at the NIGNET CORS 133

ABBREVIATIONS, DEFINITIONS, GLOSSARY AND SYMBOLS

Ap	-	A-index
CME	-	Coronal Mass Ejection
CODE	-	Centre for Orbit Determination in Europe
DCB	-	Differential Code Bias
DIC	-	Disturbed Ionospheric Condition
DOD	-	Department of Defense
DoY	-	Day of year
Dst	-	Disturbance storm time index
EUV	-	Extreme Ultra-Violet
FOC	-	Full Operational Capability
fOF2	-	Critical frequency of F2 layer
GIM	-	Global Ionospheric Map
GNSS	-	Global Navigation Satellite System
GPS	-	Global Positioning System
HSSWS	-	High Speed Solar Wind Stream
IAG	-	International Association for Geodesy
IGS	-	International GNSS Service
IONEX	-	Ionosphere Map Exchange
IRI	-	International reference ionosphere
Kp	-	K-index every three hour
NASA	-	National Aeronautics and Space Administration
NGS	-	National Geodetic Survey
NmF2	-	Electron density of F2 layer
OSGOF	-	Office of the Surveyor General of the Federation
PRN	-	Pseudo Random Noise

QIC	-	Quiet atmospheric condition
RINEX	-	Receiver INdependent EXchange format
SED	-	Storm Enhanced Density
SID	-	Sudden Ionospheric Disturbance
SSN	-	Sunspot number
TEC	-	Total Electron Content
TECs	-	Slant Total Electron Content
TECU	-	Total Electron Content Unit
TECv	-	Vertical Total Electron Content

CHAPTER ONE

INTRODUCTION

1.1 BACKGROUND TO THE STUDY

The first Global Navigation Satellite System (GNSS), known as Global Positioning System (GPS), was developed and maintained by US Department of Defense (DOD). In 1994 GPS achieved the full operational capability (FOC) with three segments: the space segment, the control segment and the user segment. The space segment is composed of a constellation of 24 satellites in six orbital planes at an altitude of approximately 20200 km above the earth surface. The orbiting period is about 11 hours and 56 minutes. The control segment contains a global tracking network of 16 monitoring stations and two master control stations which send commands and data to the constellation (NOAA, 2012). The user segment includes lots of applications such as positioning, navigation and timing.

The positional accuracy of GNSS is affected by several errors such as satellite and receiver clock errors, signal propagation delay errors due to ionosphere and troposphere, multipath error, receiver measurement noise and instrumental biases. Among all the error sources, ionospheric delay is the most predominant one and is of the order of 5-15m during mid-afternoon (El-Rabbany, 2002).

For the last seventy years scientists have studied the Earth's ionosphere quite extensively through the use of multiple techniques (i.e., radiosounders, Faraday radars, top-side soundings from satellites, GPS signals, etc). Surprisingly, however, most people are unfamiliar with its existence, despite the fact that the ionosphere plays an

integral role in many of their everyday activities. Extreme variations within the ionosphere induced by storm enhanced density (SED) events and responses to magnetic storms can adversely affect navigation and communication systems on Earth (Skone and Coster, 2008; Araujo-Pradere and Fuller-Rowell, 2002; Araujo-Pradere, *et al.*, 2002).

The ionosphere is a part of the upper atmosphere, starting at height of 50 km and extending to 1000 km. In that region free electron density affects the propagation of radio frequency electromagnetic waves (Alcay *et al.*, 2012). When solar radiation strikes the atoms and molecules of the upper atmosphere, electrons are dislodged through the process of ionization. Because of the chemical composition of the atmosphere, the shorter wavelengths of solar radiation (the extreme ultraviolet and X-Rays) are energetic enough to ionize these atoms and molecules in the Earth's atmosphere. Depending on the energy of the incident photon, photoelectrons (i.e. - electrons emitted from an atom or molecule by an incident photon) are produced, with great enough energies to ionize other nearby neutrals or moleculars. Particle precipitation occurs when energetic particles are injected into the upper atmosphere and collide with neutrals. This process produces increased and variable levels of ionization (Bothmer and Daglis, 2007). In summary, highly variable production, loss, and conditional transport of ionization are responsible for the extremely variable ionosphere.

There are various ways to study ionospheric irregularities; one of them is the total electron content (TEC) observations derived from a network of GPS stations using dual frequency measurements (Tiwari *et al.*, 2009). TEC is defined as the integral of the electron density along a trajectory, usually, vertical from the Earth's surface up to a given height in the ionosphere (hence, vertical or vTEC) or the line-of-sight (LoS) from

the satellite to the receiver (slant or sTEC). TEC is measured in TEC units (TECU), with 1 TECU being 10^{16} electrons/m^2 (Ciraolo *et al.*, 2006).

TEC is measured to estimate the impact of ionosphere to the signal transmitted by GPS satellite to the receiver on Earth. Among ionospheric parameters, the total electron content (TEC) is one of the particularly important physical quantities of the ionosphere. TEC has been extensively investigated and modelled for both scientific research of ionosphere and for applications (Mukhtarov *et al.*, 2013).

In ordinary operation the position of a GPS receiver is estimated by measuring the time delay between a radio signal transmitted from each satellite and the reception of that signal at the receiver. Assuming a constant speed of light, this time delay can be converted to a receiver-satellite distance. By comparing the distance to multiple satellites a GPS receiver can determine its three dimensional position. The ionosphere disrupts this approach since the GPS radio signal is slowed by the presence of free electrons, causing an additional time delay and hence an error in the distance to each satellite. This effect is called ionosphere refraction and has to be considered when determining the propagation velocity of signals of all space geodetic techniques operating in microwave band (Alizadeh *et al.*, 2010). The greater the TEC on the signal path, the greater the time delay. At any given GPS station, ionospheric TEC can change by tens or even hundreds of TEC units (1 x 1016 electrons m^{-2}), bringing about tens of meters of error in the given GPS position (Araujo-Pradere, 2005). Ionospheric delay correction is carried out through modelling the TEC along each satellite signal path due to high spatial variability of the ionosphere. Prediction of ionosphere vertical total electron content are crucial and remain as a challenge for GPS positioning and

navigation system , space weather forecast, as well as many other Earth Observation System (Priya and Parameswari, 2013).

The GPS system, for example, broadcasts in two frequencies and since the ionosphere is a dispersive medium the time delay on each signal, for a given TEC, will depend on the frequency of that signal. This allows the TEC to be measured by examining the differential time delay between the two frequencies (Ya'acob *et al.*, 2010). Various studies show that GPS signals are one of the best tools to study ionospheric activity, especially with low cost to high level of accuracy (Tiwari *et al.*, 2009).

With a large number of permanently tracking stations, GPS can deliver large volumes of data suitable for continuous, near or real-time ionosphere monitoring during disturbed and quiet geomagnetic conditions, and offers an attractive alternative to traditional methods (e.g., ionosonde network) (Wielgosz *et al.*, 2003).

The International GNSS Service (IGS) of the International Association for Geodesy (IAG) maintains a global GNSS tracking network of more than 200 receivers (see figure 1-1).

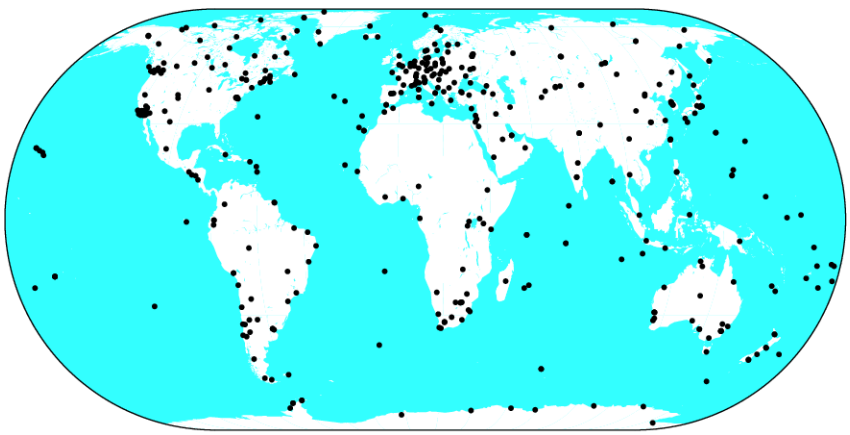


Figure 1-1: International GNSS Service Tracking Network (http://igscb.jpl.nasa.gov, last accessed October 29, 2014)

The availability of a huge number of the IGS permanent dual frequency GPS receivers, which are distributed over the Earth's surface, has made the global monitoring of the ionosphere possible and Global Ionospheric VTEC Maps (GIM) are produced routinely. Four IGS Ionospheric Analysis Centres (CODE, ESA, JPL, and UPC) individually produce daily Global Ionosphere Maps using different techniques (Perez, 2005; Wienia, 2008). The official IGS product is a combined ionosphere map from all four IGS analysis centres. The GIM files are distributed on a daily basis; they give a value for the Vertical Total Electron Content (VTEC) every two hours (0, 2, 4, to 24 hours) at the grid points. The widely used GPS-derived GIMs provided by the International GPS Service (IGS) have a spatial resolution of 2.5º and 5.0º in latitude and longitude, respectively, and a 2-hour temporal resolution (Feltens and Jakowski, 2002), and are provided in the IONEX (IONosphere map EXchange) format (Schaer 1999).

GIMs represent a new tool for monitoring global patterns of ionospheric weather, a key component of the space weather, which is driven by changes in solar ultra-violet radiation, the interplanetary particle stream known as the solar wind, and the underlying composition, wind patterns and electrodynamics of the thermosphere (the upper atmosphere at altitudes between 100 and 1000 km). GIMs are being used for global ionospheric delay calibrations, for scientific investigations of the upper atmosphere (NASA, 2012).

1.2 STATEMENT OF RESEARCH PROBLEM

Any operating or potential system which involves radio waves propagating through the ionosphere and which requires time delay measurements to an accuracy of the same order as the ionosphere time delay errors requires knowledge of TEC to correct for

these errors. The ionosphere produces retardation in the velocity of the information carried on a radio wave called group path delay. This group path delay produces timing errors in radar systems and navigation systems which must traverse the ionosphere. The group path delay timing error is directly proportional to the TEC. The group path delay timing error can be important depending upon the frequency the system uses, and the amount of the ionospheric TEC. Difficulties encountered by radio communications, and GPS users are attributed to variations in electron density and therefore, TEC throughout the ionosphere. Radio communication is dependent upon electron density because the electromagnetic wave may experience a change in propagation direction due to gradients in electron density (Dabas, 2000). According to the American Meteorological Society Policy Statement on Space Weather (2008), commercial airlines' high-frequency (HF) radio signals are often degraded or lost as a result of space weather conditions.

For example, during a strong radio blackout the electron density in the D-region increases greatly, which can render HF communications almost or completely unavailable and emergency communications used in disaster recovery on commercial flights over the Polar Regions useless (American Meteorological Society, 2008). At any given GNSS station, ionospheric TEC can change by tens or even hundreds of TEC units (1×10^{16} electrons m^{-2}), bringing about tens of meters of error in the given GPS position (Araujo-Pradere, 2005).

Despite the knowledge of the potential effect of the ionosphere on GNSS operation especially during disturbed ionospheric conditions and periods of geomagnetic storms, no study has attempted to critically examine the behaviour and variation of ionospheric TEC over the NIGerian GNSS Reference NETwork (NIGNET). Presently, surveying works carried out within Nigeria, referenced to the NIGNET are carried out with no

adequate knowledge of the behaviour and variation of the TEC over the network in order to plan for suitable campaign periods or seasons, taking into consideration the periods of disturbed and quiet ionospheric conditions. Thus, a study of the ionospheric TEC over the NIGNET will better allow us to mitigate the aforementioned effects that this parameter has on our surveying, communication and navigation industries.

1.3 AIM AND OBJECTIVES

The aim of this dissertation is to derive and analyse TEC estimates over the Nigerian GNSS Reference Network from two data sources based on GNSS observation data from the NIGNET CORS and from Global Ionospheric Maps (GIMs).

The objectives of the dissertation are to:

1. Estimate TEC values over the NIGNET from the NIGNET CORS and from the GIMs;
2. Analyse the diurnal, seasonal and spatial variations of ionospheric TEC over the NIGNET CORS;
3. Determine the effect of geomagnetic storms on GNSS-derived TEC, with particular consideration of the solar eclipse of November 03, 2013, and the correlation of ionospheric TEC with solar activity;
4. Validate the NIGNET-derived TEC with values from the Global Ionospheric Maps, for the period under study (January 2010 to June 2014);

1.4 JUSTIFICATION OF THE STUDY

Today the ionosphere remains the largest error source of GPS navigation, which in turn could interfere with precision navigation and strike operations (Coster and Komjathy, 2008, American Meteorological Society, 2008). Therefore, a technique to better

determine electron densities and thus ionospheric TECs, could lead to extensive improvements in our surveying, navigation and communication industries (Skone and Coster, 2008).

Recently, due to the wide use of GNSS receivers both on satellites at low earth orbit and on the ground, continuous and long-time ionospheric TEC data with increasing accuracy have been obtained and used to analyse the diurnal, seasonal and solar cycle variations of the ionospheric TEC over the Earth (e.g., Breed *et al*., 1998; Stamatis *et al*., 2004; Yu *et al*., 2006; Liu and Chen, 2009; Perevalova *et al*., 2010). Some new parameters, such as the Global Electron Content (GEC) (Afraimovich *et al*., 2008; Astafyeva *et al*., 2008) and the global mean TEC (Liu *et al*., 2009) have also been derived to track the global characteristics of ionospheric dynamics.

It is shown that there are annual variations, semiannual variations and regional variations in terms of TEC, and there is a strong dependence on the solar and geomagnetic activities for the TEC. At the same time, detailed analysis of temporal-spatial TEC variations have been done based on GPS receivers on the ground in some regions, such as in Australia (Wu *et al*., 2006), India (Bagiya *et al*., 2009; Rama Rao *et al*., 2006), Delhi (India) (Gupta and Singh, 2000), Brazil (Mendes *et al*., 2004), Mexico (Huang and Roussel-Dupre, 2005), and Salisbury (Breed *et al*., 1998). In the case of Nigeria, there are only very few studies for the variations of the ionospheric TEC, such as Fayose *et al.*, 2012, which was specifically over Akure, Ondo State.

Modelling TEC gives scientists the opportunity to study the temporal and spatial variation of the global ionosphere to learn more about various ionospheric structures influencing electromagnetic waves propagating from satellites to receivers. GNSS can provide a unique tool to study the ionosphere as well as help provide ionospheric

corrections for single frequency navigation, surveillance and communication systems. Studying TEC behaviour during geomagnetic storms and its correlation with solar activity will provide a better understanding of the effect of solar activity on radio signals and how to mitigate such effects.

1.5 SCOPE OF STUDY

This study of TEC is based on the data supplied NIGerian GNSS Reference NETwork (NIGNET), an infrastructure put in place and maintained by the Office of the Surveyor General of the Federation (OSGOF), Federal Republic of Nigeria, and the Global Ionospheric Maps (GIMs) supplied by International GNSS Service (IGS) in the form of IONosphere Map EXchange Format (IONEX). The data covers January 01, 2010 to June 30, 2014 (four and half years) which corresponds to GPS week 1564 to 1799 on the global GPS calendar (a total of 1,642 days considered in the study). Because of the latency in publishing the above-mentioned data, the processing is restricted to the post-process mode.

1.6 RESEARCH CONTRIBUTIONS

Currently, the network of dual frequency GNSS CORS receivers over Nigeria contains 14 operational stations, with plans for extensions in the future. Hence, the results outlined in this dissertation would be of great interest and relevance to the development of ionospheric monitoring system and correction model for the entire country. Such a system will not only be of use to the GNSS community, but also to other space related industries like the aviations, Meteorology and weather, and communication industries. In addition, the work presented here would be useful for enhancing the performance of the present and proposed future CORS of the NIGNET.

The result on the temporal, seasonal, and spatial TEC changes is useful to indigenous scientists in understanding the bounds of TEC changes in the local ionosphere. This is important for future application in high frequency radio communication, navigation, positioning, frequency management and long term studies of impact of solar outputs on climate change over Nigeria. GPS users with single-frequency receivers need ionospheric electron content information in order to achieve positioning accuracy similar to dual-frequency receivers. The study provides diurnal maps of ionospheric electron content. These maps are also of value in monitoring the effect of the ionosphere on radio signals, power grids, and on space weather as well as providing early warning systems.

As the ionospheric delay is the largest source of error affecting satellite positioning, the resulting TEC variability studied in this dissertation will enable GNSS users to better plan their surveys, avoiding periods of high ionospheric scintillations, thus leading to improved accuracy and reliability in GNSS positioning.

The resulting maps allow detecting the local ionospheric phenomena, e.g., local TEC peaks. The obtained ionosphere grids can be easily interpolated using simple linear interpolation to determine the TEC value at any point within the NIGNET. Furthermore, the computer programs in Java programming language developed during the course of the dissertation for the estimation of the TEC covering the Nigerian grid from the Global Ionospheric Maps would be essential for future TEC studies within the country.

CHAPTER TWO

LITERATURE REVIEW

2.1 Global Navigation Satellite System (GNSS)

GNSS development has an interesting aspect due to its sensitive nature. Considerable events or developments are always subject to a couple of differentiators: technological developments and political decisions. GPS and GLONASS in all stages of improvements are strictly related to those differentiators. The approval and startup of the European Galileo program is considered by far the most real innovation. Technological and political decisions in Galileo substantiate that interoperability and compatibility must be reached in the forthcoming years. Such issues are the true GNSS improvement for the benefit of institutions and organizations.

Satellite Navigation Systems has become integral part of all applications where positioning and mobility play an important role (Heinrichs *et al*., 2005). These functions will be at the heart of the mobile phone third-generation (3G) networks such as the UMTS. In transportation systems, the presence of receivers will become as common as seat belts or airbags, with all car manufacturers equipping their entry-level vehicles with these devices.

As for the past developments, GPS launched a variety of techniques, products and, consequently, applications and services. The milestone of satellite navigation is the real time positioning and time synchronization (Mulassano, *et al*., 2004). GNSS applications in all fields will play a key role, moving its use from the transportation domain to multimodal use, outdoors and indoors. It is expected that GNSS will increase significantly the precision in position domain (Lachapelle *et al*., 2002).

The main application of GNSS is focused on the potential of to determine the position in the Global reference system any where any time on the Globe in a simple, fast and cost-effective manner. The meaning of GNSS is the technical interoperability and compatibility between various satellite navigation systems such as modernized GPS, Galileo, reconstructed GLONASS to be used by civilian users without considering the nationalities of each system in order to promote the safety and convenience of life (Galileo, 2003; Feng, 2003).

The GNSS consist of three main satellite technologies: GPS, GLONASS and Galileo. Each of them consists mainly of three segments: (a) space segment, (b) control segment and (c) user segment. These segments are almost similar in the three satellite technologies, which are all together make up the GNSS. As of today, the complete satellite technology is the GPS technology and most of the existing worldwide applications related to the GPS technology. The GNSS technology will become clearer after the operation of Galileo and the reconstruction of GLONASS in the next few years.

2.1.1 GNSS signals

The overall signals (Modernized GPS, Galileo and GLONASS signals), make up the GNSS signals. Each satellite system has specific signal characteristics, but each system attempts to be compatible with the others in order to prevent the interferences and attenuation between the signals. It is important to consider that the processing of all signals should be performed using the same receiver, thus a complex receiver design is supposed to be designed and built. The GNSS frequency plan shall respect the radio-regulations as they are discussed and agreed on at ITU forums. The available spectrum

which can be used for the development of Radio-Navigation Satellite Systems (RNSS) is shown in Figure 2-1.

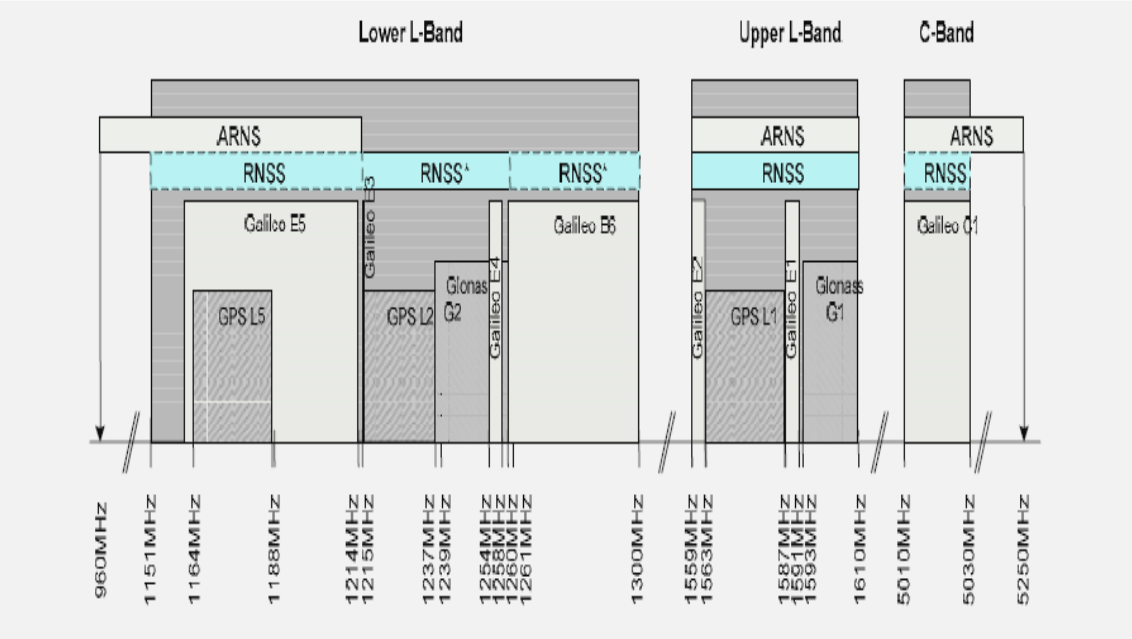


Figure 2-1: Radio-Navigation Satellite Systems (RNSS) frequency spectrum defined for GNSS signals (Galileo, 2005)

2.2 GNSS Error Sources

There are biases and errors influencing the GPS measurements, which limit the achievement of millimetre-level positioning accuracy. The major error sources of the GPS measurements are signal propagation errors due to the troposphere and ionosphere, orbital errors, satellite clock errors, multipath and receiver noise errors. These biases and errors are described in the following sections.

2.2.1 Orbital errors

The orbit quality is considered to be one of the primary accuracy-limiting factors in the GPS measurements. Orbital errors occur when the GPS message does not transmit the correct orbital parameters. There are several ways to define the satellite orbits for

determination of the position using GPS measurements. The broadcast ephemeris is transmitted in the navigation message. The broadcast ephemeris uses Keplerian elements to represent the satellite orbits and incorporates additional terms to account for the effects of the perturbing forces.

The main Keplerian elements are square root of the semi-major axis, eccentricity, mean anomaly at reference time, inclination angle at reference time, right ascension at reference time, and argument of perigee. The navigation message is generated based on observations at five ground-based monitor stations of the GPS control segment. The master control station is responsible for the computation of the ephemeris and satellite clock corrections, and the ground stations upload them to the satellites. The broadcast ephemeris is normally produced every hour and typical errors in the broadcast ephemeris are found to be 3 metres (Hugentobler *et al*., 2001).

The post-mission orbits give more accurate satellite positions. There are different agencies which provide post-mission orbits. The post-mission orbits are calculated using observations in an extended tracking network of GPS stations worldwide. The Center for Orbit Determination in Europe (CODE), the National Geodetic Survey (NGS), and the International GPS Service (IGS) provide post-mission orbit solutions. The ultra-rapid orbits are generated twice each day and contain 48 hours of orbits; the first 27 hours are based on observations and the second 21 hours are predicted. Accuracies of ultra-rapid, rapid, and final orbits have been determined by Hugentobler *et al*. (2001).

The accuracy of ultra-rapid orbits is at a level of 20 cm. The rapid orbits are available after a delay of one or two days of data collection with an accuracy of approximately 10 cm. The final orbits are the most accurate orbits with accuracies at a level of less than 5

cm. The final orbits are available after two weeks once the data is collected and the necessary analyses are conducted. The final orbits used in this dissertation are the products of IGS and NGS.

2.2.2 Satellite clock error

Satellite clock errors arise from instabilities in the oscillators of the GPS satellites, such that ranging errors are observed in user's measurements. The satellite clock error can be determined using the coefficients transmitted in the satellite navigation message. The clock errors computed using the broadcast navigation message are not accurate because the coefficients are predicted in time. If the broadcast coefficients were adequately modelled, the typical satellite clock error would be 10 ns (Hugentobler *et al*., 2001). The observed satellite clock error will be same for all receivers tracking the same satellite at the same instant.

Relativity and group delay contribute to the satellite clock error. The relativity effect occurs due to an apparent frequency shift in the satellite oscillator. The group delay correction is necessary to compensate for inter-frequency biases in the satellite transmitter. The satellite clock error can be removed by computing single differences of GPS observations between receivers. Also, the satellite clock error may be estimated post-mission using the precise clocks. Precise clocks are computed with the precise/final orbits.

2.2.3 Receiver noise

Receiver noise is a random error generated by the receiver as it processes the received signal to derive pseudorange and carrier phase measurements. It is considered as white noise because the errors are not correlated over time. There is also no correlation

between the code measurements and phase measurements taken at the same time in a given receiver because these measurements are derived using separate tracking loops. The noise in the code measurements can be isolated from all other errors using a "zero-baseline" concept where two receivers are connected to the same antenna.

The receiver noise for C/A-code measurements is in the range 30-300 cm and for P code, the values are 3-30 cm. For carrier phase L1, the phase noise would be 0.5-3 mm in a survey-grade receiver. The noise level of the code and phase measurements decreases as the elevation angle increases up to about 45^{o} and the noise level becomes constant above 45^{o} elevation (Shrestha, 2003).

2.2.4 Multipath error

Multipath is the result of GPS signals arriving at an antenna from more than one direction due to signal reflection or diffraction at various objects. In secular multipath, the incident ray remains parallel after reflection from smooth sources. In the case of diffuse multipath, the energy of the signal is scattered in many directions due to roughness of the reflecting surface, resulting in the reduction of field strength in the direction of the antenna.

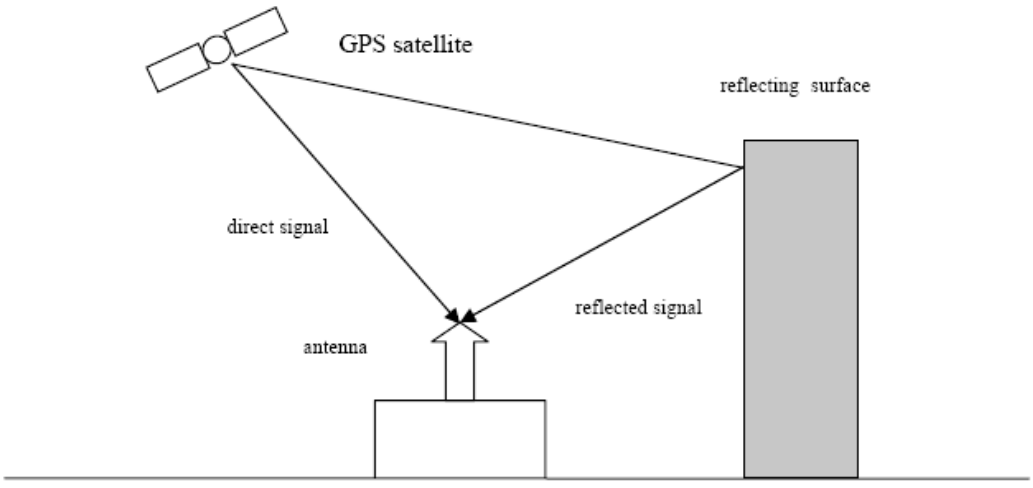


Figure 2-2: Multipath effect

Multipath has been a major source of error in precise GPS applications and a limiting factor for many DGPS applications. Multipath distorts the signal modulation and degrades the accuracy in pseudorange code measurements and carrier phase measurements, and it cannot be reduced through differential processing. Pseudorange multipath shows up as a systematic error in the GPS measurements and is correlated from day to day if the measurements are taken in the same environment. It can reach the magnitude of about 15 m for code measurements and ¼ wavelengths for phase measurements (Ray, 2000). This error can affect the ability to resolve integer ambiguities and, ultimately, degrade the accuracy of precise positioning and attitude determination.

The maximum multipath error occurs when α is equal to unity; hence maximum theoretical multipath error is 90^{o} or 5 cm for L1 measurements. However, typical phase multipath is in the order of 1 cm and less in real applications (Shrestha, 2003).

The multipath effects can be minimized by choosing the site of observation with minimum obstructions and reflecting surfaces nearby. Using a ground plane antenna or choke ring can minimize the multipath effects. Narrow correlator spacing technology may be applied in the GPS receiver to reduce the multipath effects (van Dierendonck *et al.,* 1992). Different multipath techniques have been developed to mitigate the multipath effects. Ray *et al.* (1998) have developed a system to estimate multipath parameters based on an array of closely spaced antennas in static mode.

2.2.5 Tropospheric error

The troposphere is the neutral region of the Earth's atmosphere extending from the Earth's surface up to 50 kilometres. When GPS signals propagate through the

troposphere, they experience range delays dependent on the pressure, temperature and moisture content along the signal path. The tropospheric delay is generally split into hydrostatic and wet components. The hydrostatic delay is due to the dry gases in the troposphere and the nondipole component of water vapour refractivity and can be modeled accurately using surface temperature, pressure, and humidity measurements. However, the wet delay is caused by the presence of water vapour and it exists up to 10 km from the surface of the Earth. Water vapour is highly variable in space and time such that the wet delay cannot be modeled using surface measurements very accurately (Bevis et.al., 1994).

Tropospheric delay has a great impact on GPS precise positioning because the troposphere is a non-dispersive medium at GPS frequencies and the delay cannot be eliminated using a combination of observations on two frequencies. Different models such as the Hopfield model (1969), Saastamoinen model (1973), and modified Hopfield model (Goad and Goodman, 1974) are used to estimate the tropospheric error (Hoffmann-Wellenhof *et al*., 1994). The dry part of the delay component can be determined with the accuracy of few millimetres; however the wet part of the delay component can only be estimated with an accuracy of 10-20%.

2.2.6 Ionospheric error

The ionosphere is the layer of the Earth's atmosphere extending from 50 km to 1000 km altitude. The ionosphere contains weakly ionized plasma of electrons and ions created primarily by the presence of ionizing solar radiation. GPS signals are affected as they pass through the ionosphere resulting in range errors. The magnitude of error depends on the signal frequency and the density of free electrons along the signal path.

The electron density integrated in a vertical column with a cross-sectional area of one square metre is known as the total electron content. The major effects of the ionosphere are the carrier phase advance and group delay of pseudorange. The phase advance and group delay are equal in magnitude and opposite in sign. The pseudorange ionospheric group delay ranges from 1 to 100 m (Shrestha, 2003). GPS ionospheric range errors are a function of the TEC along the signal path and the signal frequency.

The variation of TEC and ionospheric effects on GPS signals depends on different ionospheric characteristics. The electron density is directly proportional to the rate of ionization, which depends on the level of solar radiation, and solar wind characteristics (in auroral and Polar Regions). In the daytime, solar radiation is high and creates free electrons; the electrons recombine with ionospheric ions in the night time local time sector. The highest number of free electrons occurs at approximately 14:00 local time, and a secondary maximum may occur at 22:00 local time in the equatorial region. The TEC also depends on the season and geographic location. Electron densities are highest at spring equinox and two maxima in TEC are located at ±20 degrees magnetic latitude. Electron densities also increase by a factor of 3 in the period of solar maximum.

A larger number of sunspots appear in the period of solar maximum than in the period of solar minimum. TEC at mid-latitudes varies about 25% from monthly mean values due to variations in temperature and recombination processes. The measured TEC can be in the range 1016 to 1019 el/m2; these values represent the extremes of observed values in the Earth's ionosphere (Klobuchar, 1996). Figure 2-3 shows the worldwide distribution of TEC at 13:00 UT on September 27, 2001.

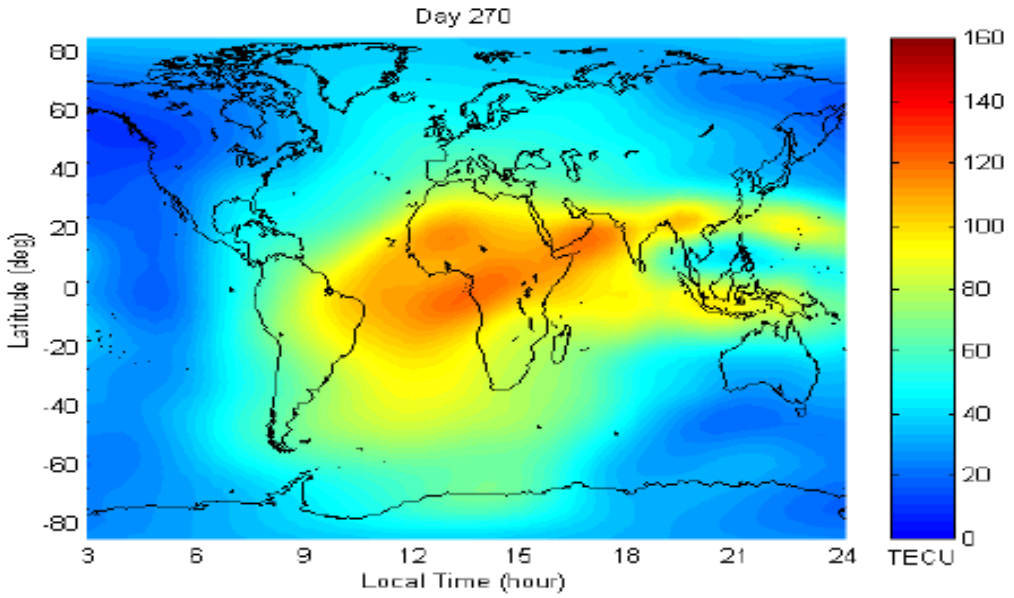


Figure 2-3: Worldwide distribution of TEC, 13:00 UT on September 27, 2001 (Shrestha, 2003).

The ionosphere is a dispersive medium: the delay depends on the frequency of the radio signal. In order to specify the propagation effects on a radio wave travelling through the ionosphere, the following equation for the refractive index of the medium given by Appleton and Hartree (Klobuchar, 1996) can be used.

$$n^2 = 1 - \frac{X}{1 - iZ - \frac{Y_T^2}{2(1-X-iZ)} \pm \left[\frac{Y_T^4}{4(1-X-iZ)^2} + Y_L^2\right]^{1/2}} \qquad (2.1)$$

Where

$X = N_e E^2/\varepsilon_0 m\omega^2, \quad Y_L = (f_H \cos\theta)/f, \quad Y_T = (f_H \sin\theta)/f, \quad Z = \vartheta/\omega,$

$\omega = 2\pi f$, and

f is the frequency of the signal,

E is the electron charge,

ε_0 is the permittivity of free space,

m is the mass of an electron,

θ is the angle of the ray with respect to the Earth's magnetic field,

N_e is the ionospheric electron density,

υ is the electron-neutral collision frequency, and

f_H is the electron gyro frequency.

The ionospheric refractive index can be determined with an accuracy of better than 1% using the following approximation:

$$n = 1 - (X/2) \quad (2.2)$$

The ionospheric group delay can then be determined using the following equation (Lachapelle *et. al*, 2002):

$$\Delta t = \frac{40.3}{f^2} TEC \quad (2.3)$$

where

Δt is the ionospheric time delay,

f is the frequency of the signal,

c is the speed of light,

TEC is the total electron content,

The temporal and spatial variations of TEC in the ionosphere cause variations in the ionospheric time delay for the GPS measurements. The phase of the carrier signal is advanced when it passes through the ionosphere. The carrier phase advance can be expressed using the following equation (Lachapelle *et al.,* 2002):

$$\Delta \emptyset = \frac{1.34\ X\ 10^{-7}}{f} TEC \quad (2.4)$$

where Δφ is phase shift due to the ionospheric refractive index.

In addition to group delay and phase advance of the radio signal, the other effects of the ionosphere are absorption, Faraday rotation or change in plane of polarization, Doppler

shift, refraction or bending of the radio waves, and scintillation. Ionospheric scintillations are rapid fluctuations in the phase and amplitude of signals and are caused by electron density irregularities in the ionosphere. The effects of ionospheric scintillations might be observed as the loss of phase lock due to lower signal strength, or due to Doppler shift outside the bandwidth of the phase lock loop.

The ionospheric effects can be virtually eliminated using dual frequency data to correct the pseudorange measurements. The ionospheric correction removes the first order ionospheric effect, but it increases the noise on the ionospherically corrected pseudorange. The ionospheric correction can be applied on the L1 carrier phase at a given epoch using dual frequency carrier phase observations and known carrier phase ambiguities for L1 and L2. However, the differential ionospheric delay correction can be applied using both L1 and L2 carriers without knowing the ambiguities in a float ambiguity positioning approach. The broadcast ionospheric model removes over 50% of the ionospheric delay at mid-latitude regions. The wide area DGPS ionospheric grid model may also be used to estimate ionospheric delays for individual satellites at a user's location (Shrestha, 2003).

2.3 Structure of the Ionosphere

The ionosphere is the ionised plasma in the atmosphere which is created by photoionisation of the neutral atmosphere by extreme ultra-violet (EUV) radiation and high energy solar particles. The ionisation process is mainly due to solar photons interacting with the atoms and molecules in the ionosphere, which results in the electrons being stripped away from the parent atoms and molecules, and creating a number of free negatively charged electrons and positively charged ions. The morphology of the ionosphere depends on altitude, time, geographic/geomagnetic

location, season and solar activity. The ionosphere lies between the altitudes of approximately 50 to at least 1,000 km. This thick layer is generally divided into four regions: D, E, F regions and topside ionosphere.

The ionosphere has distinct features at some latitudes. At low latitudes, the ionosphere has regions of high electron concentration at approximately 20◦ above and below the magnetic equator and a trough, i.e region of lower electron concentration, at the magnetic equator. This is a characteristic of the fountain effect in which electrons experience a strong upwards drift due to the Earth's magnetic field. This drift, known as the **E**×**B** vertical plasma drift, is responsible for the redistribution of the electrons to higher latitudes in the equatorial region. This equatorial region of strong horizontal electron density gradients is known as the equatorial or Appleton anomaly region and is observed during the evening and quiet magnetic conditions. At midlatitudes, the ionosphere is largely controlled by solar EUV radiation and the neutral winds, and the electron density gradient is not as steep as at low and high latitudes. At high latitudes, the ionosphere exhibits very complex behaviour because of its connection to the magnetosphere and the interplanetary medium, through the Earth's magnetic field.

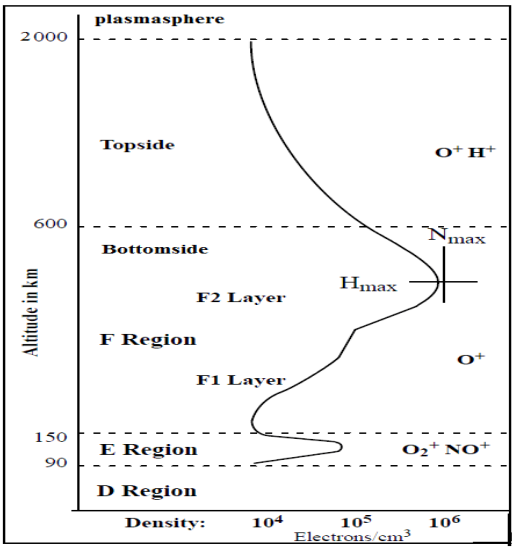


Figure 2-4: The various layers of the ionosphere and their predominant ion populations are listed at their respective heights above ground. (Katamzi, 2011).

The electron densities are generally greater during the day than at night time. The D and F1 regions disappear at night, (Hargreaves, 1992). The E, and F2 regions persist at night. The E-region is much weaker and may sometimes disappear at night. The F2 region is always present but at night it has a lower electron concentration. The peak of the F2 region appears at high altitudes in the afternoon and evening and lowers to lower altitudes at night. The diurnal variation of the ionosphere is primarily due to the fact that as the Sun rises and moves across the sky, solar radiation produces ionised particles and the number of electron concentration increases.

When the Sun sets recombination and other electron-loss processes are dominant, and thus the number of ionised particles decreases. Therefore to a rough approximation, the number of ionised electrons is greatest when the Sun is overhead, which is around noon. Another contributing factor to the diurnal variation in the Polar Regions is the $\mathbf{E}\times\mathbf{B}$ convection of ionisation from lower day lit latitudes towards the night-time. This is an important contribution for diurnal variation of the ionosphere during the long winter nights at high latitudes, (Davies, 1990).

The variation of the ionosphere with season is associated with revolution of the Earth around the Sun. The noon solar angle is higher in summer than winter. This should result in ionisation being greater in summer than in winter and is indeed observed to be the case for the D, E, and F1 region. However the F2 does not behave as expected. At mid latitudes the noon F2 electron concentration peak is greater in winter than summer. This is known as the seasonal anomaly and is more pronounced in high mid latitudes than in low and high latitudes. The anomaly is caused by the seasonal changes in the

relative concentrations of atomic and molecular species, (McNamara, 1991). More details are given in Davies (1990).

The solar activity variation is linked to the 11-year solar cycle. During the period of maximum sunspot number, which occurs when the solar cycle is at its peak, the ionisation is greater than at solar minimum because the solar radiation intensity is high thus enhancing the electron concentration in the ionosphere. Geomagnetic storms are generally initiated by solar disturbances; solar flares and coronal mass ejections (CMEs). The solar disturbances are more frequent at solar maximum than solar minimuzm, (Davies, 1990). Highly energetic particles emitted from CMEs enter the ionosphere at high latitudes. During geomagnetic storms and substorms these particles produce auroras; which are the optical manifestation of solar particles interacting with atmospheric particles observed at high latitudes, (Carlson and Egeland, 1995).

The night time E-region associated with auroras, known as the auroral E, has been observed to have high critical frequencies, almost as high at F region frequencies. At mid latitudes, the geomagnetic storms results in the critical frequency being reduced and the scale height increased in the F-region. The geomagnetic storms can have severe effects on satellites as well as electronic instruments on Earth, such as power transformers. A further exploration of the subject is found in Davies (1990).

The ionosphere acts as a refractive medium to radio signals, and the index of refraction depends on the amount of ionisation. The ionosphere affects a wide range of frequencies, from extremely low frequencies (about 3 kHz) to super high frequencies (30 GHz), Davies (1990).

The D layer is responsible for high frequency radio wave absorption, while the E and F regions are responsible for the reflection of high frequency radio waves. The absorption is explained in McNamara (1991) as follows: when a radio wave traverse the ionosphere an electron absorbs the energy from this wave and it vibrates or oscillates at a frequency equal to that of the radio wave. The energy of the radio wave is thus transformed into kinetic energy or energy of motion. The oscillating electron re-radiates this energy in the form of radio waves so the energy of the radio wave is passed forward from one electron to the next. If, however, an oscillating electron collides with a heavy neutral atom, the energy is transferred to the atom. The atom does not vibrate at the radio wave frequency, because it is not a charged particle but uses its increased energy to increase it speed. The energy of the radio waves is therefore absorbed by the neutral atom. The absorption is strongest in the D region because at those heights there is a high abundance of the neutral atom. The F region can reflect vertical radio waves with frequencies less than about 10 MHz. This frequency is known as the critical frequency, and is obtained from the plasma frequency and electron density *Ne* relation, given by:

$$f_c = \sqrt{(80.5N_e)} \qquad (2.5)$$

The typical maximum electron density in the F region is around 12×1011 electrons per cubic meter, which gives a critical frequency of approximately 10 MHz. Table 2.1 summarises the potential effects of each of the layers.

Table 2.1: Potential effects of the ionosphere on GNSS signals

Region	Coverage (Km)	Potential Effects
D	50-90	• absorption of radio signal. • has no measurable effects on GNSS frequencies
E	90-140	• causes minor scintillation effects
F1	140-210	• causes time delay of the GNSS signal when combined with the E-region thereby, accounting for 10% of the effect.
F2	210-1000	• a densed region • highest variability • causes the most potential effect on GPS

Source: Dodo, 2014

2.3.1 Ionospheric variation

As the ionosphere owes its existence to the Sun as the main ionizations energy source, the ionosphere naturally varies with time of day, season and geographic position (Ojigi, 2014). The following major variations are briefly discussed.

2.3.1.1 Diurnal variation

The day-night variations are due to the Earth's rotation. Night-time electron densities are much lower than daytime values, because of higher recombination rates in the absence of a radiation source. Daytime electron densities typically reach their peak at two hours past local noon due to the Earth's atmosphere lagging two hours behind the solid Earth's rotation (Opperman, 2007).

2.3.1.2 Seasonal variations

At different times of the year the Sun is vertically above different geographic locations. At equinox noon (March 21, Sep 23) the Sun is vertically above observers at the equator and vertically above observers at the Tropics of Capricorn and Cancer on solstice dates (21 December, 21 June). As vertical illumination from the Sun results in higher ionization rates, higher electron densit concentrations are observed at these locations on these dates than at other locations (Opperman, 2007).

2.3.1.3 Spatial variations

Similar to diurnal and seasonal variations, the Sun's position relative to the atmosphere plays a significant role in spatial variations of ionospheric densities (Opperman, 2007).

2.3.2 Major Geographic Regions of the Ionosphere

There are three major regions of the global ionosphere. These are: The equatorial regions, mid-latitude and high-latitude (see 2-5).

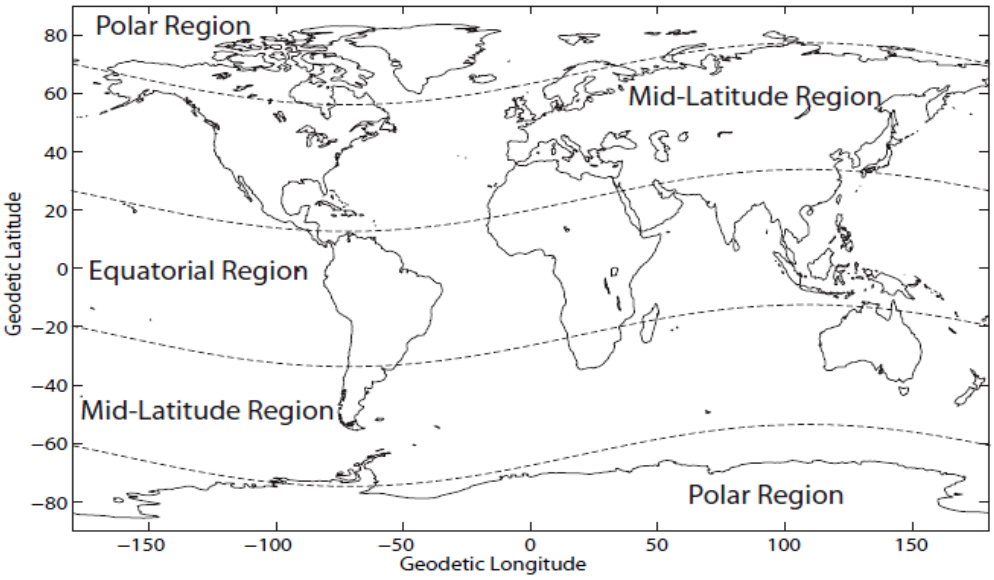


Figure 2-5: Major geographic regions of the ionosphere (Bishop *et al.*, 1991).

2.3.2.1 Equatorial regions

The equatorial regions are the geographic regions of the Earth which are centered on the equator and limited in latitude by the Tropic of Cancer in the northern hemisphere, at approximately (23.4° N), and the Tropic of Capricorn in the southern hemisphere at (23.4° S) latitude. Those regions can be characterized with the highest values of the peak-electron density with the most pronounced amplitude. The combined effect of the high radiation level from the Sun, and the magnetic fields of the earth results in the electrons rising and moving along the horizontal lines of the magnetic field, this phenomenon is called the equatorial anomaly (McNamara, 1991).

2.3.2.2 Mid-latitude region

The mid-latitude ionosphere region is known to be the best understood ionospheric region, largely due to the relatively simple physics and the reasonably good coverage of measurements. In the mid-latitude ionosphere region, transport of plasma is mostly caused by the combination of two facts, (1) the geomagnetic field line is inclined to the horizontal and (2) the ionospheric plasma is constrained to move along the geomagnetic field lines. Therefore, thermosphere neutral winds effectively transport the plasma along the field lines into higher or lower altitude regions in which recombination rates are different resulting in changes of the plasma density (Schunk and Nagy, 2000). Also, this is the region from which there are most of the ionospheric observations available due to the fact that most of the ionospheres sensing instruments are located in countries situated in the mid-latitude region (McNamara, 1991).

2.3.2.3 High-latitude region

In addition to photon ionization, collision ionization is another source of ionization in the high-latitude region. The main reason for this is the fact that the geomagnetic field lines are nearly vertical in this region leading to the charged particles descending. These particles can collide with the neutral atmospheric gases causing local enhancements in the electron concentration, a phenomenon which is associated with auroral activity. Auroral activity can also be regarded as an interaction between magnetosphere, ionosphere, and atmosphere. The auroral zones are relatively narrow rings situated between the northern and southern geomagnetic latitudes of about 64-70 degrees. In general, the intensity and the positions of the auroral ovals are related to geomagnetic disturbances, the ovals expend towards the equator with increasing levels of geomagnetic disturbance (McNamara, 1991).

2.4 Ionospheric Disturbances

Ionospheric disturbances can be resulted from solar disturbances or geomagnetic field disturbances. The ionospheric disturbances are associated directly or indirectly with the events on the Sun. The geomagnetic disturbances are also caused by events initiated from the Sun; however, these events rather affect the outer most geomagnetic field line (also called the magnetopause) and compress the geomagnetic field causing the geomagnetic disturbances (Komjathy, 1997).

2.4.1 Ionospheric sub storms

The most startling of the ionospheric irregularities is known as a Sudden Ionospheric Disturbance (SID). These disturbances may occur without warning and may prevail for any length of time, from a few minutes to several hours. Ionospheric sub storms can be caused by intense solar eruptions ejected energetic particles which also known as solar

flares that can endanger astronauts and destroy satellite electronics. X-rays which are emitted as part of the explosion can penetrate.

The energetic flares can also ejecting protons that can hit the Earth causing a polar cap absorption event. If the solar flare is sufficiently large, a cloud of plasma can also hit the Earth causing an ionospheric storm. Ionospheric disturbances can also be initiated by a High Speed Solar Wind Stream (HSSWS) which is caused by mass ejections from coronal holes. The Sun's magnetic field lines stretch out into interplanetary space making it possible for the ionized material to travel along the field lines and eventually reach the earth.

The effect of HSSWS on the ionosphere is usually not as devastating as those of a large solar flare. This is partly because HSSWS does not overtake the Earth as fast as the cloud from a solar flare hits it. Its effect also tends to last longer since it takes a couple of days to sweep over the Earth. Another potential trigger for an ionospheric storm can be sudden disappearing filaments which can be distinguished from HSSWS; they are large relatively cool structures on the Sun's surface potentially blowing out material into the interplanetary space affecting the Earth's geomagnetic field (Davies and Liu, 1991).

2.4.2 Geomagnetic storms

Ionospheric storms are disturbances in the Earth's magnetic field. They are associated, in a manner not fully understood. Geomagnetic storms usually occur in conjunction with ionospheric storms and can be caused by solar flares, high speed solar wind stream (coronal holes). The storms are usually associated with increased electron densities in the lower ionosphere and a simultaneous increase in absorption of radio waves. A geomagnetic storm usually starts with an increase in the Earth's geomagnetic field

intensity. On the other hand, a high speed solar wind stream induced geomagnetic storm (McNamara, 1991). According to Gonzalez *et al*. (1994) "*the geomagnetic storm is an interval of time when a sufficiently intense and long lasting interplanetary convection electric field leads, through a substantial energization in the magnetosphereionosphere system, to an intensified ring current sufficiently strong to exceed some key threshold of the quantifying storm time Dst index*". The definition of Dst index will be presented in detail bellow. There are other indices to describe the geomagnetic activity (Kp, Ap, ap, etc.) but all of them have a contribution from the high latitude activity and can show the increase without development of the magnetic storm, so called sub storms (Pulinets and Boyarchuk, 2003).

2.5 Solar-Terrestrial Indices

Most empirical and physics-based models of the ionosphere need solar and/or geomagnetic indices to specify the solar and geomagnetic disturbance level. These indices can be derived by continuously monitoring with groundbased equipment or they can be derived from continuously monitored parameters (Habarulema *et al.*, 2010).

2.5.1 Disturbance storm time index (Dst)

The first parameter of magnetic storm is Disturbance storm time index which define as a measure of geomagnetic activity used to assess the severity of magnetic storms. This index is a quantitative measure of the ring current forming around the Earth during the geomagnetic storm and supported by the ions with energies of several tens of keV and electrons with energy near 10 keV (Pulinets and Boyarchuk, 2003). The electric field leads to the earthward plasma convection, which permits high-energy particles to flow into near-earth space (Olwendo, *et al.,* 2012).

Dst is expressed in nanoteslas (nT) and is based on the average value of the horizontal component of the Earth's magnetic field measured hourly at four near-equatorial geomagnetic observatories. Use of the Dst as an index of storm strength is possible because the strength of the surface magnetic field at low latitudes is inversely proportional to the energy content of the ring current, which increases during geomagnetic storms. In the case of a classic magnetic storm, the Dst shows a sudden rise, corresponding to the storm sudden commencement, and then decreases sharply as the ring current intensifies.

The Dst begins a slow rise back to its quiet time level. The relationship of inverse proportionality between the horizontal component of the magnetic field and the energy content of the ring current is known as the Dessler-Parker-Sckopke relation. Other currents contribute to the Dst as well, most importantly the magnetopause current. The Dst index is corrected to remove the contribution of this current as well as that of the quiet-time ring current (Hamilton *et al.*, 1988). The minimum Dst value reached is often used to classify the strength of a geomagnetic storms as in Table 2.2**.**

Table 2.2: Geomagnetic storm classification

Dst value	**Storm type**
Minimum Dst below -20 nT	Weak storm
Minimum Dst below -50 nT	Moderate storm
Minimum Dst below -100 nT	Strong storm
Minimum Dst below -200 nT	Severe storm
Minimum Dst below -320 nT	Great storm

Source: Loewe and Prölss, 1997

2.5.2 Kp-index (Kp)

The second parameter is Kp-index which is defined as quantified disturbances in the horizontal component of Earth's magnetic field with an integer in the range (0-9) with (1) being calm and (5) or more indicating a sub-geomagnetic storm. It is derived from the maximum fluctuations of horizontal components observed on a magnetometer during a three-hour interval (Mubarak *et al.*, 2008).

The conversion table from maximum fluctuation (nT) to Kp-index varies from observatory to observatory in such a way that the historical rates of occurrence of certain levels of K are about the same at all observatories (Komjathy, 1997). In practice this means that observatories at higher geomagnetic latitude require higher levels of fluctuation for a given Kp-index as shown below in Table 2.3**.**

Table 2.3: The sudden storm scale according to Kp- index.

Kp-index	**Ap**	**Observatory measurement (nT)**	**G-scale**
0	0	0-5	G0
1	3	05-Oct	G0
2	7	44105	G0
3	15	20-40	G0
4	27	40-70	G0
5	48	70-120	G1
6	80	120-200	G2
7	140	200-330	G3
8	240	330-500	G4
9	400	> 500	G5

Source: Sethi *et al.,* 2010

2.5.3 Ap-index (Ap)

A-index provides a daily average level for geomagnetic activity, which affects radio propagation, based on the Kp-index. Because of the non-linear relationship of the K-scale to magnetometer fluctuations, it is not meaningful to take averages of a set of K indices. Instead, each K is converted into a linear scale called the "equivalent three hourly range" Ap-index where the daily Ap-index is the average of eight "A" indices (Bilitza and Reinisch, 2008).

2.5.4 Sunspot Number (SSN)

The visible surface of the Sun is known as the photosphere. A sunspot is an area seen as a dark spot on the photosphere of the Sun. They are concentrations of magnetic flux, typically occurring in bipolar clusters or groups. They appear dark because they are cooler than the surrounding photosphere. As the number of spots increase and magnetic complexity grows, they become likely sources of large eruptive energy releases known as solar flares (Dieminger *et al.*, 1996).

The daily index of sunspot activity (R) which observed is defined as

$$R = k(10g + s) \tag{2.6}$$

Where

s is the number of individual spots

g is the number of sunspot groups

k is an observatory factor.

Since for many years, solar sunspot numbers were derived at the Zurich Observatory, this index is known as the Sunspot Number. The approximately 11 year solar cycle can be clearly significant differences in the peaks of the solar cycles. Also, the climb-up

period usually takes 3 to 4 years whereas the going down period usually takes 7 to 8 years (Dieminger *et al.*, 1996).

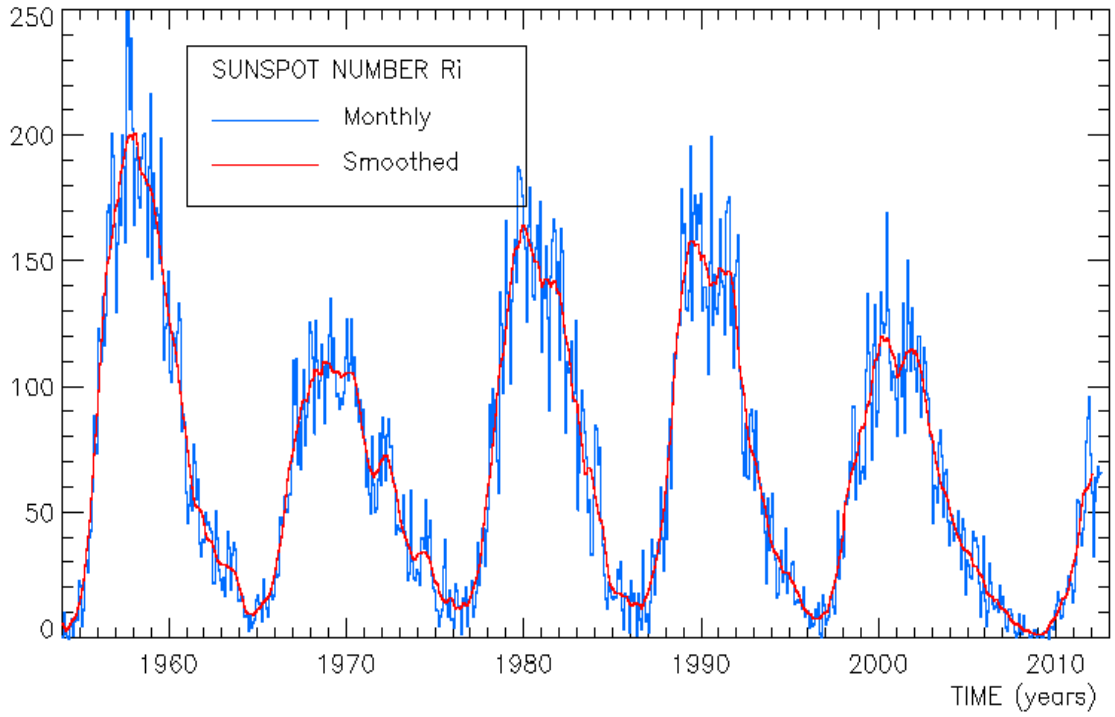


Figure 2-6: The monthly (blue) and monthly smoothed (red) sunspot numbers for the latest five cycles. (Solar Influences Data Analysis Center webpage, 09.08. 2012, http://sidc.oma.be/html/wolfmms.html, last accessed September 27, 2014)

2.6 Ionospheric Modeling

As mentioned before, propagating of a signal through the ionosphere can introduce one of the biggest errors to positioning. A significant majority of the error due to the dispersive nature of the ionosphere can be easily removed using two or more frequency communication (Jusoh, *et al.*, 2008). However, large number of GNSS receivers still use just single frequency communication. One of the possibilities how to deal with ionospheric propagation issues is using an ionospheric models. Using various inputs, ionospheric model inside a receiver models current ionospheric condition or can directly calculates assumed ionospheric delay.

There are two types of ionospheric models, deterministic and empirical. Deterministic models, based on physical laws and principles are much more precise however the deterministic modeling requires a lot of computation. Therefore, the realtime modeling or near-realtime modeling is impossible due to the high time-consumption. On the other hand, even though those empirical models are less precise, they are widely preferred in applications that require real-time or near-real time estimation of ionospheric condition (Najman, 2012).

There are several empirical models which can be used for mitigation of the second order of the ionospheric error. The most used is the Klobuchar model which is implemented in GPS receivers. Galileo system will use model NeQuick. Another model is THE IRI undertaken by NASA and quite new empirical model from DLR, Germamny, NTCM.

2.6.1 Klobuchar model

The Klobuchar model was developed by John A. Klobuchar at the Air Force Geophysics Laboratory, U.S. The algorithm was designed to correct ionospheric time-delay in GPS system for single frequency communication. The Klobuchar model is very fast and simple. It models daytime course of ionospheric time delay as a half period of cosine function which shape is determined by 8 ionospheric coefficients and with function maximum at 14:00 local time. The night time ionospheric delay is set as a constant value of 5 ns (Figure 2-7). Therefore, no integration of electron density is required since the model directly approximates time delay value (Klobuchar, 1987, as cited in Najman, 2012). The model inputs are: position, time, elevation and azimuth angle of a satellite and 8 ionospheric conefficients transmitted to a receiver by GPS navigation message. The Klobuchar model is able to reduce at average 50% of ionospheric error.

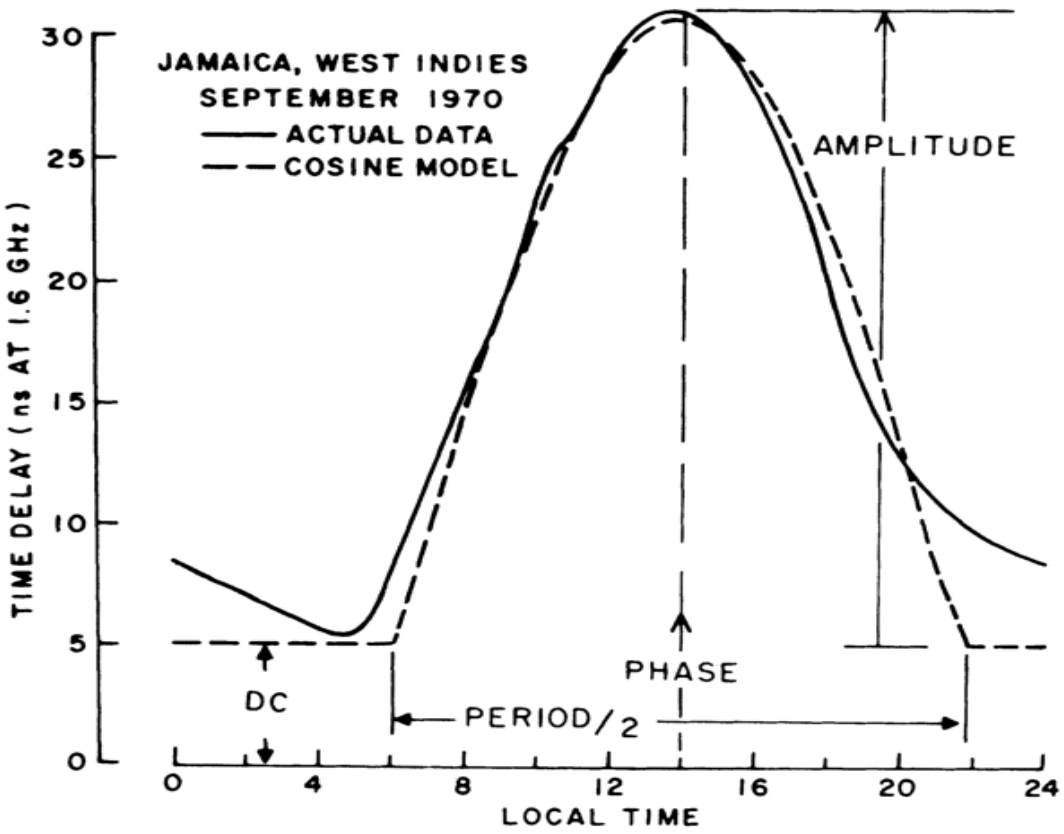


Figure 2-7: Example of actual monthly average time-delay data, along with cosine model fit to data (Klobuchar, 1987, as cited in Najman, 2012)

2.6.2 NeQuick model

The NeQuick model was developed at the Aeronom and Radiopropagation Laboratory of the Abdus Salam International Center for Theoretical Physics, Trieste, Italy, and at the Institute for Geophysics, Astrophysics and Meteorology of the University of Graz. Austria. Since the model was developed, it has been continuously improved due to the increasing amount of available ionospheric data.

The latest version, NeQuick 2, is going to be used in single frequency navigation of the system Galileo for correcting ionospheric time delay (Arbesser-Rastburg, 2006). The NeQuick computation method for the topside ionosphere has been also adopted by the IRI model as a default computation option for the topside electron density profile.

The model is able to calculate electron density at any given place of the atmosphere at any given time. FORTRAN code currently available is designed especially to create electron density profiles between two given points (usually positions of a satellite and a receiver), the value of TEC can be afterwards obtained by the integration of the electron density profile. The input parameters for the model are: position(s), time and solar flux. More information about the analytical formulation of the model and code implementation can be found in (Radicella and Nava, 2010).

2.6.3 International Reference Ionosphere

Another empirical model, which is often used to estimate TEC, is International reference ionosphere (IRI) which is currently freely available on National Aeronautics and Space Administration (NASA) webpage in version 2012. IRI serves as an international standard for the climatological specification of ionospheric parameters as ionospheric density, temperatures and chemical content (Bilitza and Reinisch, 2008).

The IRI is the international project started up in the early sixties when the first radio-observation data of the very first satellite was available. The group of specialist with name International Reference Atmosphere (CIRA) under the Committee of Space Research (COSPAR) was established as an effort to create an empirical model of the upper atmosphere. IRI became the part of CIRA which was concern with ionized part of the atmosphere (Bilitza, 1990).

Nowadays, given location and time, IRI provides possibilities to model many parameters such as the electron density, electron temperature, ion temperature and ion composition in the altitude range from 50 to 1500 km.

2.6.4 NTCM model

At Deutsches Zentrum f¨ur Luft-und Raumfahrt (DLR) Neustrelitz, GNSS based ionospheric monitoring has been carried out since 1995. Recently, they developed a simple global ionospheric model NTCM which should provide a simple way to obtain value of vertical TEC in any given time and location. The model uses 12 coefficients, value of solar radio flux and can be autonomously used for a full solar cycle. The model does not use any integration of electron density profiles, therefore it is very simple and fast (Jakowski, *et al.*, 2011).

2.6.5 Global Ionosphere Maps

The International GNSS Service (IGS) of the International Association for Geodesy (IAG) maintains a global GNSS tracking network of more than 200 receivers. The availability of a huge number of the IGS permanent dual frequency GPS receivers, which are distributed over the Earth's surface, has made the global monitoring of the ionosphere possible and Global

Ionospheric VTEC Maps (GIMs) are produced routinely. Four IGS Ionospheric Analysis Centers (CODE, ESA, JPL, and UPC) individually produce daily Global Ionosphere Maps using different techniques (Perez, 2005; Wienia, 2008). The official IGS product is a combined ionosphere map from all four IGS analysis centers. The GIM files are distributed on a daily basis; they give a value for the Vertical Total Electron Content (VTEC) every two hours (0, 2, 4, ..., 24 UTC) at the grid points. The resolution of the maps is 5° in longitude and 2.5° in latitude. The GIM are provided in the IONEX (IONosphere map EXchange) format (Schaer 1999). The maps are provided in two versions: a rapid product with a latency of 12 hours, and a final product with a latency of 3 days.

The Center for Orbit Determination in Europe (CODE), for example, employs spherical harmonics functions to model the global VTEC using about 200 worldwide GPS/GLONASS stations. The spherical harmonics are then developed into Global Ionosphere Maps. The other analysis centers use different approaches. Only the CODE distributes GIM in three versions: Predicted, Rapid and Final GIM. The predicted version contains predictions of the ionospheric delay for 1-2 days ahead. The VTEC at a certain time and location is interpolated between two consecutive maps using four surrounding grid points. The VTEC provided by GIM has a standard deviation of 2∼8 TECU (CODE, 2007) depending on the epoch in the solar cycle, season, and location is unbiased (1 TECU corresponds to an ionospheric delay of 16 cm in L1). The interpolated VTEC from the GIM is converted to the vertical ionospheric range delay V_{GIM} as

$$V_{GIM} = \frac{40.3}{f^2} . VTEC_{GIM} \qquad (2.7)$$

where f is the frequency of signal (Hz). The standard deviation of the VTEC provided by GIM is 2 ∼8 TECU (CODE, 2007). In order to get slant ionospheric delay along the line-of sight between receiver and satellite a mapping function must be used to map the VTEC to the slant TEC value. Mapping is done based on the single-layer approximation for the ionosphere and the mapping function is $F(\xi) = 1/\cos(\xi)$ where ξ is the zenith angle of the satellite at the ionospheric pierce point at the ionospheric height of 350 km (Memarzadeh, 2009).

2.7 Total Electron Content (TEC)

Global Position System is a satellite –based navigation system that sends and receives radio signals which is a powerful technique used to study the ionosphere. The ionosphere importance came from its effect on radio waves and so transmissions of

electromagnetic waves by satellite-based navigation systems, (the waves affected as they pass through the ionosphere) (Strangeways and Walsh, 2007).

GPS radio signals are slowed down as they propagate through the ionosphere, causing an increase in the propagation time of a signal when compared to the time of propagation through free space. This effect, called the propagation delay, must be taken into account when determining position (Perevalova, 2008).

The absolute value of the group delay can be written as (Ya'acob *et al*., 2009):

$$I_{\emptyset,g} = \frac{80.6}{2f^2} \int N_e \, dh \qquad (2.8)$$

Where

$I_{\phi, g}$ = the group delay of radio signal propagation
N_e = number of electrons at distance
f = system operating frequency in MHz

The TEC is defined as total number of electrons integrated along the path from the satellite to receiver. As equation,

$$TEC = N_e dh \qquad (2.9)$$

Where:

Ne=electron density along the ray paths from satellite to receiver.

TEC= total electron content, TEC is measured in unit (TECU) = 10^{16} electrons per m^2.

The ionosphere's TEC is a parameter widely used in studies of the near-Earth plasma environment which is an indicator of ionospheric variability that produces most of the effects on GPS signals. TEC is a key parameter in the ionospheric effects on radio systems, in numerous applications involving radio links between satellites and ground, which play roles in the modern technology of communications, navigation and surveillance, the propagation departs from free space conditions in various ways with

important consequences for the reliability and accuracy of the service (Jakowski, 1996). The propagation delay could characterize by the TEC by substituting TEC into equation (2.8) which yields (Ya'acob *et al*,. 2009):

$$I_{\emptyset,g} = \frac{40.3}{f^2} TEC[m] \qquad (2.10)$$

or

$$I_{\emptyset,g} = \frac{40.3}{cf^2} TEC[sec] \qquad (2.11)$$

Where:

$I_{\phi,g}$ = the group delay of radio signal propagation

f = system operating frequency in MHz

TEC= Total Electron Content e/m^2

c= *light speed* $=3x10^8$ *m/sec*

The group path delay timing error is important depending upon the frequency the system uses-and the amount of the ionospheric TEC. For Very High Frequency (VHF) and higher the relationship between time delay and TEC when the ionosphere is a dispersive medium, and since the dispersion changes with frequency in a known way, a dual frequency receiver can be used to effectively eliminate this propagation delay of GPS signals caused by the ionosphere and so provide highly accurate determinations of the position of receivers monitoring GPS, or other satellite navigation systems (Saito *et al.*, 2006).

However, because of their relative simplicity, single frequency GPS receiver systems are often used even though they have no possibility of measuring the ionosphere delay. Instead, ionospheric models must be relied on to provide the necessary correction for

the ionospheric delay. Ionospheric models generally only represent average conditions and are mostly based on ionosonde measurements that only probe the bottom-side of the ionosphere, i.e. the region below the maximum electron density which generally occurs in the range (250 – 400) km altitude (Yizengaw and Essex, 2002).

Consequently it is important that the ability to model the ionosphere, and including the topside ionosphere, is improved for GPS applications, and in fact, GPS observations can themselves be used to determine properties of the ionosphere (Ya'acob *et al.* 2009). In fact the signal propagation delay, or position correction, is proportional to the line integral of the free electron distribution along the path of the signal from the satellite transmitter to the receiver. This information can be used to determine the electron density distribution in the Earth's ionosphere and plasmasphere mean study the behaviour of the ionosphere and magnetosphere and so can be used not only to correct for the propagation delay in GPS signals, for example the changes occurring during ionospheric storms, ion composition changes, and space-weather effects on telecommunications are just a few of the phenomena that can be studied (Pedatella *et al.*, 2009).

Consequently, TEC measurements, made using transionospheric radio signals, are one of the most important methods of investigating the Earth's ionosphere and plasmasphere. However, by themselves, a series of TEC measurements are just a collection of line integrals of the free electron density and not maps of the electron density distribution or structure (Yizengaw, 2004).

2.7.1 Slant and Vertical TEC

In general, there are two types of TEC, Slant TEC (TECs) and Vertical TEC (TECv), where Slant TEC (TECs) is defined by the total electron density along the ray path between transmitter and receiver at angles deviating from the radial direction with respect to the centre of the Earth, or define as a measure of the total electron content of the ionosphere along the ray path from the satellite to the receiver, represented in Figure (2-8) as the quantity Ts or TECs. The slant total electron content, is along ray path l between a GPS satellite (T_x), and a ground-based receiver (R_x) can be written as in equation (2.1) and (2.2) (Liu *et al.*, 2004):

$$TECs = \int_{R_X}^{T_X} N_e dh = \frac{f^2}{40.3} \int_{R_X}^{T_X} (n^{-1} - 1) dh \qquad (2.12)$$

$$TECs = \frac{f^2}{40.3} \int_{R_X}^{T_X} \left[\left[\sqrt{\left(1 - \frac{f_N^3}{f^2}\right)} \right]^{-1} - 1 \right] dh \qquad (2.13)$$

Where

N_e is the electron density in e/m^3, n denotes the refractive index, and f and f_N represent radio wave and plasma frequency in MHz, respectively.

Vertical TEC (TECv) is normally given from the surface of the Earth and up enables TEC to be mapped across the surface of the earth, represented in Figure (2-8) as the quantity Tv or TECv.

The l-axis stands for the receiver-to-satellite direction. Equation (2.14) is to convert slant TEC (TECs) to vertical TEC (TECv).

$$TECv = TECs(cosx') \qquad (2.14)$$

Where

TECs is the value of slant TEC,

x' is the difference between 90° and zenith angle (90°-x).

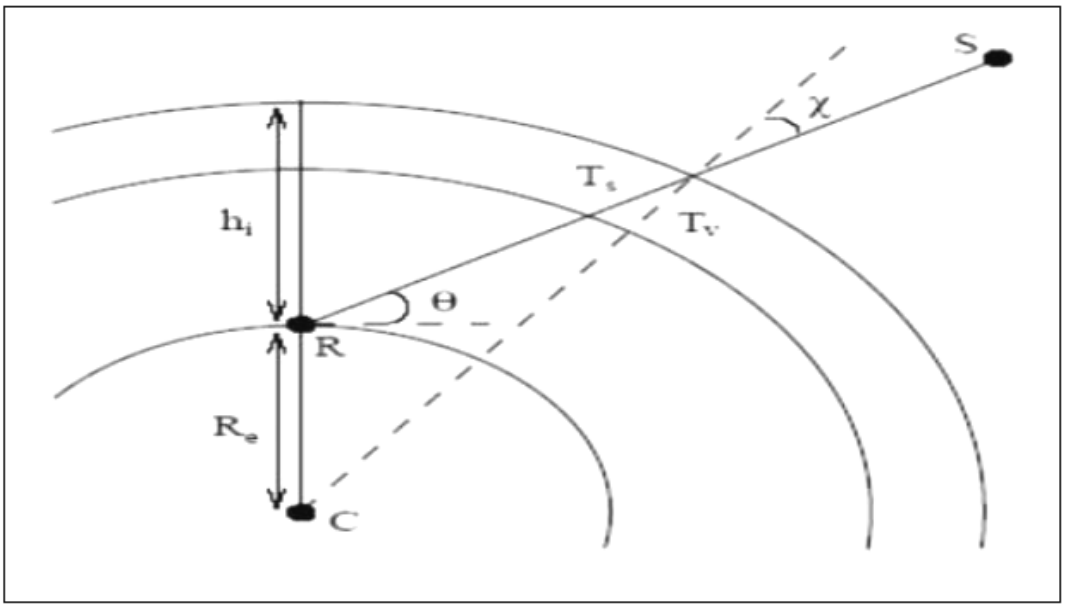


Figure 2-8: Geometry of satellite-receiver link (Liu *et al.*, 2004)

C = Centre of the Earth,

Re = Earth Equator,

Hi = the high of layer,

S = satellite (GPS),

TS, T*v* = Slant and Vertical Total Electron Content,

x, ɵ = angle of satellite

Because the effect of the TEC on GPS so it is compared which one of the widely ways to calculate TEC directly is the GPS which include currently 28 GPS satellites, at high 20,200 km altitude, and orbiting declination angle of 55°.28. Those GPS satellites, have two frequency *f*1 =1575.42 MHz and *f*2 = 1227.6 MHz. The GPS work depends on the difference in time delay of these two frequencies (Warnant. 1997).

The absolute TEC can be calculated using GPS signal, equation (2.15) (Jusoh *et al.*, 2008).

$$TEC = \frac{\Delta p.c}{40.3}\left(\frac{f_1^2.f_2^2}{f_1^2-f_2^2}\right) \qquad (2.15)$$

Where: Δp is the difference between time delays measured by the L1 and L2, c is the light speed (m/s),

$f1$ =is the frequency of the L1 wave,

$f2$ =is the second frequency of the L2 wave.

2.8 Review of Related Works

The study and estimation of the ionosphere from the GNSS perspective and the application to space geodesy are growing and active fields. In this context, it is worth noting several reports of representative works related to the study being carried out in this dissertation. From the viewpoint of ionospheric studies, for instance, Azpilicueta and Brunini (2011) wrote a paper providing a potential physical explanation for the semiannual anomaly.

Regarding the application of the ionospheric state to space geodesy, two remarkable recent examples can be highlighted, one discussing in detail different higher-order ionospheric effects in GPS (Petrie *et al.*, 2011), and another highlighting the application of these effects to problems such as long time series of accurate GPS coordinates in general, and in the provision of accurate models of glacial isostatic adjustment (GIA) in particular (King *et al.*, 2010).

From an operational standpoint, it is worth emphasizing the development of a new generation of International GNSS Service (IGS) ionospheric prediction maps: among those already computed by Center for Orbit Determination in Europe (CODE), ESA and UPC have recently started its computation (see, e.g., García-Rigo *et al.*, 2009). In addition, the forthcoming realtime ionospheric Vertical Total Electron Content (VTEC)

maps, presently computed internally by JPL, are currently in the process of being implemented as a potential future IGS product, within the context of RT-IGS pilot project products (*Caissy et al.,* 2011).

Decades of ionospheric research showed that TEC is highly variable and depends on several factors such as local time, geographical location, season and solar cycle (e.g., Jakowski, 1996; Jakowski *et al*., 1999; Tsurutani *et al*., 2005; Mannucci *et al*., 2005; Fedrizzi *et al*., 2005; Moeketsi *et al*., 2007; and Moeketsi, 2008).

Later Ezuqer *et al.* (2004) studied the behaviour of the Vertical Total Electron Content (VTEC) obtained from GPS signals, received during the high solar activity year 1999 at 10 stations of the American sector. The considered latitude range extends from 18.4°N to 64.7°N and the longitude ranges from 281.3°W to 297.7°W, the result of this study showed that the VTEC variability during daylight hours is about 30% of median or less and for night time hours is greater than the mentioned percentage, particularly at last hours of the night near the northern peak of the equatorial anomaly. The GPS signals traverse the ionosphere carrying signatures of the dynamic medium and thus offer opportunities for ionospheric research. Global distributions of TEC variations as well as its characteristics at equatorial, middle, and high latitudes have been investigated by a number of workers (Maltseva *et al*., 2012).

Jakowski *et al*., 2001 and Jakowski *et al*., 2002 illustrated that TEC monitoring using the GNSS network can contribute to space weather monitoring. On the other hand, Lui *et al*. (2007) used unique CHAMP satellite data to investigate effects of solar flares not only on the ionosphere, but also on the thermosphere and they reported important

temporal and latitudinal differences between the two components, which is crucial for improving space weather models of the upper atmosphere.

During the last decade Total Electron Content (TEC) provided by Global Navigation Satellite System (GNSS) receivers in many stations of the world allowed to study ionosphere. Many studies were done, on the comparison between in situ TEC measurement and existing ionospheric models (e.g. Jin and Park, 2007; Chauhan and Singh, 2010; Ouattara and Fleury, 2011) and on ionospheric pattern and scintillation (e.g. Mannucci *et al.*, 2005 ; Sardon *et al.*, 1994; Jakowski, 1996; Baran, *et al.*, 2001; Liu and Gao, 2001; Rama Rao *et al.*, 2006; Ray and DasGupa, 2006; DasGupta *et al.*, 2007; Spogli *et al.*, 2009; Prikryl *et al.*, 2010). Maruyama *et al.*, 2004; Guarnieri and Pillat, 2010; Jain *et al.*, 2010; Malik *et al.*, 2010; Adewale *et al.*, 2011; studied the ionospheric disturbances related to geomagnetic storms. The results of these studies showed considerable TEC rise lasting for the period of the storm and a gradual decline in the observed TEC value hours after the storm.

Total electron content (TEC) measurements have been used extensively to study the general morphology and variability of the ionosphere during both geomagnetically quiet and disturbed conditions. Codrescu *et al*. (1999, 2001) and Jee *et al.*, (2004) used TEC observations from the TOPEX satellite to study the TEC climatology over the oceans at low and middle latitudes and presented its seasonal and solar cycle variations. Jee *et al.* (2004) also presented the longitudinal variation of the TOPEX TEC data in the Atlantic, Indian, and Pacific sectors. A more detailed study of the longitudinal dependence of TEC at low-latitudes was presented by Vladimer *et al*. (1999) and Scherliess *et al.*

(2008) using the entire 13 years of TOPEX TEC data. The latter study pointed out the occurrence of a wavenumber-four pattern in the low-latitude TEC climatology.

Stankov (2009) studied TEC changes during the geomagnetic storms intensity, season, and latitude of the latest solar activity cycle using GNSS to measurements of the TEC at 50.1°N, 04.6°E and European IGS stations. The result was that the storm-time behaviour of TEC shows clear positive and negative phases, relative to the non-storm (median) behaviour, with amplitudes that tend to increase during more intense storms. The most pronounced positive phase is observed during winter, while the strongest and yet shortest negative phase is detected during equinox. Average storm-time patterns in the TEC behaviour are deduced for potential use in ionosphere prediction services.

Habarulema, *et al.,* 2010 from a study designed to investigate the ability of a newly developed neural network (NN) based model to follow total electron content dynamics over the Southern African region. The generalization of TEC behaviour by the NN model is demonstrated by producing predicted TEC maps during magnetic storm periods over South Africa. Presented results demonstrate the ability of NNs in predicting TEC variability over South Africa during magnetically disturbed conditions, and highlight areas for improvement.

Sethi *et al.* (2010) analysed values of Total Electron Content (TEC) measured by ATS-6 are used by to assess the IRI-2007 model during solar minimum over Indian sector covering equatorial to low-mid- latitudes stations. The study revealed in general, that during all seasons and at all locations the TEC predicted by NeQuick and IRI01-corr options provided in the IRI-2007 model shows much better agreement with the TEC

observations as compared to those generated by IRI-2001.option. TEC predicted using NeQuick option found to be little more closely to the observation except at equatorial station during daytime, while IRI-2001 option highly over estimates the TEC in all seasons and time.

Natali and Meza (2011) studied seasonal variations of the Vertical Total Electron Content during high solar activity in 2000 at low, mid, high latitude region by chosen two-hour at noon and at night. It reveals that the variations of VTEC at night are smaller than those obtained at noon and the seasonal variation in high and low latitude is higher than in mid latitudes region.

Stankov and Warnant (2009) reviewed the climatological and storm-time behaviour of the slab thickness at the mid-latitude site Dourbes, it was recognized that the slab thickness how diurnal, day-to-day, seasonal, spatial, solar, and geomagnetic activity variations. Guo *et al*. (2011) studied the ionospheric equivalent slab thickness which has been determined from ground-based GPS/TEC and GPS/COSMIC IRO measurements in global regions.

Climatology of the slab thickness was described as the diurnal, seasonal, and geomagnetic latitudinal variations. Some results on solar minimum phase obtained that the diurnal variations of the slab thickness are generally characterized by higher values in nighttime compared with that of daytime for non-auroral latitudes in all seasons. However, an opposite behaviour can be found in high-latitudes in summer and the pre-sunrise peaks of the slab thickness as observed for non- auroral latitudes in all seasons. At mid-latitudes, the post-sunset peaks appear in winter and equinox, and disappear in

summer. The peaks of the slab thickness at mid-noon were detected near geomagnetic equator in all seasons (Guo *et al.*, 2011).

Maltseva *et al*., (2012) studied the behaviour of the two parameters of the ionosphere, f_oF2 (or NmF2) and TEC for Period of October–November 2003 and studied the slab Thickness (τ) behaviour which is the proportionality factor between the TEC and NmF2 at low and mid latitude, and found that Both parameters have strong positive and negative variations, but synchrony of these variations exists not always even during severe disturbances. This sometimes leads to unpredictable variations of the equivalent slab thickness.

Most of the reviewed studies on ionospheric total electron content were carried out within a short time period ranging from several days to few months, or specifically during period of ionospheric disturbance. Also the total electron content was derived from single data sources. Furthermore, the study of the state of the ionosphere with radiosonde, radiosounders, Faraday radars, is limited by the spatial coverage and temporal resolution of these techniques. GNSS provides large spatial coverage with high temporal resolution of 30 seconds data rate. This research is therefore aimed at filling these gaps by deriving and analysing ionospheric total electron content over the Nigerian Global Navigation Satellite System Permanent Reference Network for a period of four and half years using data from two independent sources; the data from the Nigerian CORS network with 14 operational stations, and data from the IGS global CORS network with over 200 operational stations.

CHAPTER THREE

MATERIALS AND METHODS

3.1 Study Area

OSGOF which is the National Mapping Agency of Nigeria initiated in 2008 a project to establish NIGNET. This network, formed by state-of-the-art CORS (Continuously Operating Reference Station) GNSS (Global Navigation Satellite Systems) equipments, intends to implement the new fiducial geodetic network of Nigeria. At national level, NIGNET will serve primarily as the fiducial network that will define and materialize a new reference frame based on space-geodetic techniques (Jatau, 2010). Starting with nine stations in 2010, currently, NIGNET is formed by fifteen CORS stations covering the entire country. This nation-wide, dual-frequency, ground based GNSS receiver network provides a cost- effective means for estimation of TEC and monitoring of ionospheric activity over Nigeria. Figure 3-1 shows the spatial distribution of the nationwide stations. See Table 3.1 for details of the GNSS CORS stations used in the study.

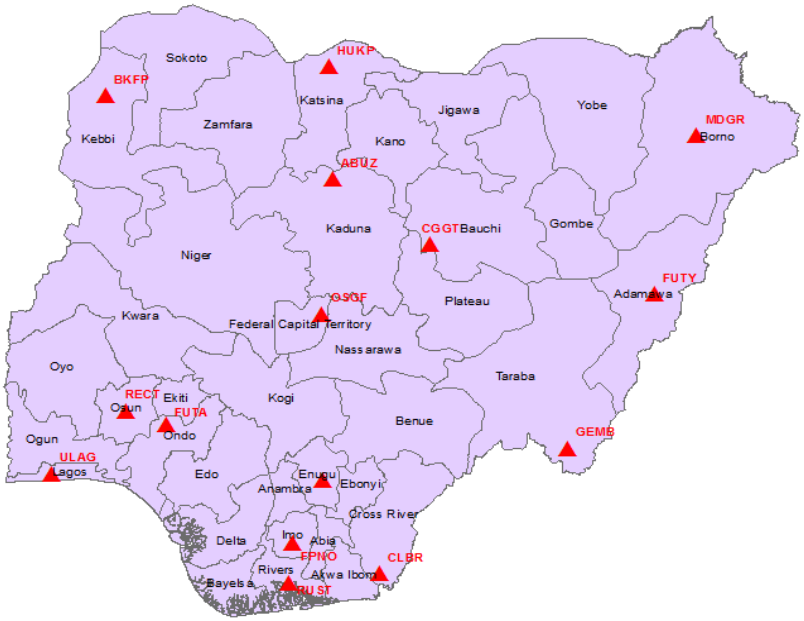


Figure 3-1: Spatial distribution of the NIGNET receiver stations in Nigeria (Source: Author)

Table 3.1: NIGNET GNSS CORS stations in Nigeria used in the study

No.	Staion ID	Latitude	Longitude	Elevation (m, ellips.)	Location	Installed date
1	ABUZ	11.15174	7.64869	706.1	Zaria	2009-10-05
2	BKFP	12.46858	4.22924	251.0	Birnin Kebbi	2009-10-05
3	CGGT	10.12309	9.11831	917.4	Toro	2009-10-05
4	CLBR	4.950301	8.35157	61.5	Calabar	2011-03-15
5	FPNO	5.4346	7.03320	92.6	Owerri	2012-07-15
6	FUTA	7.2986	5.13640	415.996	AKURE	2012-03-28
7	FUTY	9.349743	12.49780	248.4	Yola	2009-10-05
8	GEMB	6.917199	11.18394	1796.6	Gembu	2009-10-05
9	HUKP	12.9212	7.59090	565.010	Katsina	2012-04-01
10	MDGR	11.83809	13.23100	351.8	Maiduguri	2011-03-05
11	OSGF	9.027666	7.48634	533.6	Abuja	2009-10-12
12	RUST	4.801836	6.97852	46.6	Port Harcourt	2009-10-05
13	ULAG	6.517327	3.39762	45.5	Lagos	2009-10-05
14	UNEC	6.424806	7.50499	255.4	Enugu	2009-10-05

Source: Author

3.2 Materials

3.2.1 NIGNET CORS Data

The Office of Surveyor General of Federation (OSGOF) manages the NIGNET CORS that provide (GNSS) data. GNSS data collected at the CORS sites are available for download via file transfer protocol. The GNSS data collected are observation data in Receiver Independent Exchange (RINEX) format that has been compressed. RINEX files are text files that list, in text form, the L1 and L2 carrier phase and pseudocode path lengths to each satellite in view, sampled every 30 seconds. The GNSS observed

data for January 01, 2010 to June 30, 2014 were obtained from the NIGNET server. Table 3.2 provides summary of the NIGNET CORS RINEX observation data used in the study.

Table 3.2: Summary of NIGNET CORS RINEX observation data used in the study

YEAR / Station ID	2010	2011	2012	2013	2014	Total
ABUZ	283	365	364	350	87	**1,449**
BKFP	269	364	364	333	125	**1,455**
CGGT	246	264	27	112	-	**649**
CLBR	-	34	224	300	109	**667**
FPNO	-	-	84	76	9	**169**
FUTA	-	-	10	163	-	**173**
FUTY	325	352	327	318	-	**1,322**
GEMB	174	-	57	65	-	**296**
HUKP	-	-	27	160	122	**309**
MDGR	-	260	-	-8	62	**330**
OSGF	203	298	370	328	68	**1,267**
RUST	254	197	45	45	-	**541**
ULAG	207	299	363	291	-	**1,160**
UNEC	269	360	361	363	144	**1,497**
Total	**2,230**	**2,793**	**2,623**	**2,912**	**726**	**11,284**

Source: Author

The values in the table represent the number of days at each station in each year for which observations were made and the observed data archived. At ABUZ station for example, 283 days (corresponding to 283 RINEX observation files) data were available in the year 2010. 365, 364, 350, and 87 days RINEX data were available for the years; 2011, 2012, 2013 and 2014 respective. A total of 1,449 days data were considered for ABUZ station. A total of 11,284 RINEX observation files from the NIGNET CORS were used in the study.

3.2.2 Differential Code Biases (DCBs) for satellites and receivers

The differential code bias (DCB) is the differential hardware (e.g., the satellite or receiver) delay that occurs between two different observations obtained at the same or two different frequencies. The International GNSS Service (IGS) Analysis Centres have routinely provided DCB estimates for GNSS satellites and ground receivers.

DCB values on a monthly basis using the global IGS network provided by the Centre for Orbit Determination in Europe (CODE) headed by the University of Bern, Switzerland, were used in the study. The DCB files were downloaded for each month of the period under study (January 2010 to June 2014). Table 3.3 provides a summary of the DCB data used in the study.

Table 3.3: Summary of Differential Code Bias (DCBs) used in the Dissertation

DCB Data Type	Year	Number of monthly data
P1-C1	2010	12
	2011	12
	2012	12
	2013	12
	2014 (Jan-June)	6
P1-P2	2010	12
	2011	12
	2012	12
	2013	12
	2014 (Jan-June)	6
	Total	**108**

Source: Author

3.2.3 Global Ionospheric Maps (GIMs)

All IGS Global Ionospheric Maps are in IONEX format containing 13 VTEC maps per day at two hours temporal resolution. The first map refers to 00:00 UT, the last map to 24:00 UT (instead of 01:00 and 23:00 UT, respectively). Thus, a total of 4745 (13 x 365) GIMs were used for the years 2010, 2011, and 2013. The year 2012 was a leap year having 366 days. Thus, 4758 (366 x 13) GIMs were used for the year 2012. In the year 2014, the time period from January to June was considered (181 days) and

therefore, 2353 GIMs were used for the year 2014. A total of 21346 GIMs, from January 2010 to June 2014, generated on a daily basis at CODE using data from over 200 GPS/GLONASS sites of the IGS and other institutions were used in the study to evaluate the TEC over NIGNET from a global perspective. Table 3.4 provides summary of the Global Ionospheric Maps used in the study.

Table 3.4: Summary of IGS Global Ionospheric Maps used in the study

Year	**No. of GIMs data used**
2010	4745
2011	4745
2012	4758
2013	4745
2014	2353
Total	**21346**

Source: Author

3.2.4 Solar indices

Two solar indices were considered in the study for correlation with the TEC over the NIGNET. These include; daily sunspot number and f10.7 solar indices. The daily sunspot number (SSN) provides the longest record of solar activity (available since 1818). It constitutes the main reference solar index, representing the recurrence of intense magnetic loops visible on the Sun's surface. Presently, the derived International SSN is distributed by the Solar Influences Data Centre (Vanlomme *et al*. 2005). This index is based on a statistical processing of the data from a worldwide network of 86 observatories from 29 countries (Clette *et al*. 2007). The F10.7 solar flux is the integrated emission from the solar disc at 2800 MHz (10.7 cm wavelength called F10.7) which has been recorded routinely since 1947 (Covington 1969). The F10.7 is expressed in Solar Flux Units (1 SFU = 10^{-22} Wm^{-2} Hz^{-1}).

3.2.5 Software

1. crx2rnx Hatanaka to RINEX conversion program
2. GPS-TEC analysis application Developed by Dr. Gopi Krishna Seemala of Institute for Scientific Research, Boston College, USA.
3. Java Development Kit , version 1.6.0 update 14
4. MATLAB R2012b (8.0.0.783)
5. Programmers notepad
6. RTKLIB version 2.4.2, an open source program package for standard and precise positioning with GNSS. The RTKGET implementation of the RTKLIB was used to stream the IGS precise GNSS products; satellite orbit and clock information data.
7. SigmaPlot Version 11.0, Build 11.0.0.77
8. Scripter Version 5.0.848.488, program for developing and running scripts.
9. Golden Software Surfer Version 11.2.848

3.3 Methodology

3.3.1 Data Acquisition

Archived daily RINEX GNSS observation data from operational NIGNET CORS in the months and years under study were filed via file transfer protocol (ftp) from the NIGNET server (http://server.nignet.net/, last accesed September 27, 2014). The RINEX observation files were then un-compressed, and structured using crx2rnx Hatanaka to RINEX conversion program which converts the observation data from ".D" extension to ".O" ready for the TEC processing. Satellite RINEX navigation data from website (ftp://cddis.gsfc.nasa.gov/pub/gps/data/daily, last accesed September 27, 2014) and Differential Code Biases (DCBs) data for Satellites and Receivers from IGS

obtained from website (ftp://ftp.unibe.ch/aiub/CODE, last accesed September 27, 2014) were also collected using the RTKGET automatic FTP script. The geomagnetic and solar indices were obtained from SPDF OMNIWeb Plus service (http://omniweb.gsfc.nasa.gov.html, last accesed September 27, 2014).

3.3.2 TEC evaluation from NIGNET CORS data

The TEC processing for the NIGNET stations was carried out using the available observation data, satellite navigation data and the Differential Code Bias files for each day in the months and years considered in the dissertation by means of the GOPI GPS TEC processing software (Gopi, 2012). Custom computer programs written in Java high level programming language were then used for the batch processing of the GOPI software output to compute the diurnal TEC values.

3.3.3 TEC from IGS GIMs over Nigeria, interpolation and visualisation

Global Navigation Satellite Systems TEC maps are representative of the TEC values at grid points over the whole globe determined from GNSS observations. They are obtained from GPS/GLONASS data mainly from the IGS stations. The ionosphere is treated in these maps as a thin spherical shell at a specified height (usually 400 or 450 km). The spatial resolution of these maps is 2.5 degree in latitude and 5 degree in longitude, and their time resolution is 2 hours. Each daily file includes 13 ionosphere maps, starting from 0:00 to 24:00 hours, thus each map covers a 2 hours period. The GIM files used in this dissertation were obtained from CODE (Center for Orbit Determination in Europe) located at the University of Berne, Swizerland via file transfer protocol (ftp://ftp.unibe.ch/aiub/CODE, last accesed September 27, 2014). GIM is

utilized mainly to compute the VTEC at the NIGNET stations for comparison, validation and analyses with that computed from the NIGNET CORS.

Interpolation algorithms estimate the value at a given location as a weighted sum of data values at surrounding locations, with weights assigned according to functions that give a decreasing weight with increasing separation distance. In order to process the interpolation in Surfer (version 11; Golden Software), the TEC values and their corresponding time parameters and coordinates (longitude and latitude) were read from the GIMs IONEX files and transformed into XYZ arrays corresponding to longitude and latitude, and TEC using written custom batch processing JAVA programs. The program outputs were then imported into Surfer. Once all the epochs were imported into Surfer, TEC grid data covering the entire country were generated using Kriging interpolation algorithm.

Kriging is an estimation and interpolation method applied in geostatistics, which uses known sample values and a variogram to determine the unknown values at different locations/times. It utilizes the spatial and temporal correlation properties of the underlying phenomenon, and incorporates the measures of the error and uncertainty when determining the estimates (Webster and Oliver, 2001; Stanislawska *et al.*, 1999 and 2002). At each location Kriging produces an estimate and a confidence bound on the estimate, i.e., the Kriging variance. The uncertainty maps associated with Kriging appear to naturally account for insufficient sampling. Blanch (2002) demonstrated that Kriging could successfully mitigate the under-sampled problem due to sparse data points.

In order to evaluate the GIM TEC over each of the NIGNET CORS, a script (GridInterpolate.bas) written in scripter syntax was used to interpolate the TEC over each NIGNET station. The script returns the Z values from the grid at the XY locations

specified in the data file. Surfer was used for calculating interpolation statistics visualization. Figure 3-2 shows the GIM grid points covering the positions of the NIGNET CORS at which the GIM TEC values were interpolated.



Figure 3-2: GIM grid points covering the NIGNET CORS

Source: (Author)

3.3.4 Seasonal grouping

In order to study the seasonal variability of TEC over the NIGNET CORS, the derived TEC values were grouped into four seasons similar to (Mendes, *et al.*, 2004; Liu *et al.*, 2009; Chauhan *et al.*, 2011; and Fayose *et al.*, 2012). The seasons are:

i. March Equinox (February, March, April),

ii. June Solstice (May, June, July),

iii. September Equinox (August, September, October),

iv. December Solstice (November, December, January).

3.3.5 TEC validation and analyses

Using MATLAB, Microsoft Excel, and SigmaPlot plotting package, the correlation coefficients between the NIGNET and GIM TECs were computed and various TEC plots were produced to study the diurnal, spatial and temporal variations of TEC over the NIGNET in the months and years considered in the study. Figure 3-3 shows the flow chart of the applied methodology.

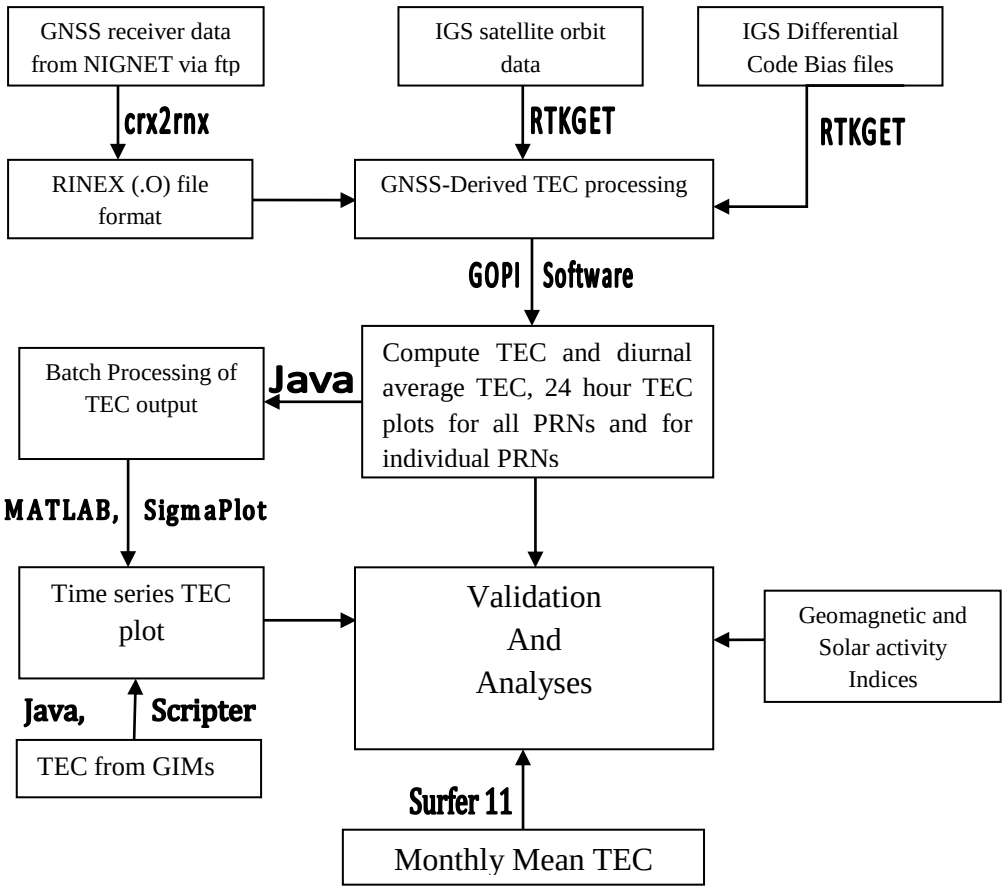


Figure 3-3: Flow chart of the TEC Evaluation and Analyses methodology
Source: Author

Analysis to study the TEC variation for geomagnetically quiet and disturbed days in the months and years under study and also for three classes (G1, G2, and G3) of geomagnetic storms that occurred during the study period was carried out by considering the TEC behaviour before, during and after the storm. Similar analysis was done to study the TEC behaviour of each station during the solar eclipse of November

03, 2013 observed from different locations in Nigeria. The local circumstances of the eclipse at some cities in Nigeria are shown in Table 3.5. Further analysis was carried out to determine the correlation of ionospheric TEC with solar activity using the daily sunspot number and f.10.7 solar indices as proxy for solar activity.

Table 3.5: Local Circumstances of the solar eclipse of November, 03, 2013

	City	Abuja	Ibadan	Kano	Lagos
	Lon.	7°19'00" E	3°55'00" E	8°31'00" E	3°20'00" E
	Lat.	9°06'00" N	7°24'00" N	12°01'00" N	6°26'00" N
	Max. Obscuration	66.05%	72.89%	56.08%	76.56%
Phenomenon	Eclipse begins (UT)	12:01:20.8	11:50:00.5	12:05:22.5	11:48:22.6
	Max. Magnitude	0.727793	0.782736	0.645811	0.812046
	Max. Magnitude (UT)	13:38:47.6	13:31:02.6	13:39:07.6	13:30:17.2
	Eclipse ends	15:02:59.0	14:59:43.6	15:00:15.5	14:59:56.2
	Eclipse duration	03:01:38	03:09:43	02:54:53	03:11:34
	City	Maiduguri	PH	Zaria	Ilorin
	Long.	13°08'00" E	7°01'00" E	7°43'00" E	4°34'00" E
	Lat.	11°50'00" N	4°46'00" N	11°07'00" N	8°30'00" N
	Max. Obscuration	56.83%	81.63%	59.14%	68.79%
Phenomenon	Eclipse begins (UT)	12:20:29.1	12:01:43.6	12:02:35.2	11:51:56.4
	Max. Magnitude	0.652263	0.852386	0.671240	0.749878
	Max. Magnitude (UT)	13:50:21.3	13:41:46.9	13:37:55.4	13:31:50.2
	Eclipse ends	15:07:03.2	15:07:45.2	15:00:31.0	14:59:20.5
	Eclipse duration	02:46:34	03:06:02	02:57:56	03:07:24

(Source: HM Nautical Almanac Office, http://astro.ukho.gov.uk/eclipse, last accessed July 23, 2014)

CHAPTER FOUR

RESULTS AND DISCUSSION

4.1 Diurnal, Seasonal and Spatial Variations of TEC over the NIGNET CORS

Ionospheric irregularities present large day-to-day variabilities and they depend on local time, season, solar cycle activity and magnetic activity. Thus, the results here are presented based on these dependencies.

4.1.1 Diurnal TEC Variation over NIGNET

Figure (4-1) shows the mean diurnal TEC profile over the NIGNET. The diurnal TEC profile at various epochs deduced from the NIGNET CORS observation data and from the Global Ionospheric Maps at each NIGNET station are shown in Figure (4-2) and (4-3) respectively.

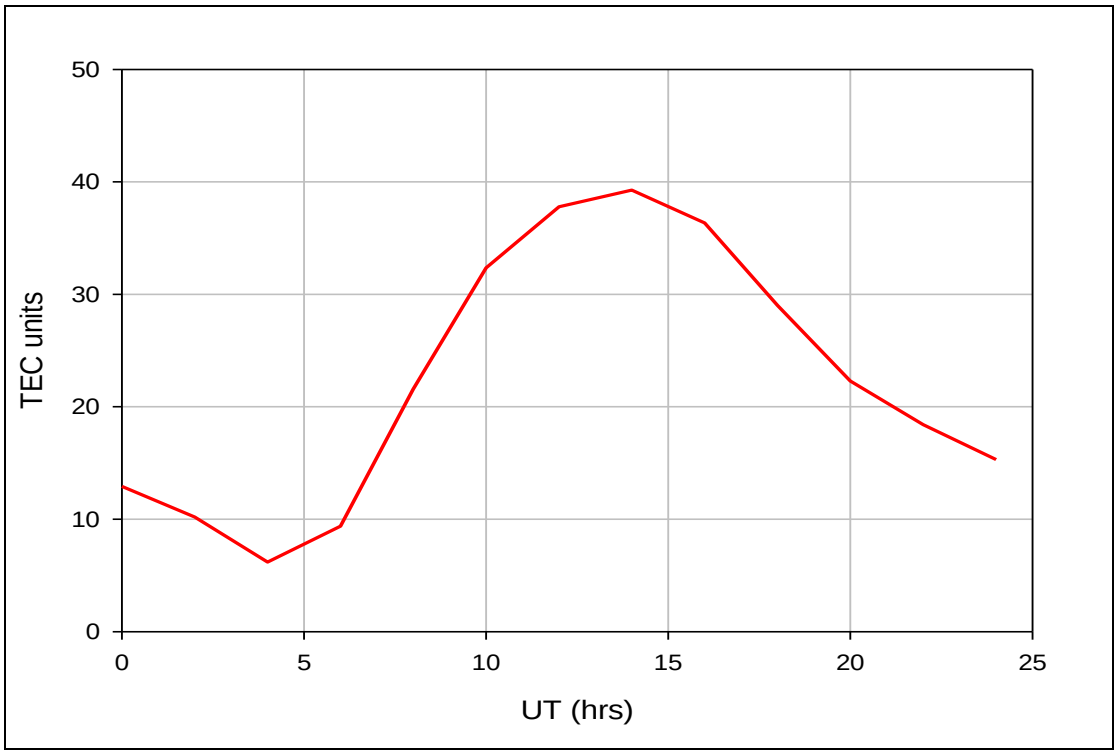
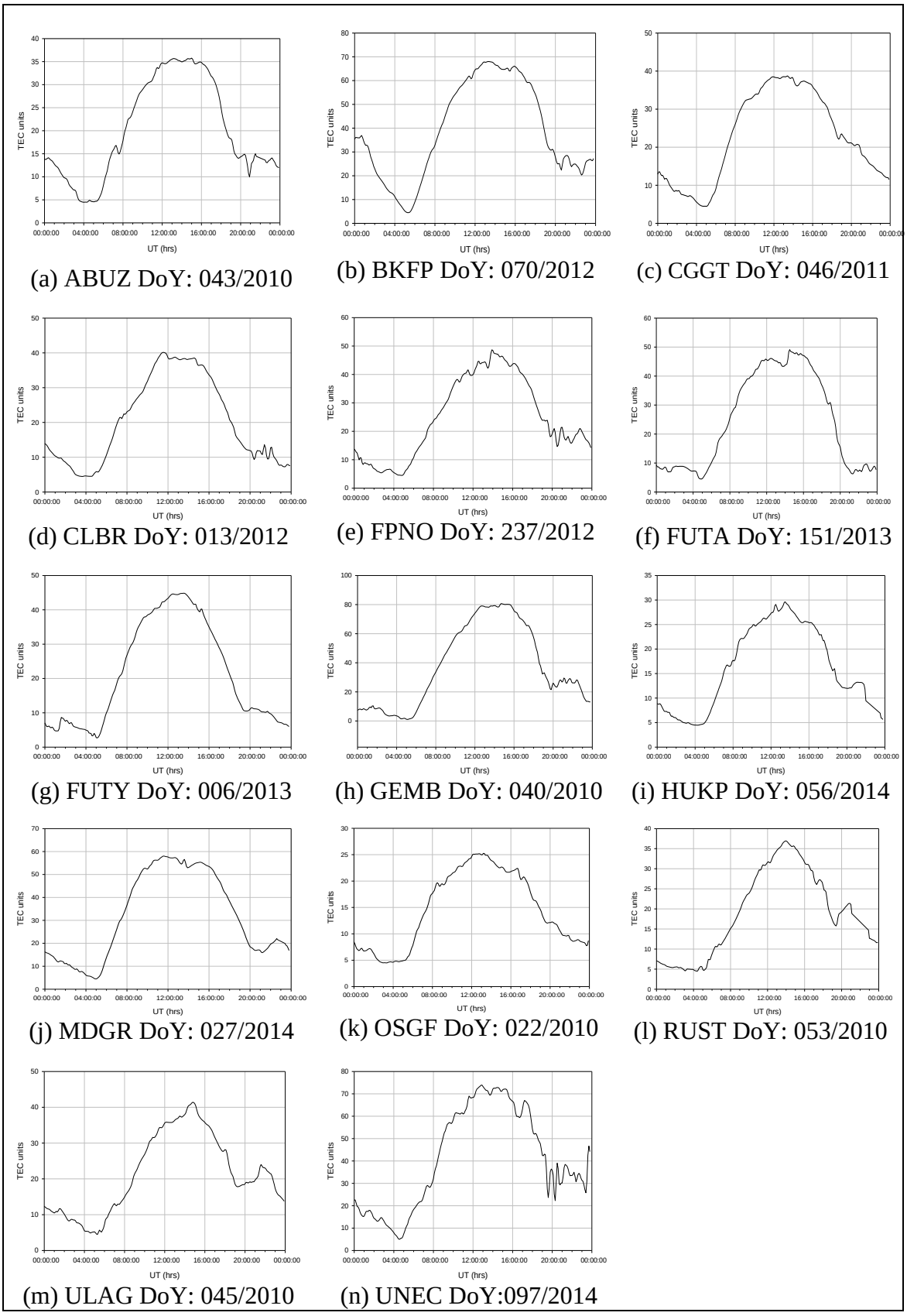


Figure 4-1: Mean diurnal TEC profile over the NIGNET



(a) ABUZ DoY: 043/2010 (b) BKFP DoY: 070/2012 (c) CGGT DoY: 046/2011

(d) CLBR DoY: 013/2012 (e) FPNO DoY: 237/2012 (f) FUTA DoY: 151/2013

(g) FUTY DoY: 006/2013 (h) GEMB DoY: 040/2010 (i) HUKP DoY: 056/2014

(j) MDGR DoY: 027/2014 (k) OSGF DoY: 022/2010 (l) RUST DoY: 053/2010

(m) ULAG DoY: 045/2010 (n) UNEC DoY:097/2014

Figure 4-2: Diurnal TEC variation over NIGNET deduced from the NIGNET CORS data

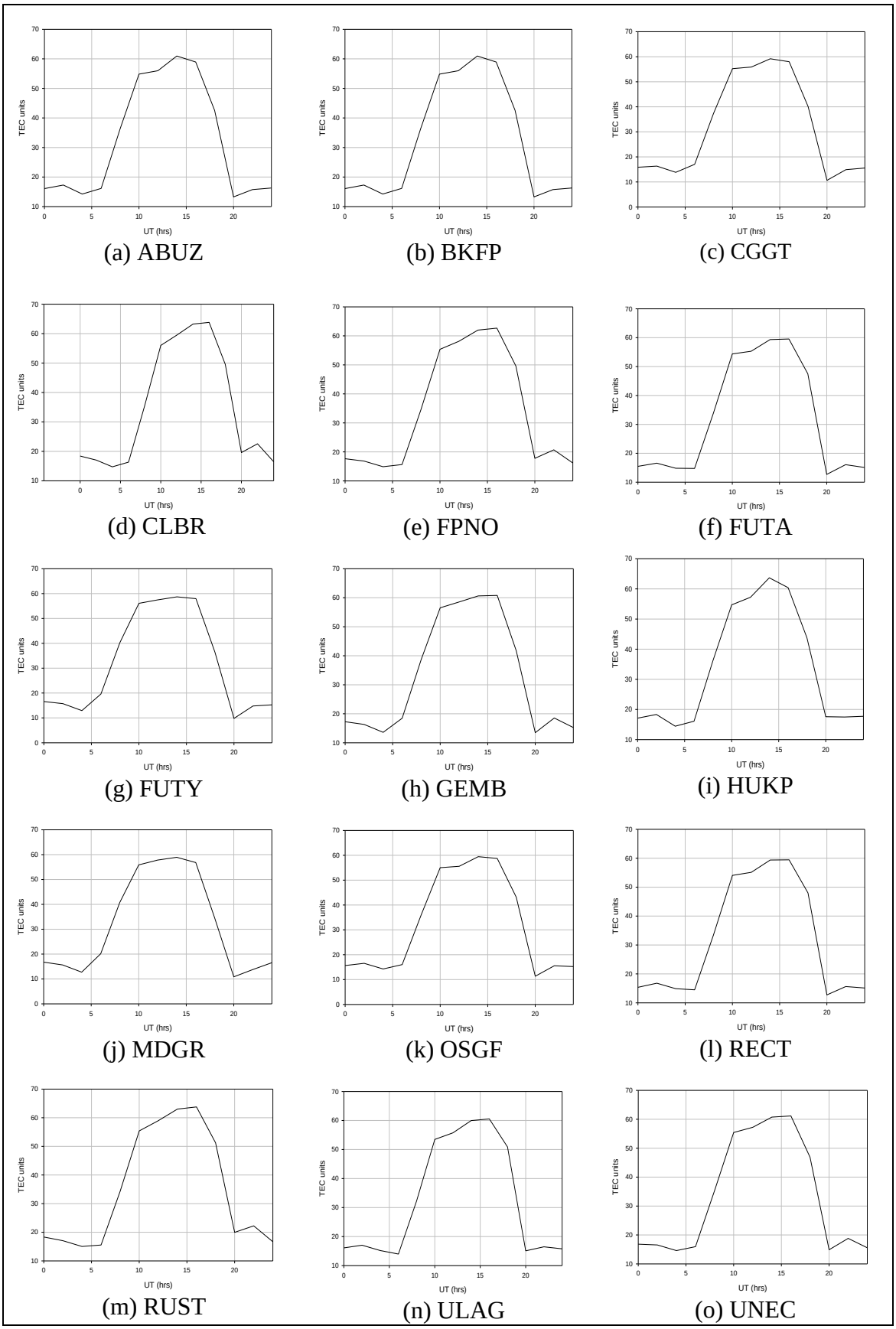


Figure 4-3: Diurnal TEC variation over NIGNET deduced from the Global Ionospheric Maps for March 06 2012, DoY: 066

The diurnal ionospheric TEC variation as observed from both data sources considered (the NIGNET CORS data and from the GIMs) showed good agreement. The results showed a gradual decline in the diurnal TEC between 00:00 hours (midnight) and 04:00 hours. The TEC declines by 20-23% between the hours of 00:00 and 02:00, and further declines by 37-40% between the hours of 02:00 and 04:00, with a minimum value occuring between the hours of 03:00 and 04:00. The TEC begins to rise gradually between the hours of 04:00 and 14:00, with the daytime peak occuring at slightly different times between past local noon and 14:00 hours at each station. At this time, the TEC has increased by above 100% its value at midnight. After this time, the TEC begins a gradual decrease till midnight. From the diurnal TEC profile, it was observed that the TEC has lower values between past midnight and 06:00, and between 18:00 and before midnight. Higher TEC values occur during the day time between 06:00 and 18:00 hours.The results confirmed the measurements reported by Gupta and Singh, 2000, for data over Delhi; Mendes *et al*., 2004, for observations over Brazil; Huang and Roussel-Dupre, 2005 for observations over Mexico; Huo *et al*., 2005, based on GPS data in China; Rama Rao *et al., 2006,* and Prasad *et al*., 2012, for measurements from the Indian GPS network of receivers; Chauhan *et al*., 2011 at a Single station in Agra, India; Fayose *et al.,* 2012, over Akure, Nigeria; Siqueira *et al.,* 2011, over South America; and Zakharenkova *et al.*, 2013, over Japan.

4.1.2 Annual TEC Time Series and Seasonal TEC Variation over NIGNET

The colour coding represents the TEC obtained using the NIGNET CORS observed data, shown in red. The corresponding TEC computed from IGS Global Ionospheric Maps are shown in blue (Figure 4-4). The red and blue horizontal solid lines in the plots show the corresponding mean values for the NIGNET and GIM annual TEC series

respectively. The vertical axis represents the total electron in TEC units (TECU), and the horizontal axis corresponds to time in days. Figure 4-4 shows the annual TEC time series at ABUZ NIGNET station. The annual TEC time series for each of the NIGNET stations are presented in Appendix I.

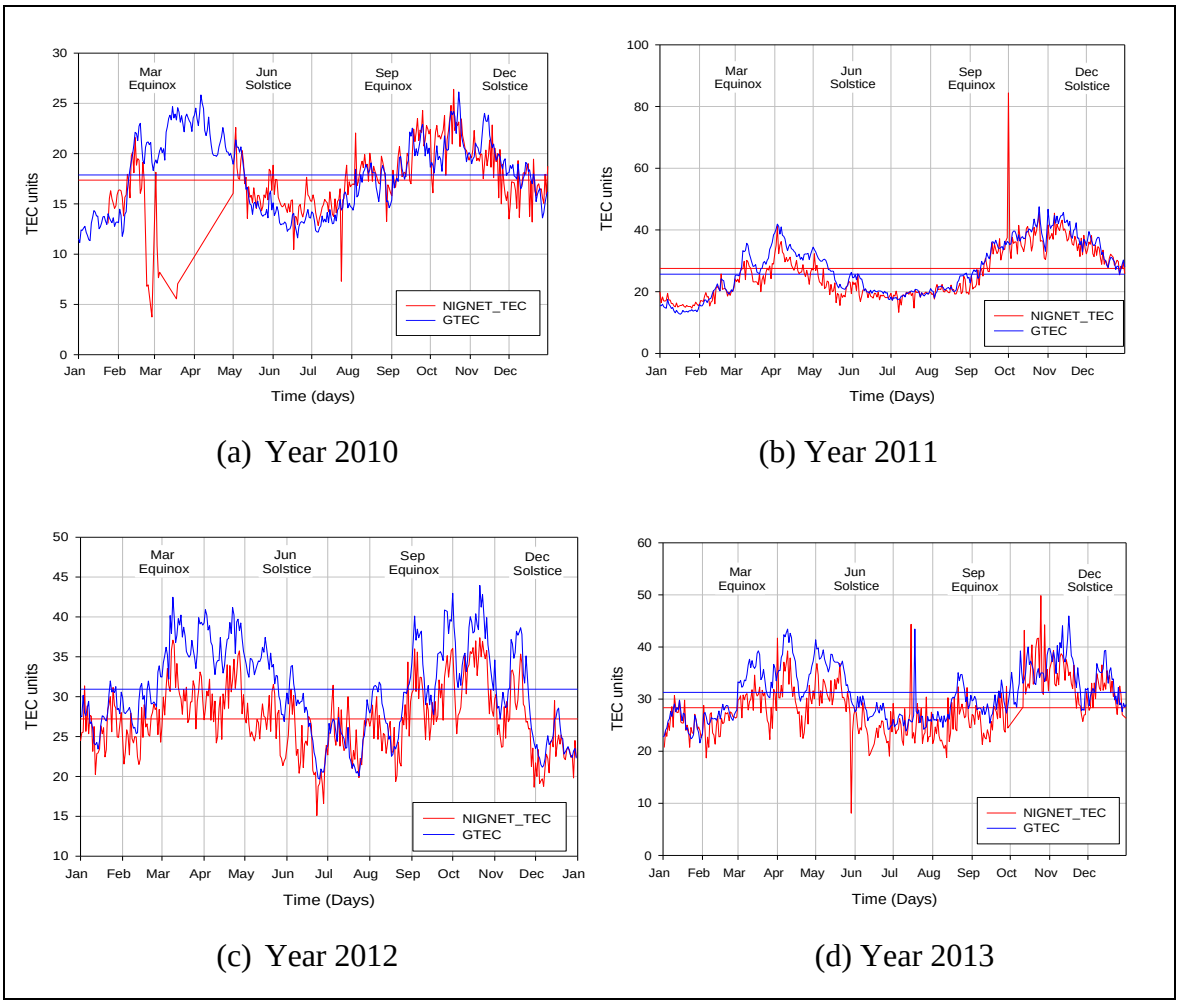


Figure 4-4: Annual TEC Time Series at ABUZ station 2010-2013

The study of seasonal dependence of TEC data was carried out. The results of seasonal dependence of TEC showed similar seasonal variation of TEC over each station and in each year considered. Also, there is a broad agreement within the experimental errors in the seasonal TEC variability between the measurements results obtained from the NIGNET data (NIGNET_TEC) and the GIM (GTEC). However, due to inconsistent and lots of missing data from the NIGNET CORS as a result of technical problems, power

failure and cycle slips due to loss of tracking signal, large deviations between the NIGNET_TEC and GTEC were observed in some days, see Figures 4-4(a), (b).

In order to examine the seasonal variation of ionospheric TEC over the NIGNET, the NIGNET annual TEC time series for 2010-2014 is shown in Figure 4-5, while four years mean annual TEC time series for the NIGNET is shown in Figure 4-6.

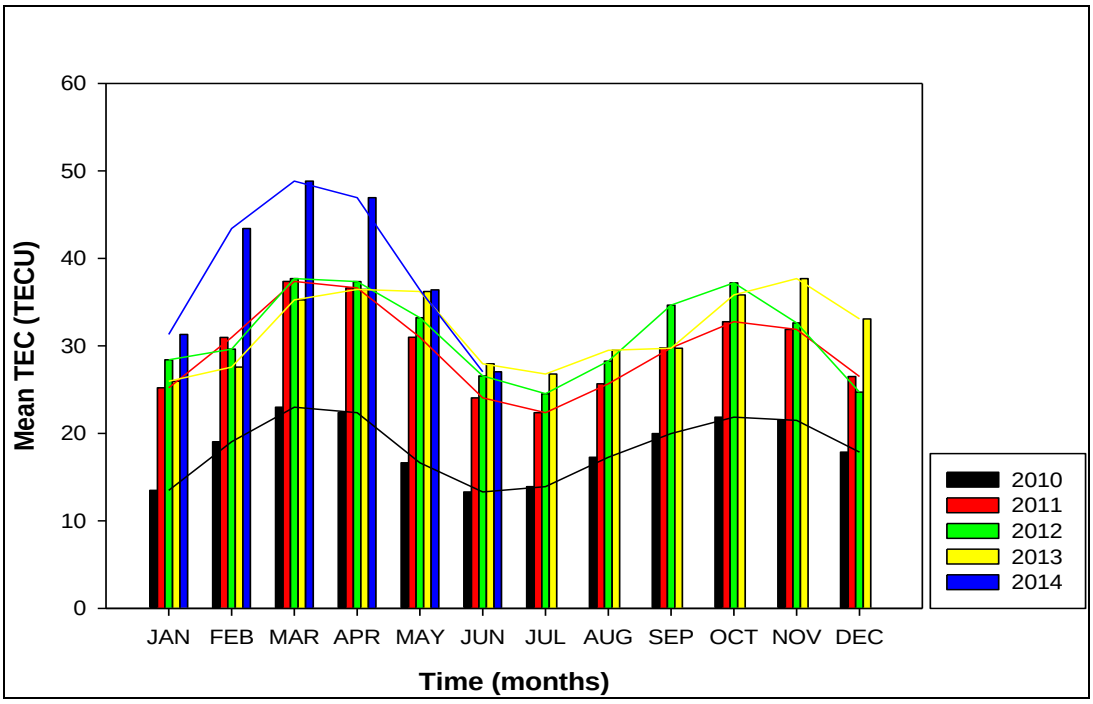


Figure 4-5: NIGNET annual TEC time series for 2010-2014

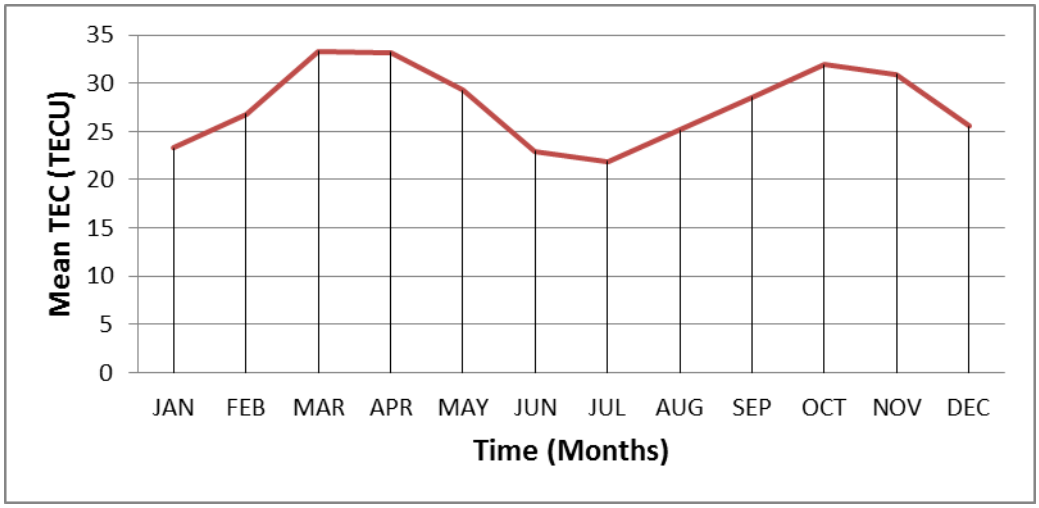


Figure 4-6: Mean annual TEC time series for the NIGNET

The NIGNET annual TEC time series for 2010-2014 (Figure 4-6) shows that the ionospheric TEC is on the rise between year 2010 and year 2014, having 50-55% rise between year 2010 and 2011, 12-13% rise between 2011 and 2012, 1-2% rise between 2012 and 2013, and 22-25% rise between year 2013 and 2014.

Thus, the TEC profile over NIGNET is characterised by two minima occurring within December to January, and June to July, and two maxima occurring within March to April, and October to November yearly. The results are consistent with earlier observations reported by Gupta *et al.*, 2000*;* Mendes *et al*., 2004; Huang and Roussel-Dupre, 2005; Huo *et al*., 2005; Wu *et al*., 2006; Astafyeva *et al*., 2008; Bagiya *et al*., 2009; Liu *et al*., 2009; Chauhan *et al*., 2011; Prasad *et at.*, 2012.

4.1.3 Spatial Variation TEC over NIGNET

For the purpose of examining the spatial variations of TEC over the NIGNET CORS, monthly TEC means from each station were computed and the corresponding TEC map generated. Figures (4-7) to (4-15) represent the monthly mean TEC map for the relation between the values of TEC with geographic latitude and longitude from January 2010 to June 2014. The maps presented here cover only the extent of the NIGNET CORS, and showing the geographical position of each of the stations. See Appendix II for the values of monthly mean TEC at each of the NIGNET CORS.

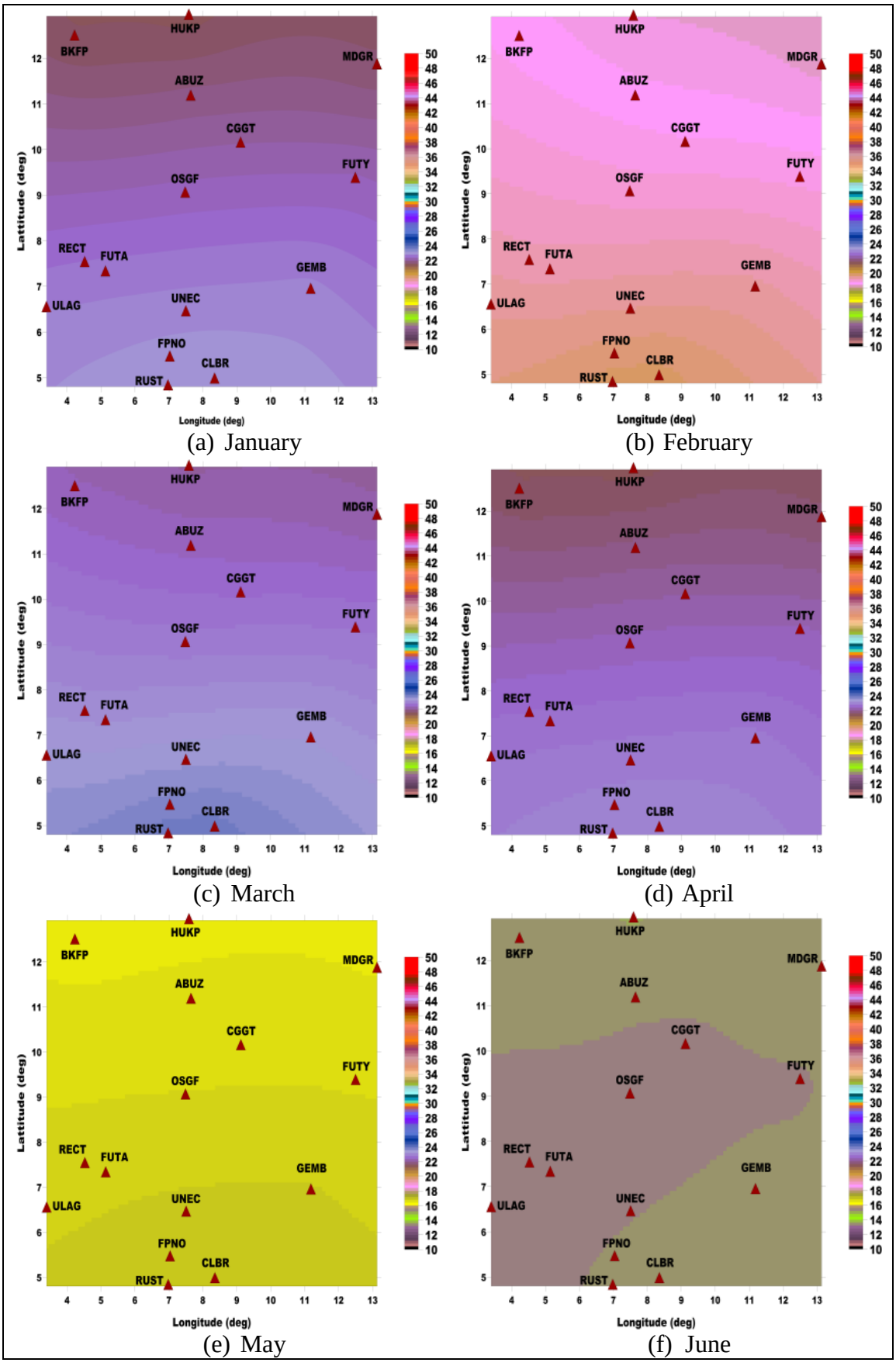


Figure 4-7: Spatial Variation of Monthly Mean TEC over NIGNET Jan – Jun 2010

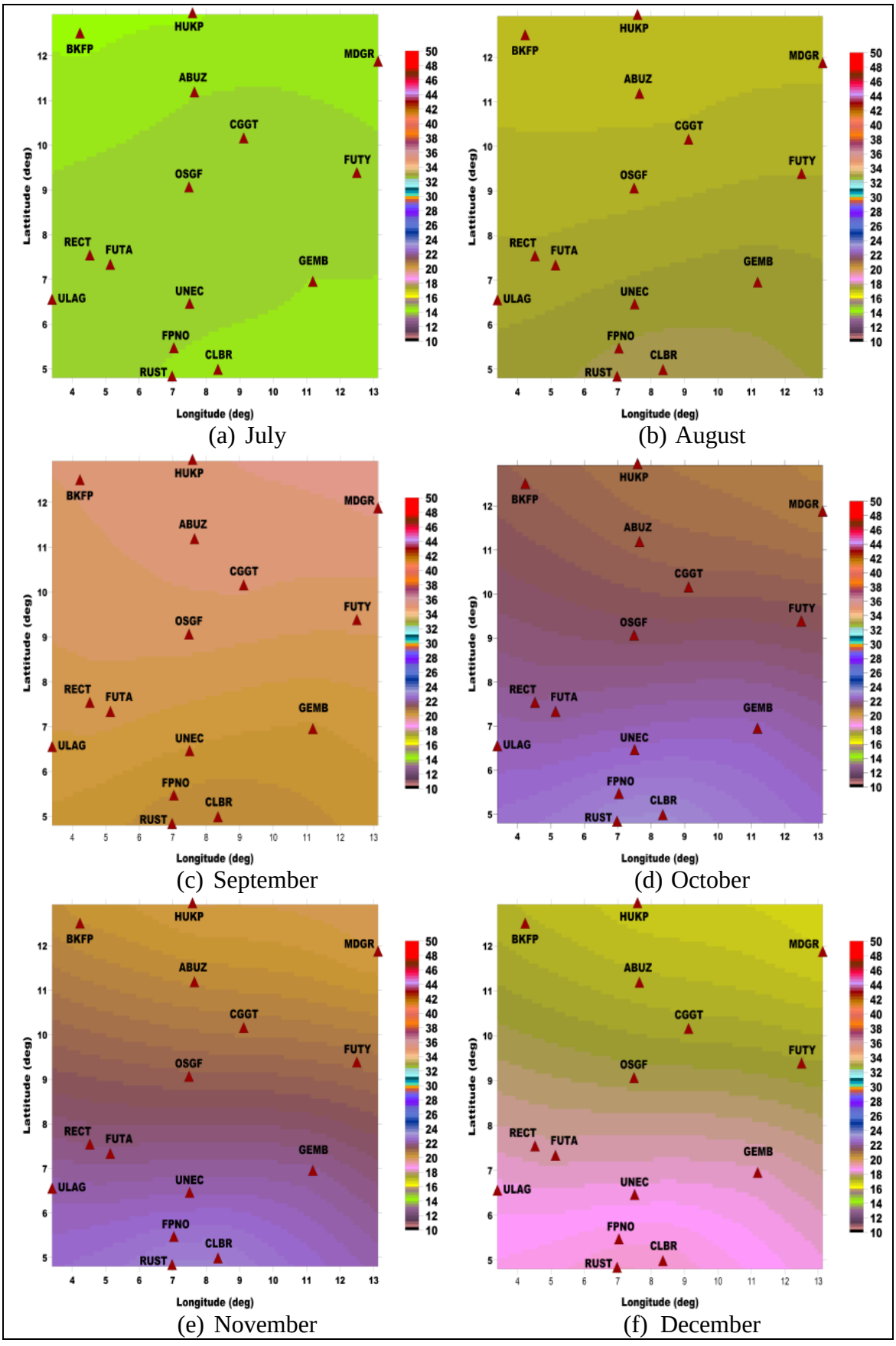


Figure 4-8: Spatial Variation of Monthly Mean TEC over NIGNET Jul – Dec 2010

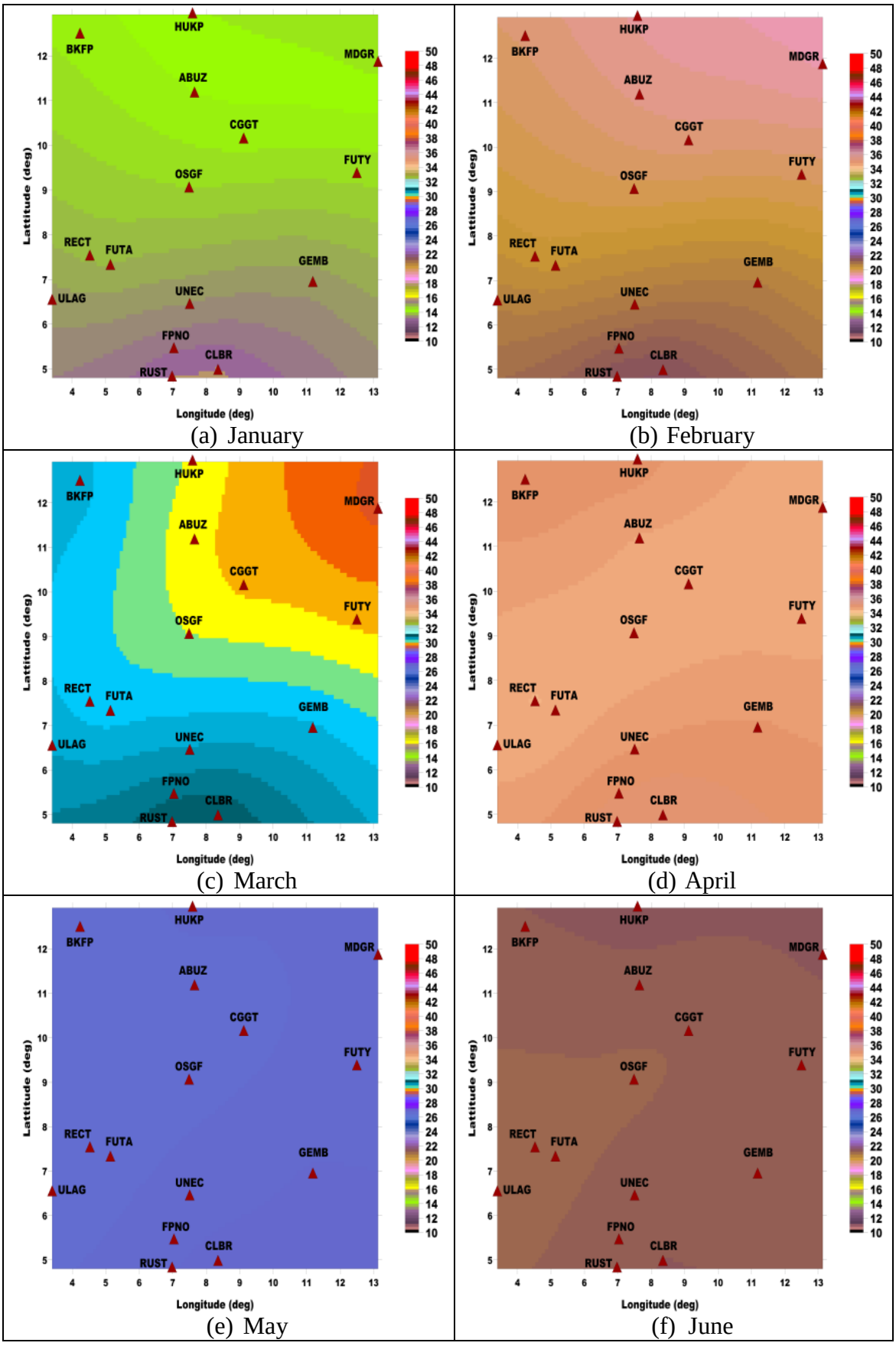


Figure 4-9: Spatial Variation of Monthly Mean TEC over NIGNET Jan – Jun 2011

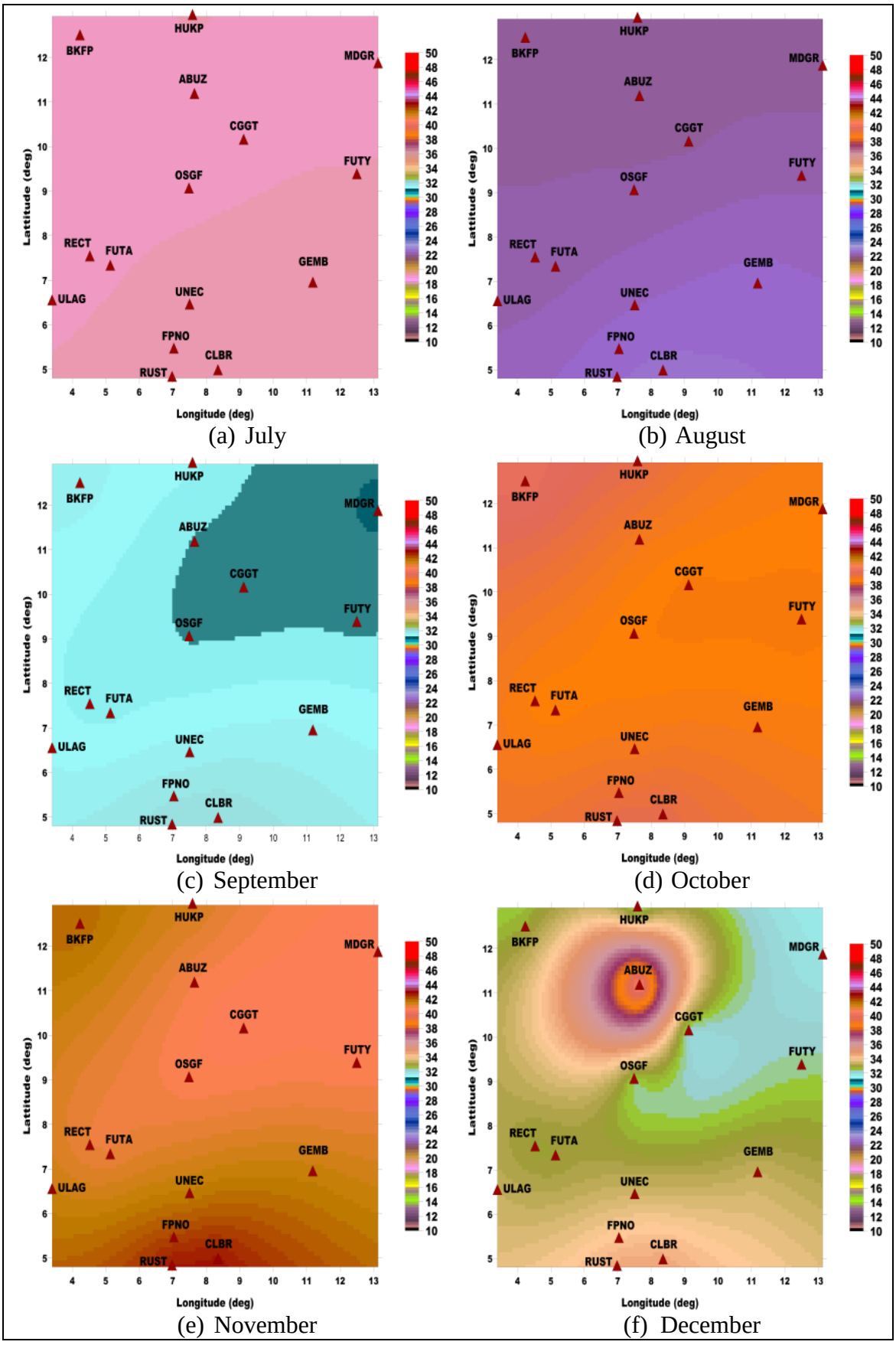


Figure 4-10: Spatial Variation of Monthly Mean TEC over NIGNET Jul – Dec 2011

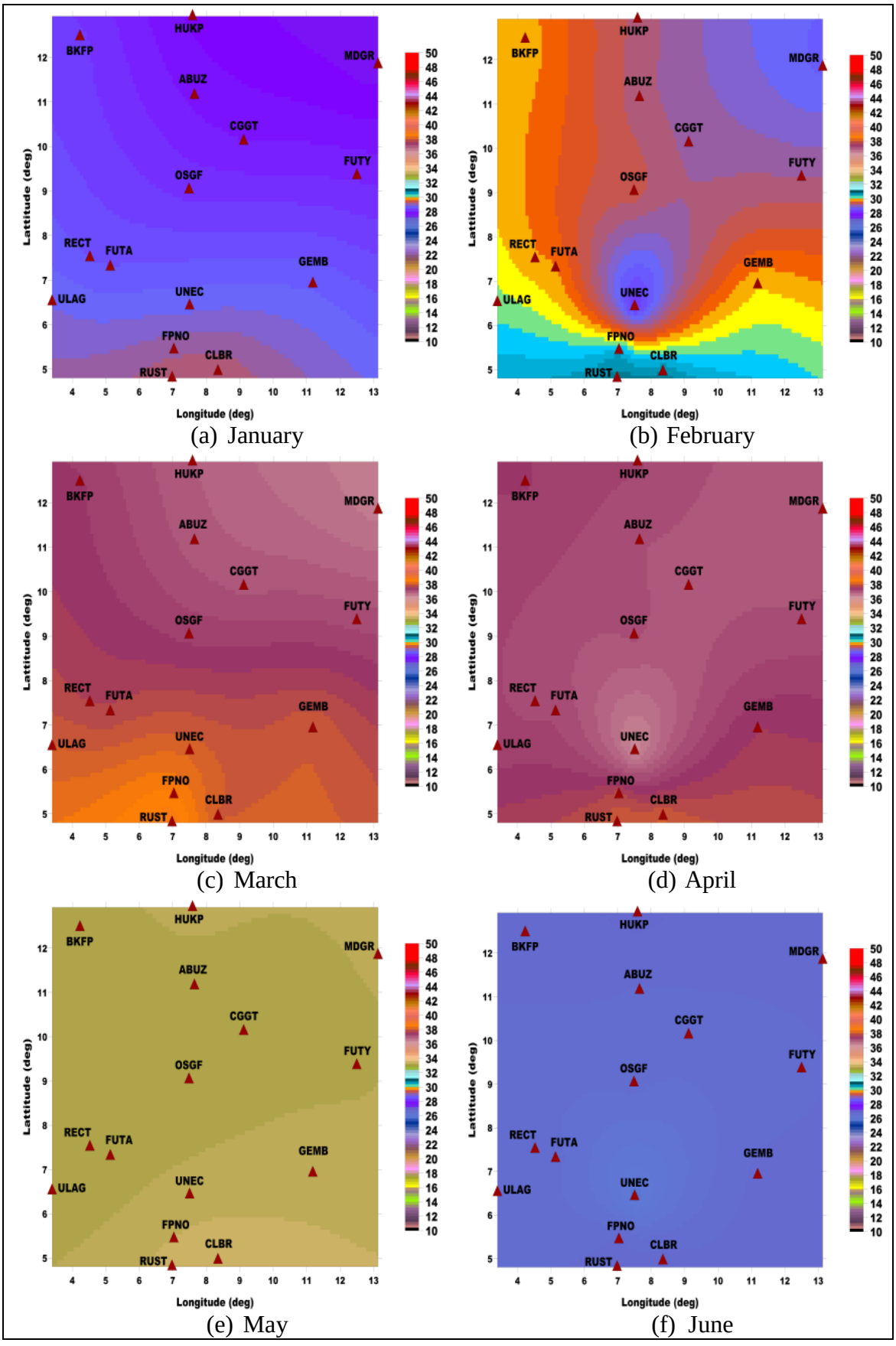


Figure 4-11: Spatial Variation of Monthly Mean TEC over NIGNET Jan – Jun 2012

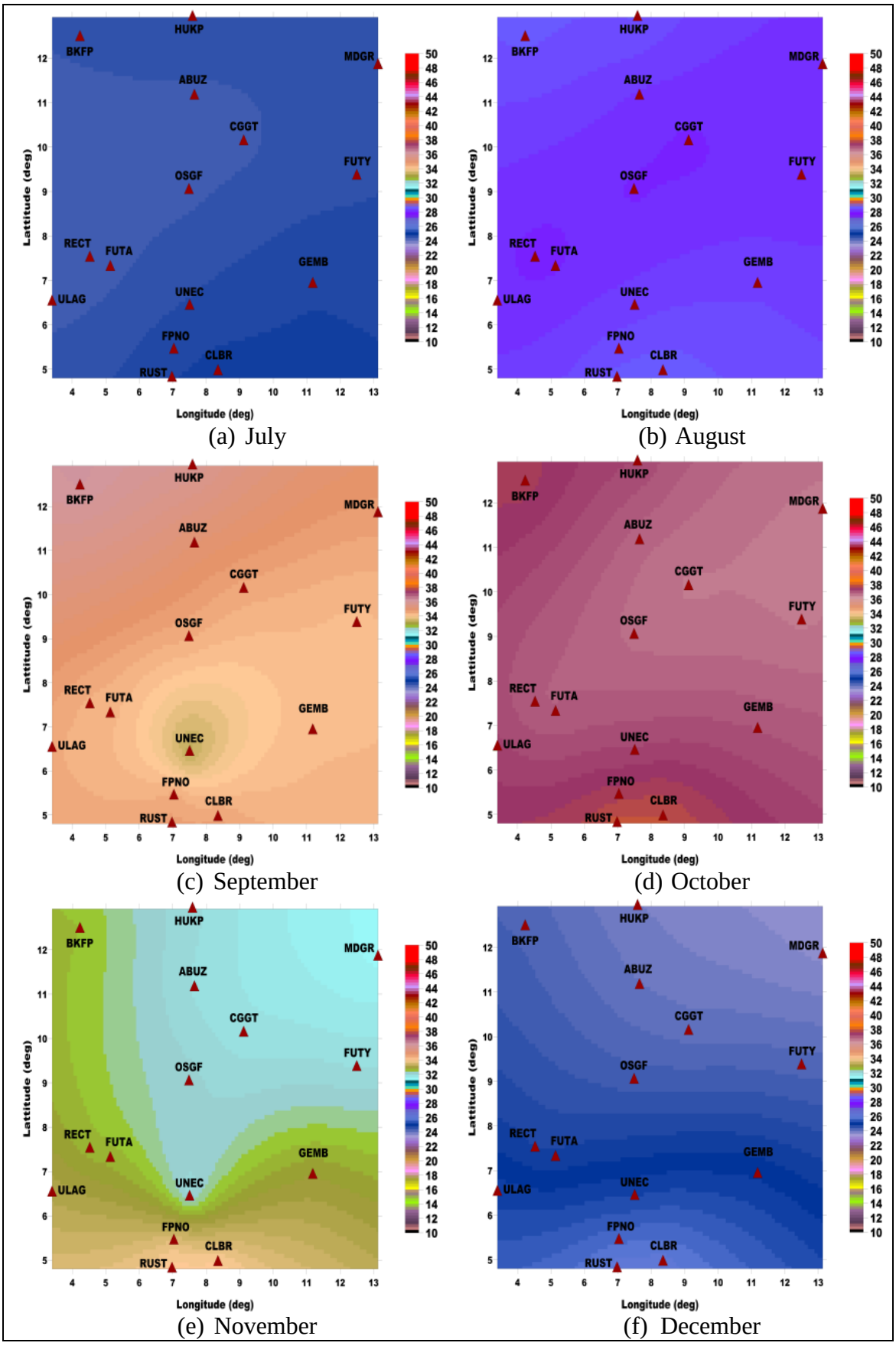


Figure 4-12: Spatial Variation of Monthly Mean TEC over NIGNET Jul – Dec 2012

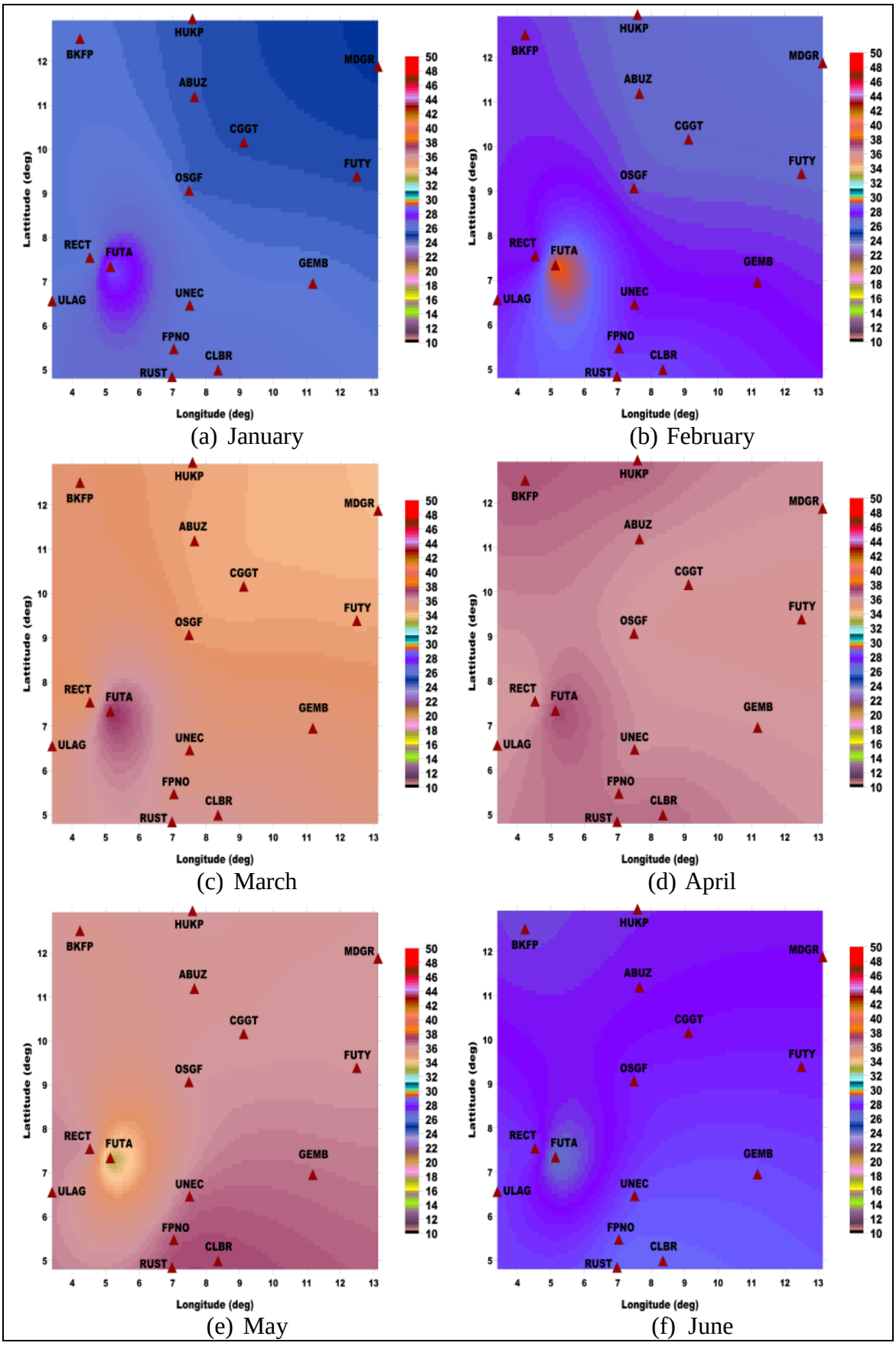


Figure 4-13: Spatial Variation of Monthly Mean TEC over NIGNET Jan – Jun 2013

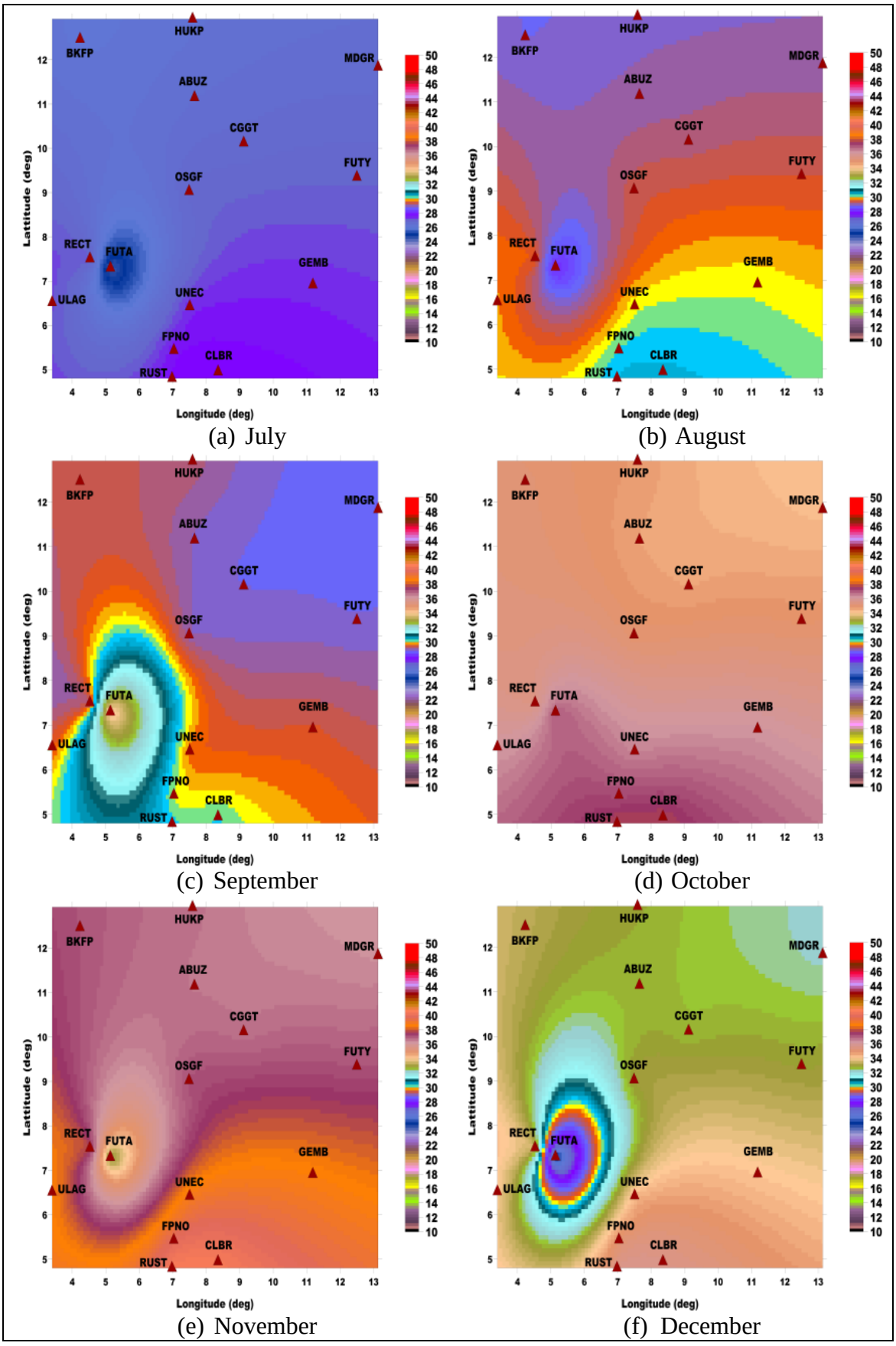


Figure 4-14: Spatial Variation of Monthly Mean TEC over NIGNET Jul – Dec 2013

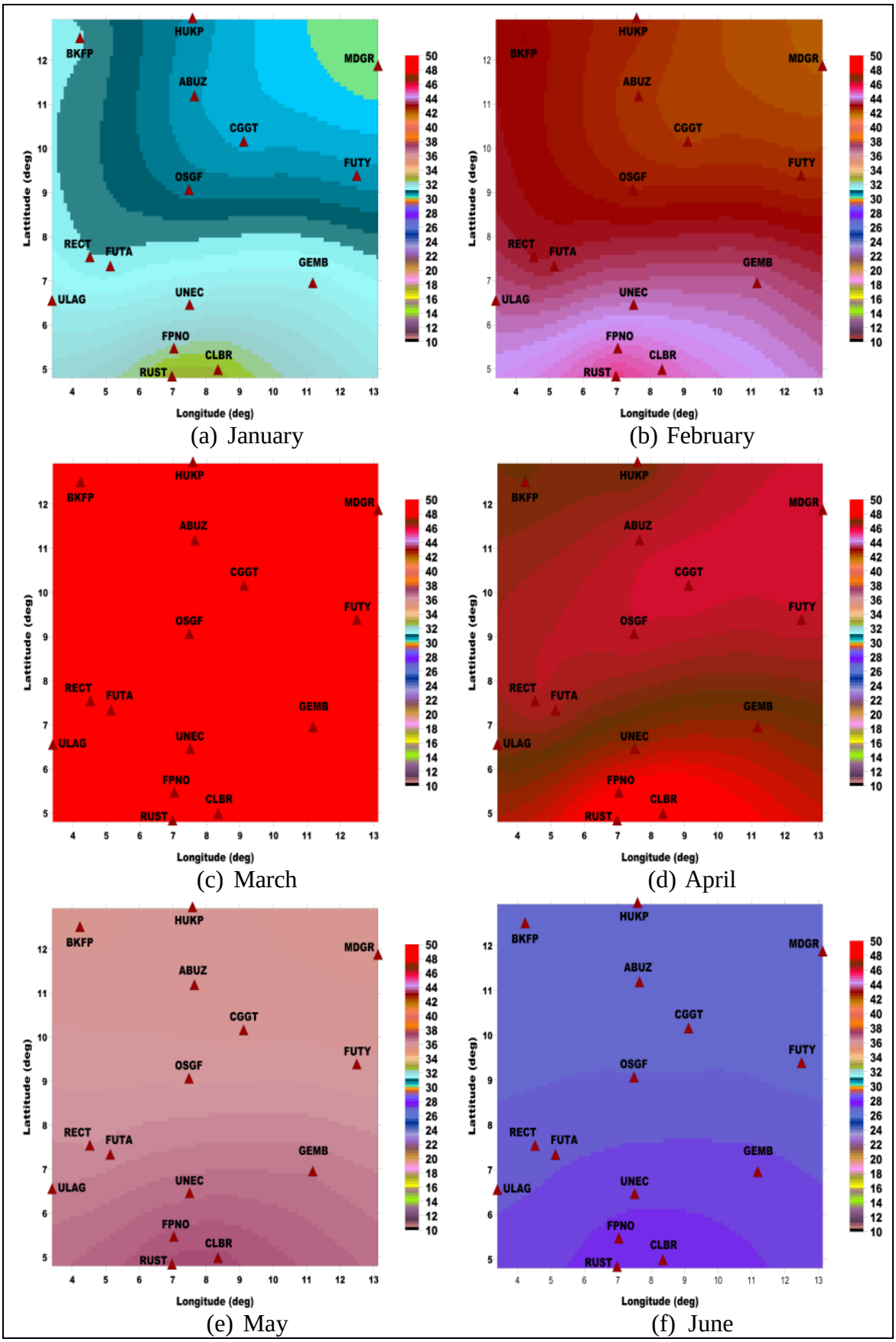


Figure 4-15: Spatial Variation of Monthly Mean TEC over NIGNET Jan - Jun 2014

Due to the irregular nature and variable effect of solar and geomagnetic activities at different geographical locations, deviations from the above results were observed in some months within the study period, where some stations tend to exhibit higher or lower monthly mean TEC values compared to the other stations. ABUZ station in December 2011 [Figure 4-10(f)] had higher mean TEC value (40.883 TEC units) compared to the other stations. UNEC station had the lowest mean TEC values in February (28.157 TEC units), April (36.399 TEC units), June (25.77 TEC units), and September (33.303 TEC units), 2012 as observed from Figures 4-11(b), (d), (f) and Figure 4-12(c) respectively. Similar results were observed at FUTA in year 2013. This station had higher monthly mean TEC compared to other stations in the months of January (28.51 TEC units), February (29.788 TEC units), March (37.799 TEC units), April (37.277 TEC units), and in September (34.368 TEC units), 2013, as seen in Figures 4-13(a) to 4-13(d) and 4-14(c) respectively. However, the station exhibited lower monthly mean TEC values compared to other stations, for May to August (33.105, 26.509, 24.392, 28.027 TEC units respectively), November and December (32.688 and 24.792 TEC units respectively), in the year 2013. See Figures 4-13(e) to 4-14(b), 4-14(e) and 4-14(f) respectively. These variabilities are due to sudden rapid ionospheric changes over these stations during these periods.

The results revealed the spatial variation of TEC within the extent of the NIGNET CORS. The TEC is proportional inversely with both longitudes and latitudes. However, the variation of the TEC with latitude is more easily observed from the TEC maps. The TEC values increase from the north to the south of the NIGNET extent, with stations such as CLBR, FPNO and RUST which are closer to the equator having higher TEC values for most period of the year. This presupposes that stations at low latitude and at equatorial region are highly susceptible to ionospheric effect. These results agree well

with studies reported by (Dabas *et al.,* 1984; Komjathy, 1997; Yue *et al.,* 2007; Bagiya *et al*., 2009; Zhang *et al*., 2011; 2012). These longitudinal differences are caused by the difference in magnetic declination which gives rise to upward and downward ion drifts across the zero declination for a given thermospheric zonal wind direction (Wu *et. al,* 2012), thereby resulting to higher effects of geomagnetic activities within the low latitude region. Furthermore, there is larger enhancement in the relative TEC variation that exhibits significant latitudinal variations during March equinox, September equinox and December solstice compared to the June solstice.

4.2 Effect of Geomagnetic Storms and Solar Activities on TEC over NIGNET

GNSS satellites have been used to study the effects of solar disturbances on ionospheric TEC behaviour (Krankowski *et al*., 2005). The ionosphere is the ionized component of Earth's upper atmosphere; it is a complex medium that varies with time and space, it is important to understand the behaviour of the steady state ionosphere for expecting and forecasting disturbances in the ionosphere by studying the magnetic storm effects (Yoshimura *et al.,* 2002).

4.2.1 Relation to Geomagnetic storms (Solar Flares)

On February 15, 2011 sunspot group 1158 produced an X2.2-class solar flare. Dubbed the Valentine's Day solar event by the scientific community, it was the first Solar Cycle 24 flare reaching X class level. In fact, it was the first of its class since December 2006. NOAA issued a R3 (strong) radio blackout alert pertaining this prominent x-ray flux event. In addition to flashing Earth with X and UV radiation, the explosion also hurled a CME in Earth's direction (NASA, 2011, Spaceweather, 2011).

AR1429, rotating toward the other side of the Sun, still generated a M6.3-class flare on March 9, a M8.5 flare one day later and a G2 (moderate) M7.9 flare on March 13. (http://www.space.com/14780-sun-storm-solar-flare-eruption.html, last accessed September 27, 2014; The Watchers, 2012). The active region 1429 erupted a powerful X5.4-class flare at 00:24 UTC the March 7. The related CME impacted the Earth on March 8, causing a G3 (strong) geomagnetic storm. This event marked the second strongest solar flare of Cycle 24 in terms of X-ray flux. NOAA launched a R3 (strong) radio blackout and a S3 (strong) solar radiation storm alerts (Universe Today, 2012).

Table 4.1 shows the details of each of the three solar flares considered in the study.

Table 4.1: Solar Flares of Solar Cycle 24 examined in the study

	Class	**Year**	**Date**	**Sunspot region**	**Radio B.**	**SR Storm**	**CME**	**GM Storm**
1.	X2.2	2011	Feb-15	1158	R3	-	Yes	G1
2.	M7.9	2012	Mar-13	1429	R2	S2	Yes	G2
3.	X5.4	2012	Mar-07	1429	R3	S3	Yes	G3

Source: (Solarham.com http://solarham.com/top10.txt and NOAA's SWPC (http://www.swpc.noaa.gov, last accessed September 27, 2014).

The Coronal Mass Ejection (CME) field indicates whether the solar flare hurled a CME (oriented or not to Earth). The Radio B./SR Storm/GM Storm fields indicate the NOAA scales of radio blackouts/solar radiation storms/geomagnetic storms, being G1 (minor), G2 (moderate), G3 (strong).

Figures (4-16) to (4-18) show the TEC behaviour at each NIGNET station before, during and after each of the three solar flares examined.

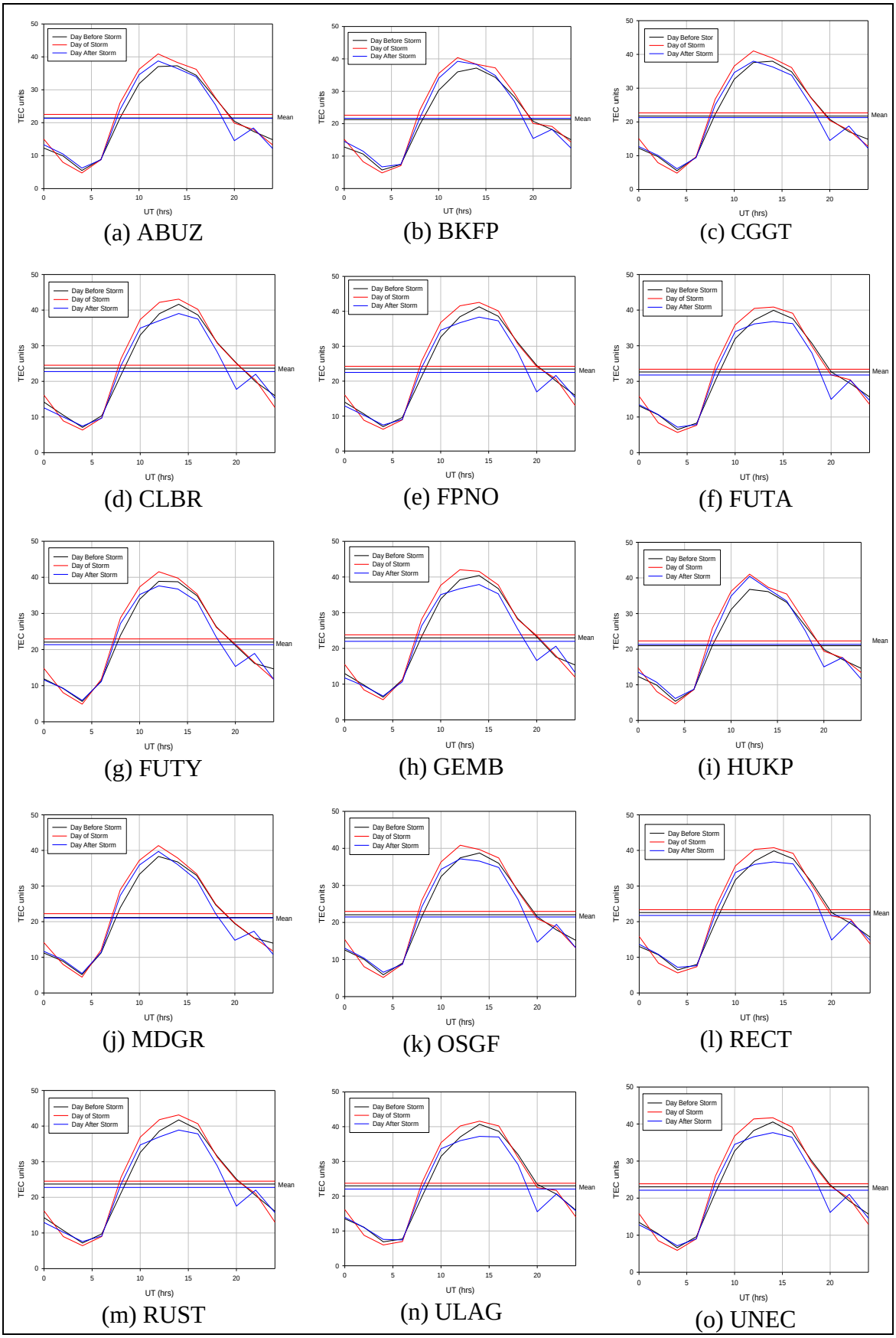


Figure 4-16: TEC Behaviour over the NIGNET stations during the 'Valentine's Day' 2011 X2.2-class G1 minor solar flare of February 15 2011

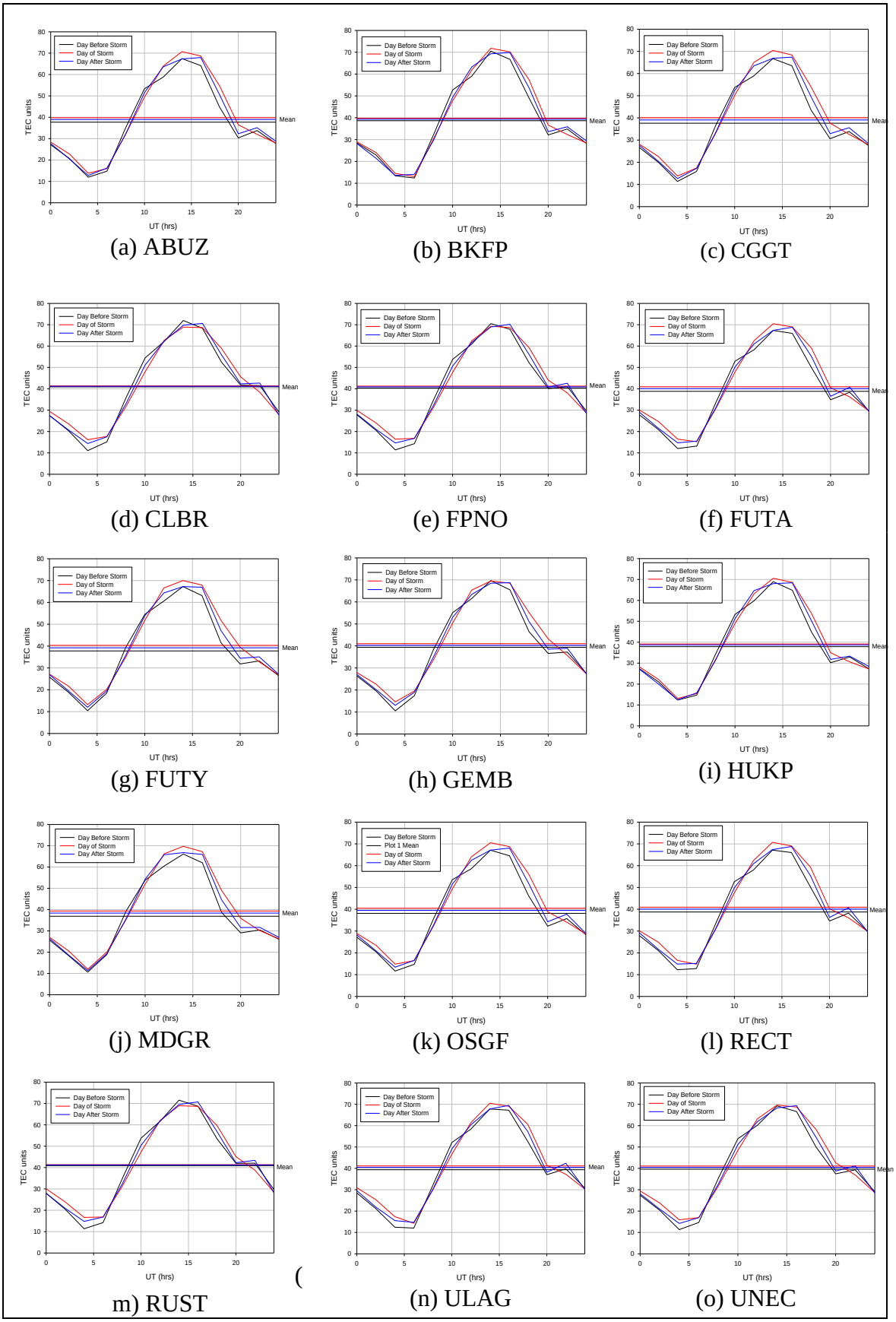


Figure 4-17: TEC Behaviour over the NIGNET stations during the M7.9-class G2 moderate solar flare of March 13 2012

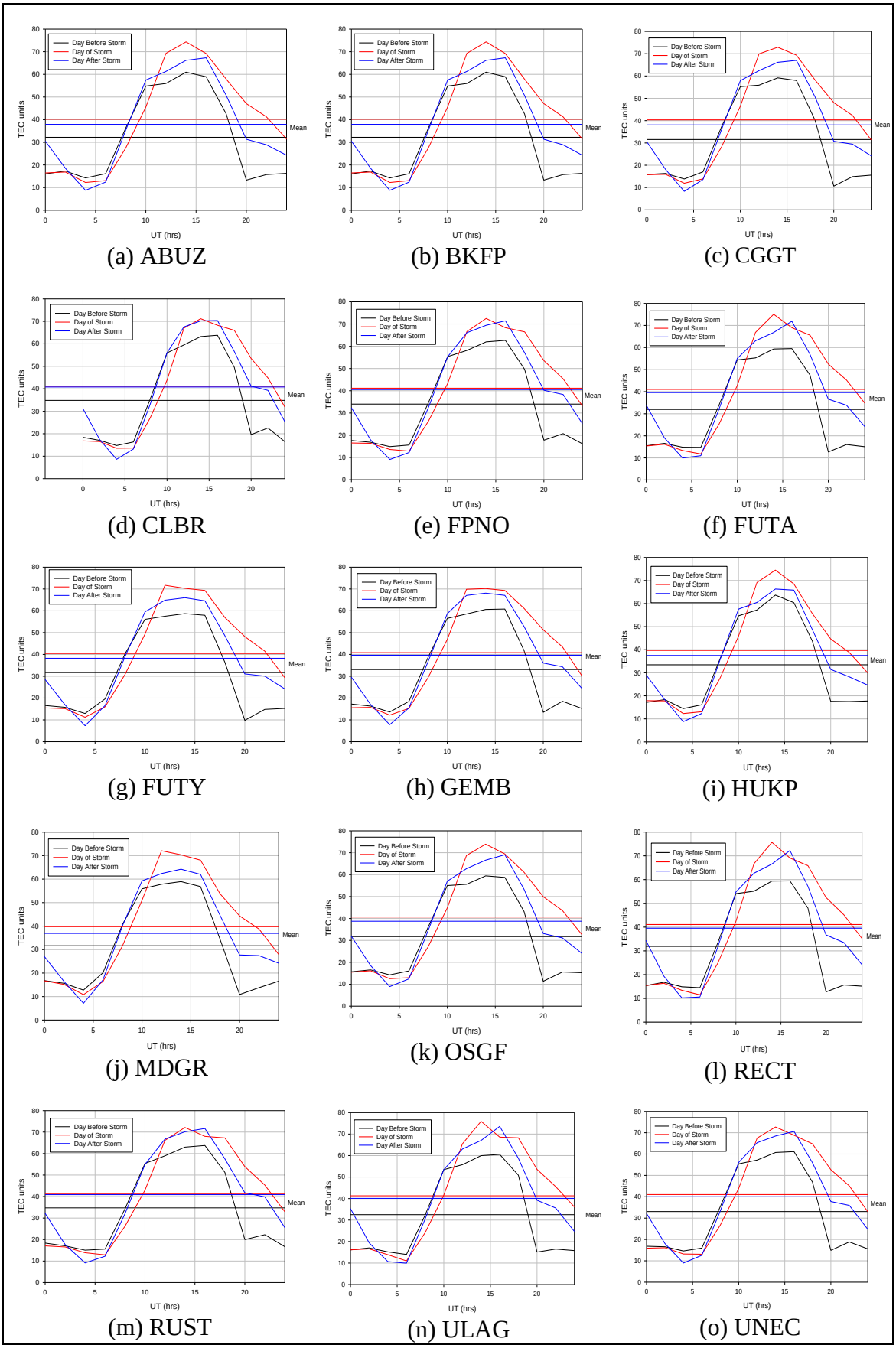


Figure 4-18: TEC Behaviour over the NIGNET stations during the X5.4-class G3 strong solar flare of March 07 2012

The results showed that the average diurnal TEC is higher during the day of the flare. The difference in diurnal amplitude between the day before, the day of, and the day after the flare is dependent on the magnitude of the flare. For the minor G1 (Figure 4-16) and moderate G2 (Figure 4-17) flares, the difference in the diurnal mean TEC was observed to be in the range of 1-3 TECU (4 - 4.5% increment from the day before the storm). Similar TEC behaviour was observed at all the NIGNET stations for the G1 and G2 geomagnetic storms, with the exception of CLBR, FPNO and RUST, having very negligible difference in their mean diurnal TEC values of less than 1 TECU between the day before and the day of the storm. These three stations had lower daytime maxima but slightly higher mean TEC values during the day of the G2 storm (see Figures 4-17(d), (e) and (m)). However, for the strong G3 X5.4-class flare, it was evident that the TEC enhancement with respect to the background values was significantly higher during the day of the storm, reaching up to 37% increment in the mean diurnal TEC on the day of the storm. Large TEC maxima up to 10 TECU higher than the value of the day before the flares were observed at all of the NIGNET stations [see Figure (4-18)]. These very high TECs were followed by the dramatic collapse of the ionisation a day after the flare, which is characteristic of such conditions. Similar TEC behaviour have also been observed during other solar flares from previous studies; Cander and Mihajlovic, 2005; Fedrizzi *et al.*, 2005; Mannucci *et al*., 2005; Choi *et al*., 2011; Bolzan *et al*., 2012.

4.2.2 Solar Eclipse of November 03, 2013

Observations of ionospheric disturbances during solar eclipses make it possible to obtain information on processes in the Moon's shadow and its vicinities. The final event of 2013 is the most interesting eclipse of the year. It is one of the rare hybrid or annular/total eclipses in which some sections of the path are annular while other parts

are total. The results in this section are depicting the ionospheric behaviour over the NIGNET CORS during this event. To study the effect of this solar eclipse on the ionosphere, diurnal TEC data at each NIGNET station were obtained a day before, during and a day after the solar eclipse. These results were analysed for each of the stations. Figures (4-19) show the ionospheric TEC response during total solar eclipse of 03 November 2013 at 15 of the NIGNET stations.

From the results shown in Figure (4-19), a sharp declination of (3-6) TECU was observed in the daytime TEC peak on the day of the eclipse when compared to the day before the eclipse (compare the black and red plots in Figure 4-19). This declination was dependent on station location and time of the eclipse. The declination starts at the commencement of the eclipse, attaining a minimum value within the time period the eclipse attains a maximum magnitude, and then recovering gradually as the eclipse elapses progressively. This trend was observed at all the NIGNET stations, except for BKFP [Figure 4-19(b)] and CLBR [Figure 4-19(d)] stations where the decline in the daytime TEC peak was almost constant during the period of the eclipse.

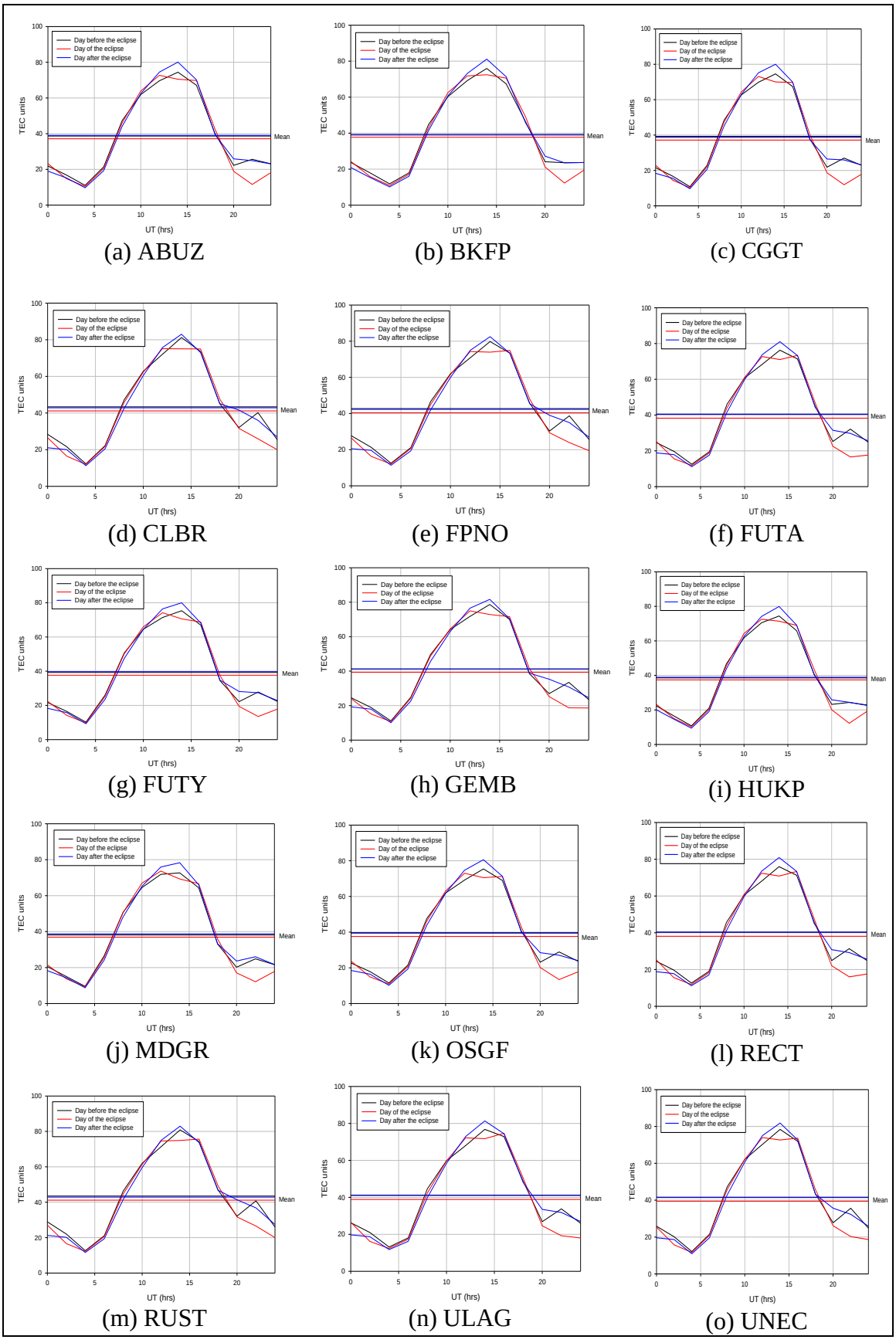


Figure 4-19: TEC Behaviour over the NIGNET stations before, during and after the solar eclipse of 03 November 2013

The study found considerable reduction of (1-3) TECU in the mean daily TEC on the day of the eclipse, compared to quiet mean TEC a day before the eclipse at all the stations. The reduction in the mean TEC on eclipse day compared to quiet mean TEC is attributed to less production of plasma due to less amount of solar radiation during the solar eclipse reaching the Earth. Furthermore, it was observed at all the stations that the daytime peak TEC was higher the day after the eclipse than the day before the eclipse (compare the red and blue plots in Figure (4-19). However, it was astonishing to observed that the mean daily TEC returns to almost exact same value a day after the eclipse as it were a day before the eclipse (compare the horizontal black, red and blue solid lines in Figure (4-19), indicating the mean daily TEC values for the day before, day of, and day after the eclipse respectively).

Thus, from the findings it shows that TEC level will reduce during solar eclipse due to the reduction of ionizing radiation. This is in agreement with earlier findings for other eclipses in other regions. GPS TEC measurements in Spain show a significantly reduced ionization during the annular eclipse on 3 October 2005 (Jakowskia *et al*., 2008). Comparable results were obtained in India (Sharma *et al*., 2010) and China (Jia-Chun *et al*., 2010), during the solar eclipse of July 22, 2009, also at a single station Bengaluru in India during the eclipse of 15 January 2010 (Galav *et al*., 2010). Also, similar results have been reported by Liu *et al*., 1999; Afraimovich *et al*., 2002; Baran *et al*., 2003 and Abidin *et al.,* 2006.

4.2.3 TEC Correlation with Solar Activity

Solar activity is characterized by a number of activity indices. For the purpose of this work, the daily averaged sunspot number and f10.7 solar indices were used as proxies for solar activity. These solar indices were compared with the daily mean ionospheric TEC obtained from GNSS data for a period of four and half years to better understand the ionization response to solar activity variations.

Figure (4-20) shows the correlation coefficient between the NIGNET CORS-derived TEC and the solar indices at ABUZ, BKFP and UNEC stations for 2011 epoch. These stations were used for the correlation analysis between the TEC derived from the NIGNET CORS data and the solar indices due to data availability from these stations covering the entire or almost the entire year since the solar indices data covers the entire year. Figures (4-21) and (4-22) show the comparative results for the NIGNET CORS-derived TEC and the solar indices at ABUZ, BKFP and UNEC for 2011 epoch.

The results for the correlation between the GIM-derived TEC at each NIGNET station with the solar indices are shown in figure (4-23), while the comparative plots results are shown in figures (4-24) and (4-25).

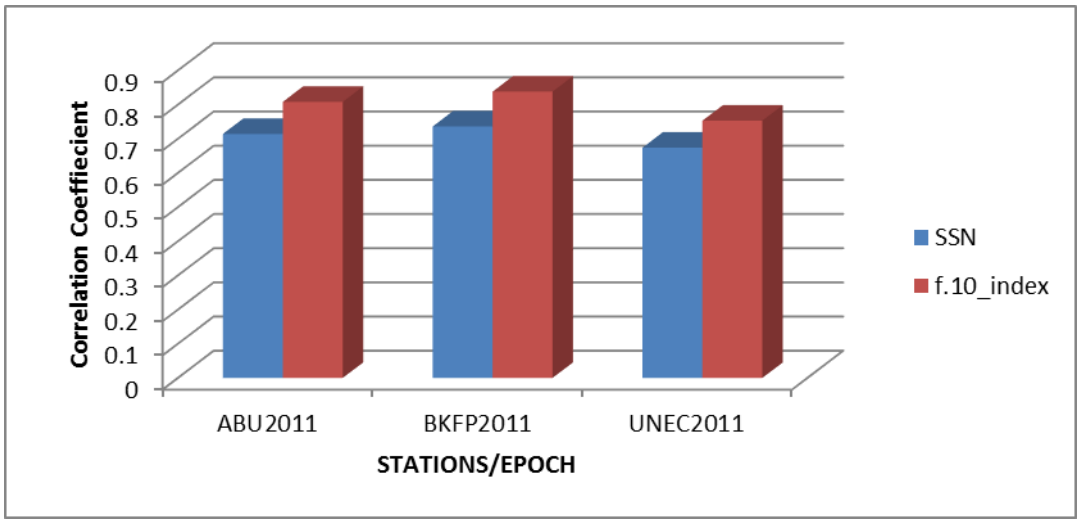


Figure 4-20: NIGNET TEC Correlation with Sunspot Number and f.10_index at ABUZ, BKFP and UNEC for 2011 epoch

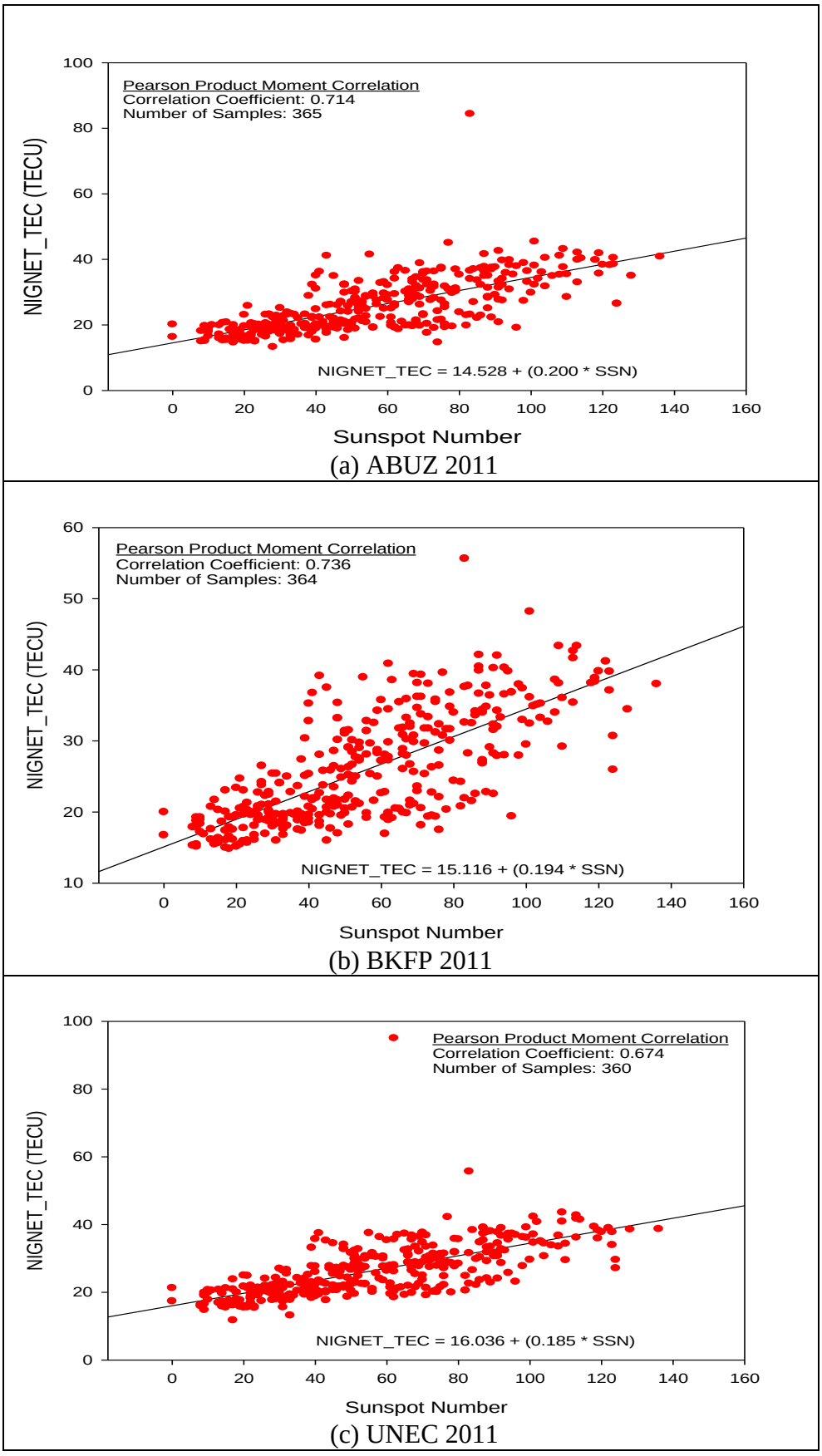


Figure 4-21: Comparative plots of NIGNET TEC and Sunspot Number at ABUZ, BKFP and UNEC for 2011 epoch

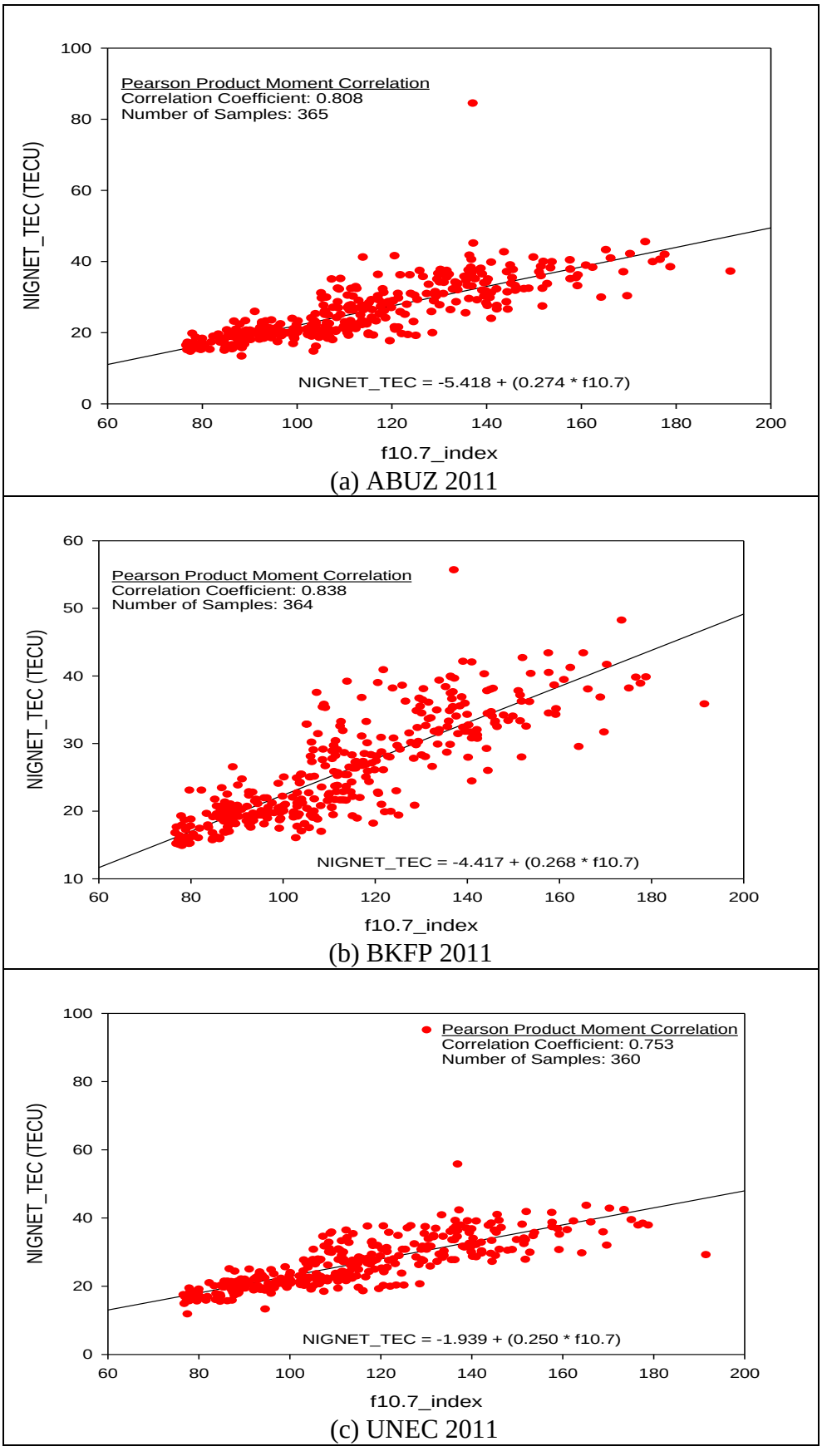


Figure 4-22: Comparative plots of NIGNET TEC and f.10_index at ABUZ, BKFP and UNEC for 2011 epoch

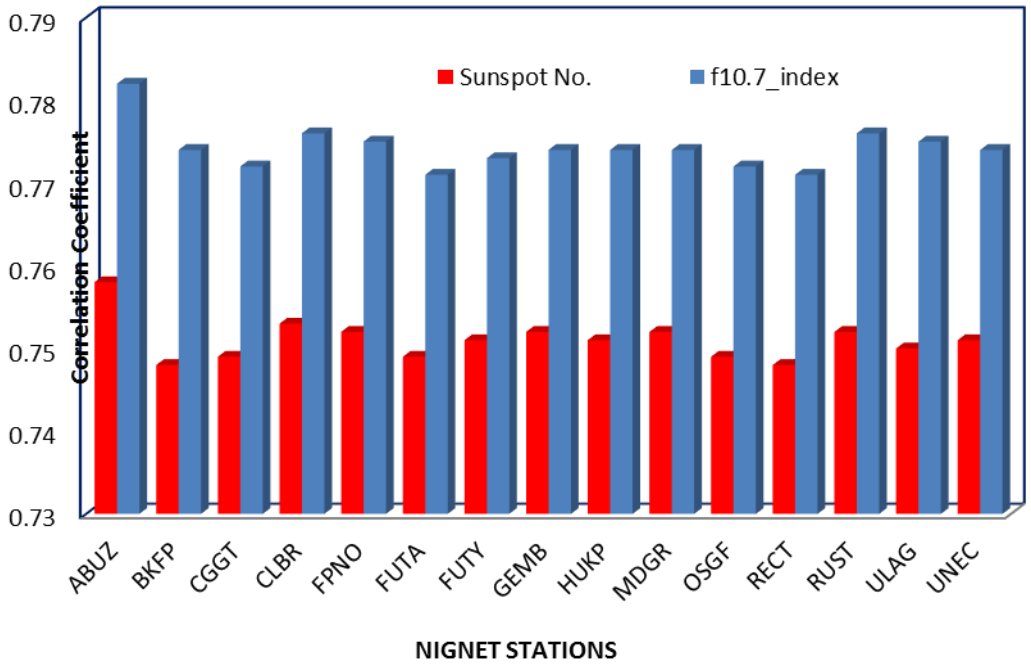


Figure 4-23: GTEC Correlation with Sunspot Number and f.10_index at the NIGNET stations for the period of January 2010 to June 2014

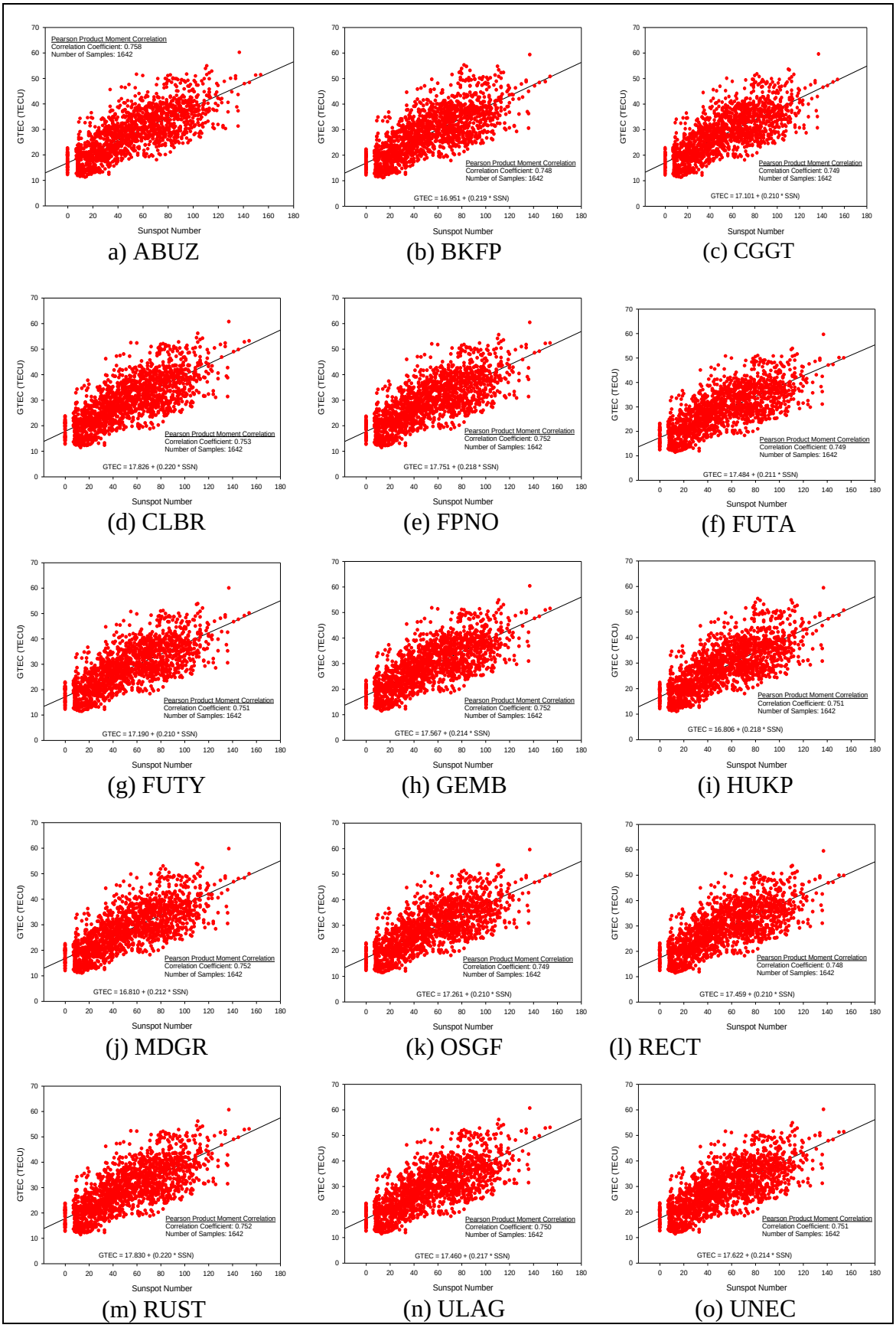


Figure 4-24: Comparative plots of GTEC and Sunspot Number at the NIGNET stations for January 2010 to June 2014

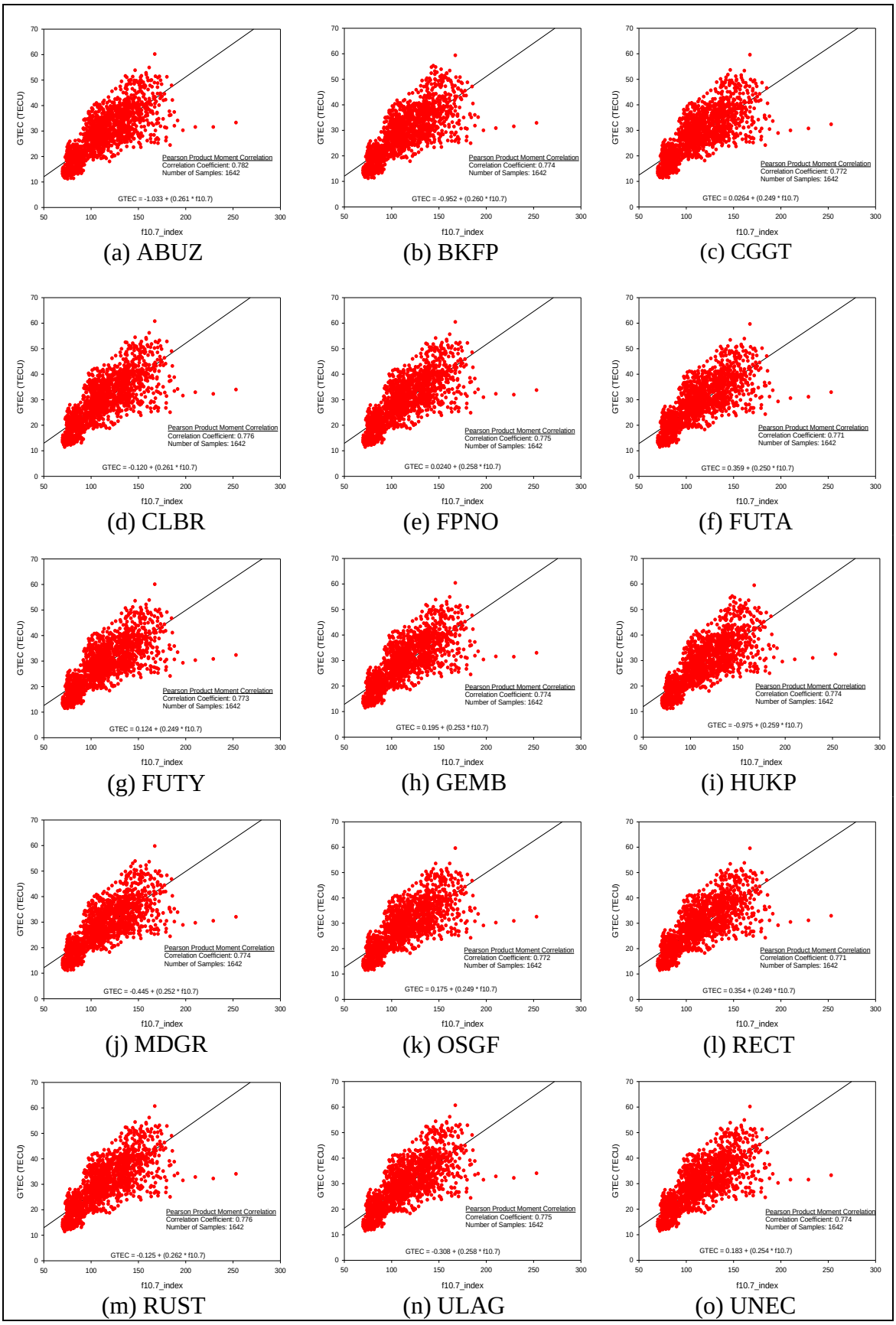


Figure 4-25: Comparative plots of GTEC and f.10_index at the NIGNET stations for January 2010 to June 2014

From the results, it was found that TEC follows a synchronous variation with both solar indices considered. The correlation was found to be remarkably high. The correlation analysis based on 2011 NIGNET data for ABUZ, BKFP and UNEC and for the 1642-day sample length for the GTEC showed an average of 71% correlation between the NIGNET_TEC and the sunspot number, and 80% average correlation with with the f10.7 solar index. On the other hand, 75% and 77% average correlations between GTEC with sunspot number and f10.7 indices respectively were observed. Thus, the findings showed good positive correlations above 60% for all stations for both the NIGNET and GIM derived TECs recorded over the four and half years period with the two solar indices considered. Hence, it is certain that TEC increase actually corresponds normally with increased solar activity. Similar positive correlation has also been observed by Dabas *et al.*, *1994;* Liu *et al*., 2007; Bagiya *et al*., 2009; Liu and Chen, 2009; Mansoori *et al*., 2013; Oron *et al*., 2013.

However, a close observation of the results showed that the variation of TEC with F10.7 index has closer agreement than with sunspot number as observed from both the NIGNET_TEC and GTEC. The result is quite obvious since the primary source of ionospheric ionization is solar radiation flux. Also, higher correlation was observed between both solar indices with the GTEC than with the NIGNET_TEC. This can be attributed to the global nature of the Global Ionospheric Maps from which the GTEC was derived, since solar activity is usually on a global scale than on a local or regional scale.

4.3 Validation of NIGNET – Derived TEC with GIM TEC

In order to validate the NIGNET - derived TEC, the comparison between NIGNET-Derived TEC with IGS GIMs as performed. It should be noted that the IGS GIMs are a combination of GIMs resolution of the final IGS GIMs is 2.5º in latitude and 5.0º in longitude. For validation purposes, an area covering the NIGNET extent was extracted from the IGS GIMs, and the validation carried out using NIGNET stations with consistent and significant numbers of sample data. Figures (4-26) shows the correlation coefficient between NIGNET CORS derived TEC (NIGNET_TEC) and the GIM derived TEC (GTEC) for 7 stations based on data availability for 2011 to 2013 epoch. Figure (4-27) shows the comparative plot results of the validation of the NIGNET_TEC with the GTEC.

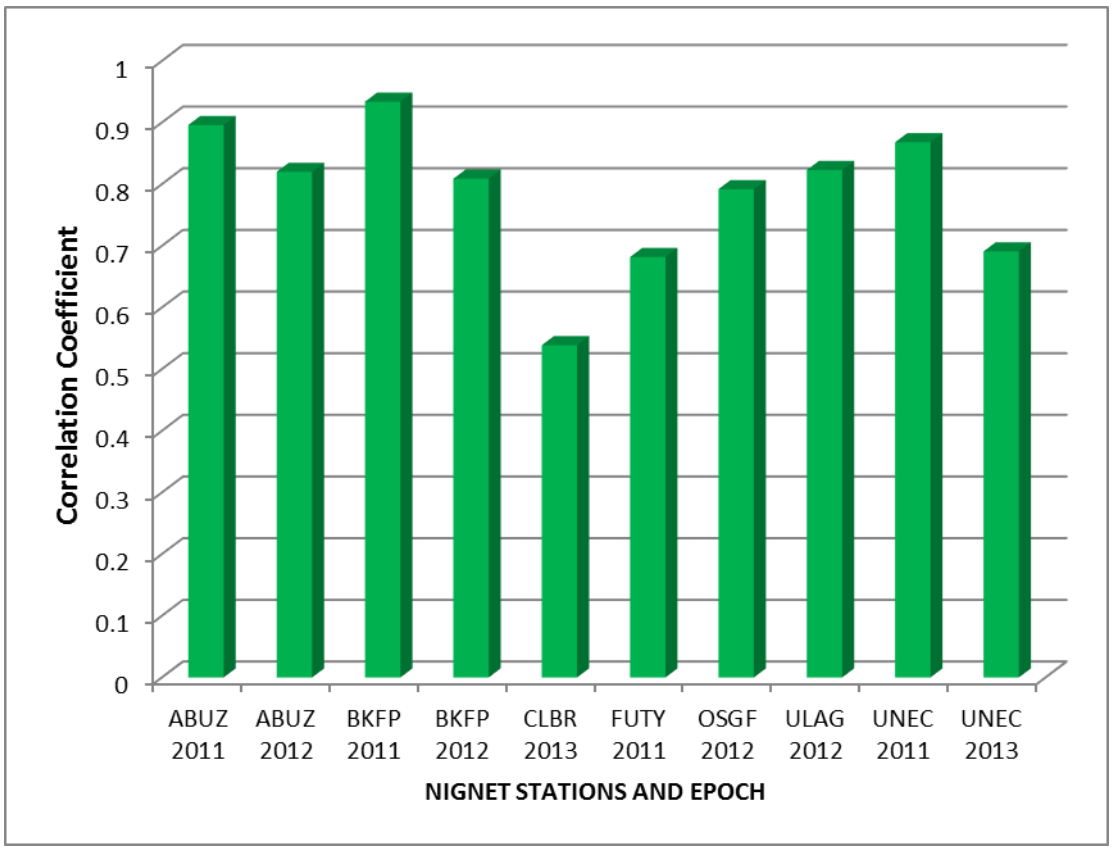


Figure 4-26: Correlation coefficient between the NIGNET CORS derived TEC (NIGNET_TEC) and the GIM derived TEC (GTEC)

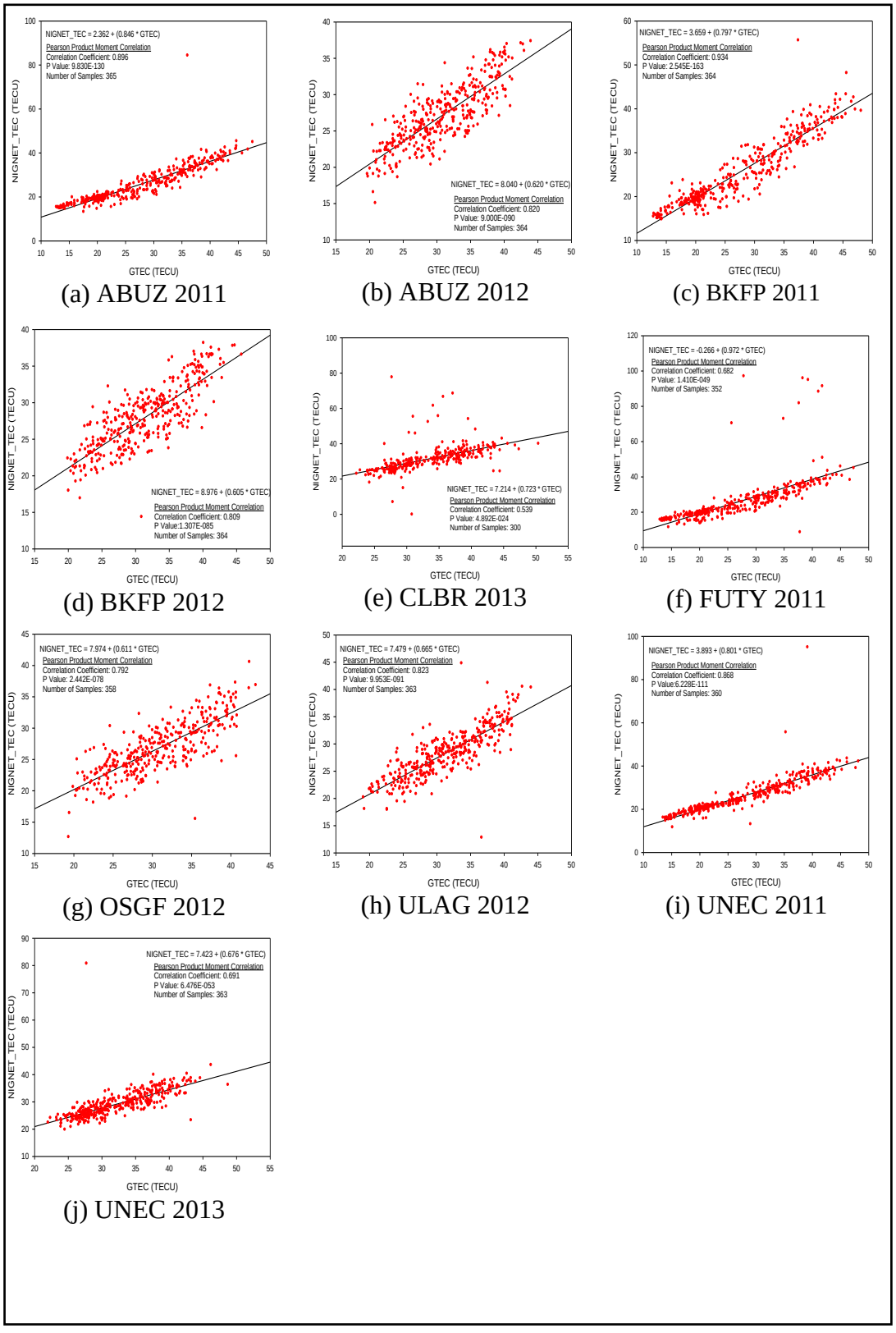


Figure 4-27: Comparative plots of equivalent vertical TECs obtained from NIGNET CORS data (NIGNET_TEC) and vertical TECs obtained from the GIMs data (GTEC)

The comparative plots show good statistical agreement between the data sets. The results show positive correlation between the NIGNET TEC and the GIM TEC for each station of the NIGNET CORS used for validation purpose, each station having more than 50% correlation. BKFP, ABUZ, UNEC and ULAG stations have higher correlations of 93.4%, 89.6%, 86.8%, and 82.3% respectively with the GIM TEC. CLBR station has the lowest correlation of 53.9%. This can however, be attributed to the smaller number of sample data used for the station based on data availability. However, it was noted that some apparently rogue points can be seen in the comparative plots. This can be attributed to local ionospheric disturbances that are station dependent. In general, the obtained results from the NIGNET CORS are comparable to the IGS GIMs. It is noticeable however, that TEC from GIM is higher by about 0 to 5 TECU, as compared with TEC generated by processing the NIGNET CORS data. This can be attributed the global nature of GIMs and the very low spatial coverage of IGS stations in the Nigerian region.

The key findings of the dissertation from the results presented are outlined below:

i. The total electron content can be evaluated from the NIGNET CORS data and from the Global Ionospheric Maps.
ii. The TEC is a highly variable parameter with diurnal, seasonal and spatial variations.
iii. TEC profile varies considerably during geomagnetic storms and solar eclipse. The TEC increases during geomagnetic storms depending on the magnitude of the storm, while during solar eclipse there is a general decline in the observed TEC value.

iv. The TEC time series generated and the validation of the NIGNET CORS data-derived TEC with the GIM-derived TEC show good positive correction between the TEC from both data sources and thus the GIM-derived TEC can be used in situations where there are no available observed data from any of the NIGNET stations.

CHAPTER FIVE

CONCLUSION AND RECOMMENDATIONS

5.1 CONCLUSION

The study of the estimation and analysis of ionospheric TEC over the Nigerian GNSS Reference Network (NIGNET) has been carried out. The results from the study were compared to results from earlier works and reports where applicable. In this study, different methods for processing TEC which utilize different techniques have been presented. Two scenario of obtaining TEC were studied such as TEC from the dual frequency NIGNET CORS and TEC derived Global Ionospheric Maps. More than 11,000 observation data from 14 operational CORS within the Nigerian sector, and over 21,000 Global Ionospheric data from more than 200 IGS globally distributed GNSS receivers have been used to estimate and describe the TEC variation in the ionosphere over NIGNET in terms of diurnal, seasonal and spatial variations for a period of four and a half years (January 01, 2010 - June 30, 2014).

It is concluded that the TEC measurements from the two independent techniques agree well on a statistical basis within the limits of experimental observation, as some outlying points were found in the data set from the NIGNET CORS due to technical and/or power problem. Thus, GIM-derived TEC values can be used for the locations where continuous NIGNET TEC data are not available.

From the analysis carried out, it was observed that a persistent diurnal variation with larger intensity during daytime and seasonal variation with high TEC values in the equinox months and low values in the solstice months, were common features at all the NIGNET stations for the period considered in the study. On the spatial variation of TEC over the NIGNET, it was found that the TEC increase from north to south of the

country, with stations closer to the equator having higher TEC values for most period of the year.

On the effect of geomagnetic storms on TEC behaviour over the NIGNET network, the results showed that there are several types of storms which affect the TEC behaviour at a GNSS station. The impact of the storm was found to be directly proportional to the strength of the storm. In general, for all types of geomagnetic storms, the profile of diurnal TEC variation showed an increased daytime peak on the day of the storm compared to the day before the storm, and a gradual recovery of the mean diurnal TEC a day after the storm. Analysis of the solar eclipse of November 03, 2013 which was visible from most part of the country showed a general decline in the daytime peak TEC value during the time period of the eclipse at each of the stations. The TEC gradually recovered a day after the eclipse, attaining almost same mean diurnal TEc value as observed the day before the eclipse.

The long term variation of the solar activity indices were compared with the variability of ionospheric TEC. The correlation analysis was performed to access the magnitude of correlation between the long term solar cycle variations and the ionospheric behaviour. From the analysis it was found that NIGNET and GIM derived TEC follow a strong correlation with the sunspot number and f10.7 solar activity indices considered in the study. The ionospheric TEC follows a synchronous variation with the solar cycle variations, as the TEC exhibits an extremely good positive association with the solar indices.

A major challenge encountered during the research work was the capacity to manage and process the large amount of data involved in the work. Also, due to technical and power problem, there were so many missing data from the NIGNET CORS. Furthermore, data for some days of the year at some of the stations were just for a short

period of observation time in contrast to the 24 hours of continuous observation expected.

5.2 RECOMMENDATIONS

i. There are several potential areas that would be worthwhile further exploring both from the scientific and application points of view. From the scientific point of view, the results presented in this dissertation have shown that the NIGNET CORS could potentially be used to monitor ionospheric and solar disturbances.

ii. The real-time processing of a continuously operating network of GNSS receivers could possibly allow monitoring of ionospheric disturbances caused by solar and/or geomagnetic disturbances. From the application point of view, GNSS users should be aware from the results outlined in this dissertation, of the likely times, seasons and regions of strong ionospheric disturbances and should attempt to avoid positioning at those times and seasons when possible.

iii. With optimism of improvements in the latency of data from NIGNET, it is recommended that further studies should be carried out to improve this study into a real or near-real time ionospheric monitoring system for Nigeria. Presented in this study is the evaluation of the ionosphere TEC over the Nigerian GNSS network, with no inclusion of ionospheric correction model to the positioning results. Therefore, future study should cover the development of an ionospheric correction model for NIGNET using the TEC data from the Nigerian CORS and GIMs obtained in this study. The monitoring system and model can be developed using data presently made available in this dissertation in such a way as to allow for future improvements and updates.

iv. Furthermore, only dual frequency data for L1 and L2 were used to investigate the ionospheric TEC. Thus, it would be necessary to include new improved signals, such as the L5 for more detailed analysis. A period of four and half years was considered in the study, future works should consider a long time period of about 11 years which corresponds to the solar cycle in order to ascertain the long time correlation of TEC with the solar cycle variation.

v. Considered in this dissertation is the estimation and analysis of the TEC profile and variation over the NIGNET with no inclusion of the effect of the ionospheric TEC on GNSS positioning. Therefore, future works should consider the effect of the TEC on GNSS positioning accuracy and reliability.

REFERENCES

Abidin, A. R. Z., Awad, M. M, Sulaiman, S. (2006). GPS ionospheric TEC measurements during the 23rd November 2003 total solar eclipse at Scott Base Antarctica, *Journal of Atmospheric and Solar-Terrestrial Physics*, 68, 1219-1236.

Adewale, A. O., Oyeyemi E. O., Adeloye, A. B., Ngwira, C. M. and Athieno, R. (2011). Responses of equatorial F region to different geomagnetic storms observed by GPS in the African sector. *Journal of Geophysical Research*, 116, A12319. doi:10.1029/2011JA01699.

Afraimovich, E. L., Kosogorov, E. A., Lesyuta, O. S. (2002). Effects of the August 11, 1999 total solar eclipse as deduced from total electron content measurements at the GPS network, *Journal of Atmospheric and Solar-Terrestrial Physics*, 64, 1933_1941.

Alcay, S., Inal, C., Yigit, C. O., and Yetkin, M. (2012). Comparing GLONASS only with GPS only and hybrid positioning in various length of baselines. *Acta Geodaetica et Geophysica*, 47(1), 1-12. doi: 10.1556/AGeod.47.2012.1.1.

Alizadeh, M., Schuh, H. and Schmidt, M. (2010). Multi-dimensional modelling of electron density using spherical harmonics and chapman function. *Geophysical Research Abstracts*, vol 12, EGU2010-4103-1.

American Meteorological Society, (2008). Space Weather. A Policy Statement of the American Meteorological Society. *Bulletin of the American Meteorological Society*, 89, (6), 16-18.

Araujo-Pradere, E. A. (2005). GPS-derived Total Electron Content response for the Bastille Day Magnetic Storm of 2000 at a low mid-latitude station. *Geofisica Internacional*, 5, 211-218.

Araujo-Pradere, E. A. and Fuller-Rowell, T. J. (2002). STORM: An empirical storm-time ionospheric correction model, 2, Validation. *Radio Science*, 37(5), 1071, doi: 10.1029/2002RS002620.

Araujo-Pradere, E. A., Fuller-Rowell, T. J., and Codrescu, M. V. (2002). STORM: An empirical stormtime ionospheric correction model, 1, Model description, *Radio Science*, 37(5), 1070, doi: 10.1029/2001RS002467.

Arbesser-Rastburg, B. (2006). The Galileo single frequency ionospheric correction algorithm. Retrieved from sidc.be/esww3/presentations/Session4/Arbesser.pdf.

Astafyeva, E. I., Afraimovich, E. L., Oinats A. V., Yasukevich, Y. V., and Zhivetiev, I. V. (2008). Dynamics of global electron content in 1998–2005 derived from global GPS data and IRI modeling, *Advances in Space Research*, 42, 763–769.

Azpilicueta, F., and Brunini, C. (2011). A new concept regarding the cause of ionosphere semiannual and annual anomalies. *Journal of Geophysical Research*. 116:A01307. doi:10.1029/2010JA015977

Bagiya, M. S., Joshi, H. P., Iyer, K. N., Aggarwal, M., Ravindran, S., and Pathan, B. M. (2009). TEC variations during low solar activity period (2005–2007) near the Equatorial Ionospheric Anomaly Crest region in India, *Annals of Geophysics*, 27, 1047–1057. doi:10.5194/angeo-27-1047-2009.

Baran, L. W., Ephishov, I. I., and Shagimuratov, I. I. (2001). Ionospheric Total Electron Content Behavior during November 1997 Storm. *Physical Chemistry of Earth*, 26, pp. 341-345.

Baran, L. W., Ephishov, I. I., and Shagimuratov, I. I. (2003). The response of the ionospheric total electron content to the solar eclipse on August 11, 1999, *Advances in Space Research*, 31(4), 989-994.

Bevis, M., Businger, S., Chiswell, S., Herring, T. A., Anthes, R. A., Rocken, C., and Ware, R. (1994). GPS meteorology: mapping zenith wet delays onto precipitable water. *Journal of Applied Meteorology*, Vol. 33, pp. 379-386.

Bilitza, D. (ed.) (1990). International Reference Ionosphere 1990. Report Number NSSDC/WDC-A-R&S 90-22, National Space Science Data Center/World Data Center A for Rockets and Satellites, Lanham, MD.

Bilitza, D., and Reinisch, B. W. (2008). International reference ionosphere 2007: improvements and new parameters. *Advances in Space Research*, 42, pp. 599–610.

Bishop, G. J., Coco, D. S., and Coker, C. (1991). Variations in Ionospheric Range Error with GPS Look Direction. *Proceedings of ION GPS-91, the 4th International Technical Meeting of the Satellite Division of The Institute of Navigation*, Albuquerque, NM, 11-13 September, The Institute of Navigation, Alexandria(VA), pp.1045-1054.

Blanch, J. (2002). An Ionospheric Estimation Algorithm for WAAS Based on Kriging. *Proceedings of ION GPS*, 2002, Portland.

Bolzan, M. J. A. and Rosa, R. R. (2012). Multifractal analysis of interplanetary magnetic field obtained during CME events, *Annals of Geophysics*, 30, 1107–1112. doi:10.5194/angeo-30-1107-2012.

Bothmer, V. and Daglis, I. A. (2007). *Space Weather: Physics and Effects*, 213, 315-318, 438 pp., Praxis Publishing Ltd., Chichester, UK.

Breed, A. M., GoodWin, G. L., and Silby, J. H. (1998). Total electron content measurement in the southern hemisphere using GPS satellites, 1991 to 1995, *Radio Science*, 33, 1705–1726.

Caissy M., Weber, G., Agrotis, L., Wübbena, G., and Hernández-Pajares, M. (2011). The IGS real-time pilot project—the development of realtime IGS correction products for precise point positioning.

Cander, L. R., and Mihajlovic, S. J. (2005). Ionospheric spatial and temporal variations during the 29–31 October 2003 storm, *Journal of Atmospheric and Solar-Terrestrial Physics*, 67, 1118–1128.

Carlson, H. C., and Egeland, A. (1995). Introduction to Space Physics, chap. *The aurora and the auroral ionosphere*. Cambridge University Press, Cambridge, U.K.

Chauhan, V., and Singh, O. P. (2010). A morphological study of GPS-TEC data at Agra and their comparison with the IRI model. *Advances in Space Research*. 46, 280–290.

Chauhan, V., Singh, O. P., and Singh, B. (2011). Diurnal and seasonal variation of GPS-TEC during a low solar activity period as observed at a low latitude station Agra. *Indian Journal of Radio & Space Physics*, 40(1), 26-36.

Choi, B. K., Lee, S. J., and Park, J. U. (2011). Monitoring the ionospheric total electron content variations over the Korean Peninsula using a GPS network during geomagnetic storms, *Earth Planets Space*, 63, 469–476. doi:10.5047/eps.2011.03.004.

Ciraolo, L., Azpilicueta, F., Brunini, C., Meza, A., and Radicella, S. M. (2006). Calibration errors on experimental slant total electron content (TEC) determined with GPS. *Springer-Verlag*.

Clette, F., Berghmans, D., Vanlommel, P., Van der Linden, R., Koeckelenbergh, A., and Wauters, L. (2007). From the Wolf number to the International Sunspot Index: 25 years of SIDC, *Advances in Space Research*, 40 (7), 919–928, ISSN: 0273-1177, DOI: 10.1016/j.asr.2006.12.045.

Codrescu, M. V., Beierle, K. L., Fuller-Rowell, T. J., Palo, S. E., and Zhang, X. (2001). More total electron content climatology from TOPEX/Poseidon measurements. *Radio Science*, 36, 325-333.

Codrescu, M. V., Palo, S. E., Zhang, X., Fuller-Rowell, T. J., and Poppe, C. (1999). TEC climatology derived from TOPEX/POSEIDON measurements, *Journal of Atmospheric Solution*, 61, 281-298.

Coster, A., and Komjathy, A. (2008). Space Weather and the Global Positioning System. *Space Weather*, 6, S06D04, doi: 10.1029/2008SW000400.f.

Covington, A. E. (1969). Solar Radio Emission at 10.7 cm, 1947–1968, *Journal of the Royal Astronomical Society of Canada*, 63, 125–132.

Dabas, R. S., Bhuyan, P. K., Tyagi, T. R., Bhardwaj, R. K., Lal, J. B. (1984). Day-to-day changes in ionospheric electron content at low latitudes. *Radio Science*, 19, 749–756.

Dabas, R. S., Lakshmi, D. R., Reddy, B. M. (1994). Solar activity dependence of ionospheric electron content and slab thickness using different solar indices, *Journal of Pure and Applied Geophysics*, 140(4).

Dabas, S. R. (2000). Ionosphere and its Influence on Radio Communication. *Journal of Science Education*, 5, 28 – 43.

Davies, K. (1990). Ionospheric radio. *IEE Electromagnetic waves series*, 31, Peter Peregrinus Ltd, Exeter.

Davies, K., and Liu, X. M. (1991). Ionospheric slab thickness in middle and low latitudes. *Radio Science*, vol.26, pp. 997-1001.

Dieminger, W., Hartmann, G. R, and Leitinger, R. (Eds.). (1996). *The Upper Atmosphere, Data Analysis and Interpretation.* New York: Springer Verlag.

Dodo, J. D. (2014). Advanced GNSS Methods, GEOM 810 Lecture Notes, Department of Geomatics, Ahmadu Bello University, Zaria, Nigeria.

El-Rabbany, A. (2002). *The Global Positioning System.* Massachusetts, USA : Artech House Inc. Retrieved from www2.pv.infn.it/~genova/gps/Rabbani.pdf.

Ezuqer, R. G., Brunini, C., Meza, A., Azpilicueta, F., Mosert, M., and Radicella, S. (2004). VTEC behavior in the American sector during high solar activity. *Advances in Space Research*, 33, pp.855-861.

Fayose, R. S., Babatunde, R., Oladosu, O. and Groves, K. (2012). Variation of Total Electron Content [TEC] and Their Effect on GNSS over Akure, Nigeria, *Applied Physics Research*,4(2). doi:10.5539/apr.v4n2p105.

Fedrizzi, M., Paula, E., Kantor, I. J., Langley, R., Komjathy, A., and Batista, I. (2005). Study of the March 31, 2001 magnetic storm effects on the ionospheric GPS data, *Advances in Space Research*, 36, 534–545.

Feltens J. and N. Jakowski (2002) The International GPS Service (IGS) Ionosphere Working Activity, SCAR Report No. 21.

Feng, Y (2003), Combined Galileo and GPS: A Technical Perspective. Journal of Global Positioning Systems, 2 (1): 67-72.

Galav, P., Sharma, S., Pandey, R. (2010). Total electron content in peninsular India during the eclipse of 15 January 2010, *Current Science*, 99 (6), 732.

Galileo (2003). Mission Requirement Document (MRD). *European Commission*, Issue 5–Rev. 1.1, 27. March 2003. Available at http://www.Galileoju.com.

Galileo (2005). Mission High Level Definition (HLD) (2002). *European Commission Communication Document, W. Doc. 2002/05,* Version 3, 23. Retieved from http://www.Galileoju.com.

García-Rigo A., Hernández-Pajares, M., Monte, E., Juan, J. M, Sanz, J., Krankowski, A., and Wielgosz, P. (2009). Assessment of UPC model for ionosphere VTEC prediction (Poster). *Geodesy for Planet Earth (IAG)*, Buenos Aires, Argentina.

Goad, C. C., and Goodman, L. (1974). A modified Hopfield tropospheric refraction correction model. *Paper presented at the American Geophysical Union Annual Fall Meeting at CA*, 12-17 December, pp. 28.

Gonzalez, W. D., Joselyn, J. A., Kamide, Y., Kroehl, H. W., Rostoker, G., Tsurutani, B. T., and Vasyliunas, V. M. (1994). What is geomagnetic storm? *Journal of Geophysical Research*, 99, No. A4, Pages 5771-5792.

Gopi, S. (2012). Rinex GPS-TEC program Version 2.2.0, Boston College.

Guarnieri, F. L., and Pillat, V. G. (2010). Response of the ionospheric F region in the Brazilian sector during the super geomagnetic storm in April 2000 observed by GPS. Advances in Space Research, 45, 1322–1329, doi:10.1016/j.asr.2010.02.003.

Guo, P., Xu, X. G., and Zhang, X. (2011). Analysis of the ionospheric equivalent slab thickness based on ground-based GPS/TEC and GPS/COSMIC RO measurements. *Journal of Atmospheric and Solar Terrestrial Physics*, vol.73, pp. 839–846.

Gupta, J. K. and Singh, L. (2000). Long term ionospheric electron content variations over Delhi, *Annals of Geophysics*, 18, 1635–1644. doi:10.1007/s00585-001-1635-8.

Habarulema, J. B., McKinnell, L. A., and Opperman, B. D. (2010). TEC measurements and modeling over Southern Africa during magnetic storms; a comparative analysis. *Journal of Atmospheric and Solar Terrestrial Physics*, 72, pp. 509–520.

Hamilton, D. C., Gloeckler, G., Ipavich, F.M., Stedemann, W., Wilken, B. and Kremser, G. (1988). Ring current development during the great geomagnetic storm of February 1986. *Journal of Geophysical Research*, vol. 9, pp.148-227.

Hargreaves, J. K. (1992). *The solar-terrestrial environment*. Cambridge: Cambridge University Press, 2nd ed.

Heinrichs, G., Germany, G., Winkel, J., Drewes, C., Maurer, L., Springer, A., ... Wicpalek, C., (2005). A Hybrid Galileo/UMTS Receiver Architecture for Mass-Market Applications. *GNSS 2005*. Retrieved from http://www.gawain-receivers.com/publications/IfEN_Paper_GAWAIN_GNSS2005.pdf.

Hoffmann-Wellenhof, B., Lichtenegger, H., and Collions, J. (1994). *GPS theory and practice*, 3rd Edition. New York, NY, USA: Springer-Verlag.

Hopfield, H.S. (1969). Two quartic tropospheric refractivity profile for correcting satellite data. *Journal of Geophysical Research*, 74, No. 18, pp. 4487-4499.

Huang, Z., and Roussel-Dupre, R. (2005). Total electron content (TEC) variability at Los Alamos, New Mexico: A comparative study: FORTE-derived TEC analysis, *Radio Science*, 40, RS6007. doi:10.1029/2004RS003202.

Hugentobler, U., Schaer, S., and Fridez, P. (2001). *Bernese GPS software, Version 4.2*. Switzerland: Astronomical Institute, University of Bern.

Huo, X. L., Yuan, Y. B., and Ou, J. K. (2005). The diurnal variations, semiannual and winter anomalies of the ionospheric TEC based on GPS data in China, *Progress in Nature Science*, 15, 56–60.

Jain, A., Tiwari, S., Jain, S., Gwal, A. K.(2010). TEC response during severe geomagnetic storms near the crest of equatorial ionization anomaly. *Indian Journal of Radio Space Physics*, 39, 11–24, 2010.

Jakowski, N. (1996). TEC Monitoring by using satellite positioning system, in Modern Ionospheric Science. *Journal of Atmospheric and Solar Terrestrial Physics*, 60, 371-390, 1996.

Jakowski, N., Heise, S., Wehrenpfenning, S., and Schluter, S. (2001). TEC monitoring by GPS – a possible contribution to space weather monitoring. *Physics and Chemistry of the Earth*, (C) 26, 609–613, 2001.

Jakowski, N., Heise, S., Wehrenpfenning, S., Schluter, S., and Reimer, R. (2002). GPS/GLONASS-based TEC measurements as a contributor for space weather forecast. *Journal of Atmospheric and Solar Terrestrial Physics*, 64, 729–735, 2002.

Jakowski, N., Mayer, C., Hoque, M. M., and Wilken, V. (2011). Total electron content models and their use in ionosphere monitoring. *Radio Science*, 46, pp. 1–11, Sept. 2011.

Jakowski, N., Schluter, S., and Sardon, E. (1999). Total electron content of the ionosphere during the geomagnetic storm on 10 January 1997. *Journal of Atmospheric and Solar Terrestrial Physics* 61, 299–307, 1999.

Jakowskia, N., Stankova, S. M., Wilkena, V., Borriesa, C., Altadillb, D., Chumc, J., ... Cander, R. (2008). Ionospheric behavior over Europe during the solar eclipse of 3 October 2005. *Journal of Atmospheric and Solar-Terrestrial Physics*, 70, 836–853.

Jatau, B., Fernandes, R. M. S., Adebomehin, A., and Gonçalves, N. (2010). NIGNET – The New Permanent GNSS Network of Nigeria.. *FIG Congress 2010 Facing the Challenges – Building the Capacity*, Sydney, Australia, 11-16 April 2010.

Jee, G., Schunk, R. W., and Scherliess, L. (2004). Analysis of TEC data from the TOPEX/Poseidon mission, *Journal of Geophysical Research*, 109, A01301, doi:10.1029/2003JA010058.

Jia-Chun, A., Ze-Min, W., Dong-Chen, E., and Wei, S. (2010). Ionospheric behavior during the solar eclipse of 22 July 2009 and its effect on positioning, *Chinese Journal of Geophysics*, 53(5), 731-739.

Jin S., and Park, J. U. (2007). GPS ionospheric tomography: a comparison with the IRI-2001 model over South Korea. Earth Planet Space 59, 287–292, 2007.

Jin, S. G., Cho, J. H., and Park, J. U. (2007). Ionospheric slab thickness and its seasonal variations observed by GPS. *Journal of Atmospheric and Solar-Terrestrial Physics*, 69, pp.1864–1870, 2007.

Jusoh, M. H., Bakar, F. N. A., Sulaiman, A. A., Baba, N. H., Awang, R. A., and Khan, Z. I. (2008). Determination of traveling ionospheric disturbances of geomagnetic storm by using dual frequency GPS data. *2008 IEEE International RF and Microwave Conference*, pp. 361–366, Dec. 2008.

Katamzi, Z. T. 2011. *Statistical Analysis of Ionospheric Total Electron Content*. A thesis submitted for the degree of Doctor of Philosophy University of Bath Department of Electronic and Electrical Engineering March 2011.

King, M. A, Altamimi, Z., Boehm, J., Bos, M., Dach, R., Elosegui, P., ... Willis, P. (2010). Improved constraints on models of glacial isostatic adjustment: a review of the contribution of ground-based geodetic observations. *Surveys in Geophysics*, vol.31,465–507. doi:10.1007/s10712-010-9100-4

Klobuchar, J.A. (1996). Ionospheric effects in Global Positioning System: theory and applications, I, ed. Parkinson, B. W., and Spilker, J. J., American Institute of Aeronautics and Astronautics, Washington, D.C., USA.

Komjathy, A. (1997). *Global Ionospheric Total Electron Content Mapping Using the Global Positioning System.* (Doctoral dissertation, Department of Geodesy and Geomatics Engineering Technical Report", University of New Brunswick, Fredericton, New Brunswick, Canada). Retrieved from www2.unb.ca/gge/Pubs/TR188.pdf, last accessed October 29, 2014.

Krankowski, A., Kosek, W., Baran, L. W., and Popinski, W. (2005). Wavelet analysis and forecasting of VTEC obtained with GPS observations over European latitudes, *Journal of Atmospheric and Solar-Terrestrial Physics*, 67(12), 1147–1156.

Lachapelle, G., Cannon, K., and Alves, P. (2002). How Will Galileo Improve Positioning Performance? *GPS World*, 13 (9): 38 – 48.

Liu, J. Y., Chuo, Y. J., Shan, S. J., Tsai, Y. B., Chen, Y. I., Pulinets, S. A. and Yu, S. B. (2004). Preearthquake Ionospheric Anomalies Registered by Continuous GPS TEC Measurements. *Annals of Geophysics*, pp. 1588- 1589. Retrieved from http://www.ann-geophys.net.

Liu, J. Y., Tsai, H. F., and Tsai, L. C. (1999). Ionospheric total electron content observed during the 24 October 1995 solar eclipse, *Advances in Space Research*, 24(11), 1495-1498.

Liu, L. B. and Chen, Y. D. (2009). Statistical analysis of solar activity variations of total electron content derived at Jet Propulsion Laboratory from GPS observations, *Journal of Geophysical Research*, 114, A10311. doi:10.1029/2009JA014533.

Liu, L. B., Zhao, B. Q., Wan, W. X., Ning, B. Q., Zhang M. L., and He, M. S. (2009). Seasonal variations of the ionospheric electron densities retrieved from Constellation Observing System for Meteorology, Ionosphere, and Climate mission radio occultation measurements, *Journal of Geophysical Research*, 114, A02302. doi:10.1029/2008JA013819.

Liu, L., Wan, W., Yue, X., Zhao, B., Ning, B., and Zhang, M. L. (2007). The dependence of plasma density in the topside ionosphere on solar activity level, *Annals of Geophysics*, 25(6), 1337–1343.

Liu, Z. Z., and Gao, Y. (2001). Ionospheric tomography using GPS measurements. *Proceedings of the International Symposium on Kinematic Systems in Geodesy, Geomatics and Navigation*, June 5-8, Banff, Alberta, Canada, 111-120.

Loewe, C. A. and Prölss, G. W. (1997). Classification and mean behaviour of magnetic storms. *Journal of Geophysical Research*, 102, pp. 14209- 14213.

Lui, H., Luhr, H., Watanabe, S., Kohler, W., and Maoj, C. (2007). Contrasting behavior of the thermosphere and ionosphere in response to the 28 October 2003 solar flare. *Journal Geophysical Research*, 112, A07305, doi:10.1029/ 2007JA012313, 2007.

Malik, R., Sarkar, S., Mukherjee, S., and Gwal, A. K. (2010). Study of ionospheric variability during geomagnetic storms. *Journal of Indian Geophysics Union*, 14, 47-56, 2010.

Maltseva, O. A., Mozhaeva, N. S., Poltavsky, O. S., and Zhbankov, G. A. (2012). Use of TEC global maps and the IRI model to study ionospheric response to

geomagnetic disturbances. *Advances in Space Research*, vol.49, pp. 1076–1087, 2012.

Mannucci, A. J., Tsurutani, B. T., Iijima, B. A., Komjathy, A., Saito, A., Gonzalez, W. D., ... Skoug, R. (2005). Dayside global ionospheric response to the major interplanetary events of October 29–30, 2003 ‘‘Halloween storms,’’, *Geophysical Research Letters*, 32, L12S02. doi:10.1029/2004GL021467.

Mansoori, A. A., Khan, P. A., Bhawre, P., Gwal, A. K. Purohit, P. K. (2013). Variability of TEC at mid latitude with solar activity during the solar cycle 23 and 24, *Proceeding of the 2013 IEEE International Conference on Space Science and Communication (IconSpace)*, 1-3 July 2013, Melaka, Malaysia pp139-143.

Maruyama, T., Ma, G., and Nakamura, M. (2004). Signature of TEC storm on 6 November 2001 derived from dense GPS receiver network and ionosonde chain over Japan. *Journal of Geophysical Research*, 109, A10302, doi:10.1029/2004JA010451, 2004.

McNamara, L. (1991). The Ionosphere: Communications, Surveillance, and Direction Finding. *Orbit: A Foundation Series*, Kreiger Publishing Company, Malabar, Florida, 1991.

Memarzadeh, Y. (2009). *Ionospheric modeling for precise GNSS applications*. (Doctoral thesis, Delft University of Technology). Retrieved from http://repository.tudelft.nl.

Mendes, C. A, Vilas, B., Williams, J., and Edvaldo S. (2004). GPS Total Electron Content measurements at low latitudes in Brazil for low solar activity. *Geofísica Internacional*, january-march-2004, 129-137.

Moeketsi, D. M. (2008). *Solar cycle effects on GNSS-derived ionospeheric total electron content observed over Southern Africa*. (Doctotral thesis, Rhodes University, South Africa).

Moeketsi, D. M., Combrinck, W. L., McKinnell, L. A., and Fedrizzi, M. (2007). Mapping GPS¬derived ionospheric total electron content over southern Africa during different epochs of solar cycle 23, *Advances in Space Research*, 39, 821–829.

Mubarak, W. A., Abdullah, M., and Misran, N. (2008). Total Electron Content variation before the Sumatra earthquake of 12 September 2007. *Proceedings of the Engineering Postgraduate Conference 2008*, pp. 1-6, 2008.

Mukhtarov, P., Pancheva, D., Andonov, B., and Pashova, L. (2013). Global TEC maps based on GNSS data: 1. Empirical background TEC model. *Journal of Geophysical Research: Space Physics*, 118, doi:10.1002/jgra.50413.

Mulassano, P., Dovis, F., and Cllomb, F. (2004). European projects for innovative GNSS-related applications. *GPS Solutions*, 7, 268-270.

Najman, P. (2012). Nature of the GNSS ionospheric error and modeling of mid-latitudes ionospheric structures in relation to the space weather. *Kvalifacijski Doktorski Ispit*, August 2012.

NASA (2012). Global Ionospheric (TEC) Maps. Retrieved July 10, 2014, from http://www.iono.jpl.nasa.gov/gim.html, last accessed Octoer 29, 2014.

NASA. (2011). *Valentine's Day Solar Flare, NASA, February 17, 2011*. Retrieved Semptember 09, 2014, from http://www.nasa.gov/mission_pages/sunearth/news/News021411-xclass.html, last accessed Octoer 29, 2014.

Natali, M. P. and Meza, A. (2011). Annual and semiannual variations of vertical total electron content during high solar activity based on GPS observations. *Annals of Geophysics*, 29, pp. 865–873. Retrieved from http://www.ann-geophys.net, last accessed Octoer 29, 2014

NOAA (2012). What is GPS? Retrieved from http://www.gps.gov/systems/gps, last accessed Octoer 29, 2014.

Ojigi, L. M. (2014). *GEOM 810 Satellite Altimetry and Applications, Course Notes*. Department of Geomatics, Ahmadu Bello University, Zaria, Nigeria.

Olwendo, O. J., Baki, P., Cilliers, P. J., Mito, C., Doherty, P. (2012). Comparison of GPS TEC measurements with IRI-2007 TEC prediction over the Kenyan region during the descending phase of solar cycle 23. *Advances in Space Research*, vol.49, pp. 914–921.

Opperman, B. D. L. (2007). *Reconstructing Ionospheric TEC over South Africa using signals from a regional GPS network.* (Doctoral thesis, Rhodes University).

Oron, S., D'ujanga, F. M., and Ssenyonga, T. J. (2013). Ionospheric TEC variations during the ascending solar activity phase at an equatorial station, Uganda. *Indian Journal of Radio & Space Physics*, 42, 7-17.

Ouattara, F., Fleury, R. (2011). Variability of CODG TEC and IRI 2001 total electron content (TEC) during IHY campaign period (21 March to 16 April 2008) at Niamey under different geomagnetic activity conditions. *Scientific Research and Essays*, 6 (17), 3609-3622.

Pedatella, N. M., Lei, J., Larson, K. M., and Forbes, J. M. (2009). Observations of the ionospheric response to the 15 December 2006 geomagnetic storm: Long-duration positive storm effect. *Journal of Geophysical Research*, 114, pp.12313-12323.

Perevalova, N. P., Afraimovich, E. L., Voeykov, V., and Zhivetiev, I. V. (2008). Parameters of large-scale TEC disturbances during the strong magnetic storm on 29 October 2003. *Journal of Geophysical Research*, vol.113, pp.13-26.

Perevalova, N. P., Polyakova, A. S., and Zalizovski, A. V. (2010). Diurnal variations of the total electron content under quiet heligeomagnetic condictions, *Journal of Atmospheric and Solar-Terrestrial Physics*, 72, 997–1007.

Perez, R. O. (2005). *Contributions on the improvement, assessment and application of the Global Ionospheric VTEC Maps computed with GPS data.* (Doctoral thesis, Universitat Politechnica de Catalunya (UPC) Spain, Research group of Astronomy and Geomatics).

Petrie, E. J., Hernández-Pajares, M., Spalla, P., Moore, P., and King, M. A. (2011). A review of higher order ionospheric refraction effects on dual frequency GPS. *Surveys in Geophysics*, 32, 197–253. doi:10.1007/s10712-010-9105-z.

Prasad, S. N. V. S., Rama Rao, P. V. S., Prasad, D. S. V., Venkatesh, K., Niranjan, K. (2012). On the variabilities of the Total Electron Content (TEC) over the Indian low latitude sector, *Advances in Space Research*, 49(5), 898-913, ISSN 0273-1177.

Prikryl, P., Jayachandran, P. T., Mushini, S. Pokhotelov, C. D., MacDougall, J. W., Donovan, E., ... St. Maurice, J. P. (2010). GPS TEC, scintillation and cycle slips observed at high latitudes during solar minimum. *Annals of Geophysics*, 28, 1307–1316. Retrieved from http://www.ann-geophys.net.

Priya, S., and Parameswari, A. (2013). Predictive Models for Vertical Total Electron Content in Ionosphere. *International Journal of Innovative Technology and Exploring Engineering (IJITEE) ISSN: 2278-3075*, 2, Issue-5.

Pulinets, S., and Boyarchuk, K. (2003). *Ionospheric Precursors of Earthquakes*. Berlin Heidelberg New York : Springer.

Radicella, S. M. and Nava, B. (2010). NeQuick model: Origin and evolution. *Proceedings of the 9th International Symposium on Antennas, Propagation and EM Theory*, 2, pp. 422–425.

Rama Rao, P. V. S., Gopi, K. S., Niranjan, K., and Prasad, D. S. V. T. (2006). Temporal and spatial variations in TEC using simultaneous measurements from the Indian GPS network of receivers during the low solar activity period of 2004–2005, *Annals of Geophysics*, 24, 3279–3292, doi:10.5194/angeo-24-3279-2006.

Ray, J. (2000). *Mitigation of GPS code and carrier phase multipath effects using a multiantenna system.* (Doctoral Thesis, Department of Geomatics Engineering, University of Calgary, Calgary, Canada). Retrieved from www.ucalgary.ca/engo_webdocs/MEC/00.20136.JayantaRay.pdf.

Ray, J., Cannon, M. E., and Fenton, P. (1998). Mitigation of static carrier phase multipath effects using multiple closely-spaced antennas. *Proceedings of ION GPS-98, Nashville, Tennessee, Institute of Navigation*, pp. 1025-1034.

Ray, S., Paul, A., and DasGupa, A. (2006). Equatorial scintillation in relation with the development of ionization anomaly, Annals of Geophysics, 24, 1429-1442. Retrieved from http://www.ann-geophys.net.

Saastamoinen, J. (1973). Contribution of the theory of atmospheric refraction. *Bulletin of Geodesique*, No. 105, pp. 279-298, No. 106, pp. 383-397, No. 107, pp. 13-34.

Saito, A., Fukao, S., and Unnikrishnan, K. (2006). Differences in magnetic storm and quiet ionospheric deterministic chaotic behavior: GPS total electron content analyses. *Journal of Geophysical Research*, 111, pp.6304-6318.

Sardon, E., Rius A., Zarraoa, N. (19994). Estimation of the Transmitter and Receiver Differential Biases and the Ionospheric Total Electron Content from Global Positioning System Observations. *Radio Science*, Vol.29, 577-586.

Schaer, S. (1999). Mapping and predicting the Earth's ionosphere using the Global Positioning System. Geod.-Geophys. Arb. Schweiz, 59, 59.

Scherliess, L. D., Thompson, C., and Schunk, R. W. (2008), Longitudinal variability of low-latitude total electron content: Tidal in uences. *Journal of Geophysical Research*, 113, doi:10.1029/2007JA012480.

Schunk, R. W., and Nagy, A. F. (2000). *Ionospheres*. New York : Cambridge University press.

Sethi, N. K., Pandey, V. K., Mahajan, K. K. (2010). Comparative study of TEC with IRI model for solar minimum period at low latitude. *Advances in Space Research*, 27, pp. 45–48.

Sharma, S., Dashora, N., Galav, P., and Pandey, R. (2010). Total solar eclipse of July 22, 2009: its impact on the total electron content and ionospheric electron density in the Indian zone, *Journal of Atmospheric and Solar-Terrestrial Physics* , 72, 1387–1392.

Shrestha, S. M. (2003). *Investigations into the Estimation of Tropospheric Delay and Wet Refractivity Using GPS Measurements.* (Master's thesis, University of Calgary, Alberta). Retrieved from http://www.geomatics.ucalgary.ca/links/GradTheses.html, last accessed October 29, 2014.

Siqueira, P. M., Paula, E. R., Muella, M. T. A. H., Rezende, L. F. C., Abdu, M. A. and Gonzalez, W. D. (2011). Storm-time total electron content and its response to penetration electric fields over South America, *Annals of Geophysics*, 29, 1765–1778. doi:10.5194/angeo-29-1765-2011.

Skone, S., and Coster, A. (2008). Potential for issuing ionospheric warnings to Canadian users of marine DGPS. *Space Weather*, 6, S04D03, doi:10.1029/2007SW000336.

Spaceweather. (2011). *Time Machine*. Retrieved September 27, 2014 from http://spaceweather.com/archive.php?view=1&day=15&month=02&year=2011.

Spogli, L., Alfonsi, L., De Franceschi, G., Romano, V., Aquino, M. H. O., and Dodson, A. (2009). Climatology of GPS ionospheric scintillations over high and mid-latitude European regions. *Annals of Geophysics*, 27, 3429–3437, 2009. Retrieved from http://www.ann-geophys.net.

Stamatis, S. K., Xenos, T. D., Polimeris, K. V., and Stergiou, D. (2004). TEC and *fo*F2 variations: preliminary results, *Annals of Geophysics*, 47, 1325–1332.

Stanislawska, I. and Cander, L. R. (1999). Coordinated SRC and RAL Centres for ionospheric weather specification and forecasting. *ESA Workshop on Space Weather*, 11-13 November 1998, ESTEC, Noordwijk, The Netherlands, WPP-155, pp. 499-552.

Stanislawska, I., Bradley, P. A. and Juchnikowski, G. (2002). Spatial correlation assessment of ionospheric parameters for limited-area mapping. *Proceedings of the XXVIIth General Assembly of the International Union of Radio Science*, Maastricht, Netherlands, 17-24.

Stankov, S. M. (2009). Trans-ionospheric GPS signal delay gradients observed over mid-latitude Europe. *Advances in Space Research*, 43, pp. 1314–1324.

Stankov, S. M., and Warnant, R. (2009). Ionospheric slab thickness analysis, modelling, and monitoring. *Advances in Space Research*, 44, pp. 1295–1303.

Strangeways, A. M., and Walsh, H. J. (2007). Effects of ionospheric horizontal gradients on differential GPS. *Acta Geophysica*, 55, pp.509-523.

The Watchers. (2012). *Major X1.1 Solar Flare peaked around sunspot 1429*. Retrieved September 27, 2014 from http://thewatchers.adorraeli.com/2012/03/05/major-x1-1-solar-flare-peaked-around-sunspot-1429-on-march-5th-2012/.

Tiwari, R. A., Soumi, B., Purohitb, P. K., and Gwala, A. K. (2009). Effect of TEC Variation on GPS Precise Point at Low Latitude. *The Open Atmospheric Science Journal*, 3, 1-12.

Tsurutani, B. T., Judge, D. L., Guarnieri, F. L., Gangopadhyay, P., Jones, A. R., Nuttall, J., ... Viereck, R. (2005). The October 28, 2003 extreme EUV solar flare and resultant extreme ionospheric effects: Comparison to other halloween events and the Bastille Day event. *Geophysical Research Letters*, 32, DOI: 10.1029/2004GL021475.

Universe Today. (2012). *Sun releases a powerful X5 flare*. Retrieved September 27, 2014 from http://www.universetoday.com/94018/sun-releases-a-powerful-x5-flare/

Van Dierendonck, A. J., Fonton, P., and Ford, T. (1992). Theory and performance of narrow correlator spacing in a GPS receiver. *Navigation*, 30, No. 3 Fall, pp. 265-283.

Vanlomme, P., Cugnon, P., Van Der Linden, R., Berghmans, D., and Clette, F. (2005). The SIDC: World Data Center for the Sunspot Index, Solar Physics, 2004-10-01, Springer Netherlands, 0038-0938, *Phys. Astron.*, 224 (1), 113–120. doi: 10.1007/s11207-005-6504-2.

Vladimer, J. A., Jastrzebski, P., Lee, M. C., Doherty, P. H., Decker, D. T., and Anderson, D. N. (1999). Longitude structure of ionosphere total electron content at low latitudes measured by the TOPEX/Poseidon satellite. *Radio Science*, 34, 1239-1260.

Warnant, R. (1997). Reliability of the TEC computed using GPS measurements -the problem of hardware biases. *Acta Geodaetica et Geophysica*, 32, pp. 451-459.

Webster, R. and Olivier, M. (2001). *Geostatistics for Environmental Scientists*. New York: John Wiley and Sons.

Wielgosz, P., Dorota, G., and Kashani, I. (2003). Regional Ionosphere Mapping with Kriging and Multiquadric Methods. *Journal of Global Positioning Systems*, 2, No. 1: 48-55.

Wienia, R. J. (2008). *Use of global ionospheric maps for precise point positioning*. (Master's scriptie, Delft University of Technology, Faculty of Aerospace Engineering, Section Mathematical Geodesy and Positioning (MGP)). Retrieved

from http://repository.tudelft.nl/assets/uuid:dec284ff-7f52-4ad3-bfc0-28b4b1851bcd/ae_wienia_2008.pdf.

Wu, S., Zhang, K., Yuan, Y., and Wu, F. (2006). Spatio-temporal Characteristics of the Ionospheric TEC Variation for GPSnet-based Realtime Positioning in Victoria, *Journal of Global Positioning Systems,* 5, 52–57.

Wu, Y. W., Liu, R. Y., Zhang, B. C., Wu, Z. S., Ping, J. S., Liu, J. M., and Hu, Z. J. (2012). Variations of the ionospheric TEC using simultaneous measurements from the China Crustal Movement Observation Network, *Annals of Geophysics*, 30, 1423-1433. doi:10.5194/angeo-30-1423-2012.

Ya'acob, N., Abdullah, M. E, and Ismail, M. (2010). GPS Total Electron Content (TEC) Prediction at Ionosphere Layer over the Equatorial Region, Trends in Telecommunications Technologies, Christos J Bouras (Ed.), ISBN: 978-953-307-072-8, InTech, DOI: 10.5772/8474. Retrieved from: http://www.intechopen.com/books/trends-in-telecommunications-technologies/gps-total-electro-content-tec-prediction-at-ionosphere-layer-over-the-equatorial-region.

Ya'acob, N., Abdullah, M., Ismail, M., and Zaharim, A. (2009). Model Validation for GPS Total Electron Content (TEC) using 10th Polynomial Function Technique at an Equatorial Region. *WSEAS Transactions on Computers*, 8, pp.1533-1542. Retrieved from www.wseas.us/e-library/transactions/computers/2009/32-418.pdf.

Yizengaw, E. (2004). *Imaging the Ionosphere.* (Doctoral thesis, La Trobe University, Australia). Retrieved from http://www.igpp.ucla.edu/public/ekassie/Publications/PHD_thesis_title.pdf.

Yizengaw, E., and Essex, E. A. (2002). Storm Time Seasonal Variation of TEC on the Southern Hemisphere Mid-Latitude Regions Using Signals from Gps Satellite. *OIST-4 proceedings*, pp.221-224.

Yoshimura, R., Maruyama, T., and Kawamura, S. (2002). Application of dynamical equilibrium model to topside ionosphere specification, *Journal Geophysics Research,* 107, 1468- 1471.

Yu, T., Wan, W. X., and Liu, L. B. (2006). Using IGS data to analysis the global TEC annual and semiannual variation, *Chinese Journal of Geophysics,* 49, 943–949.

Yue, X., Wan, W., Liu, L., and Mao, T. (2007). Statistical analysis on spatial correlation of ionospheric day-to-day variability by using GPS and Incoherent Scatter Radar observations. *Annals of Geophysics*, 25, 1815–1825.

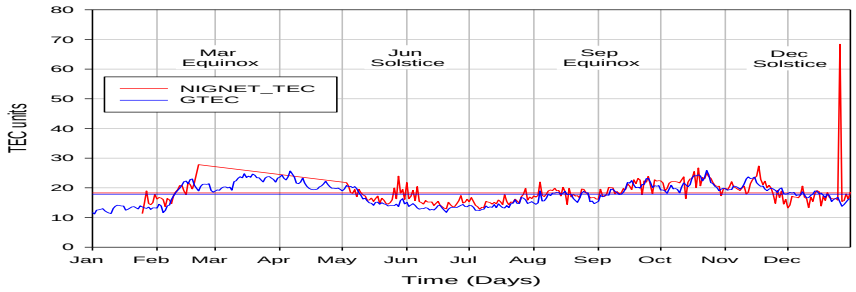
Zakharenkova, I. E., Cherniak, U. V, Krankowski, A., and Shagimuratov, I. I. (2013). Analysis of electron content variations over Japan during solar minimum: Observations and modeling, *Advances in Space Research,* 52(10), 1827-1836. ISSN 0273-1177.

Zhang, S. R., Coster, A., Holt, J., Foster, J., and Erickson, P. (2012). Ionospheric longitudinal variations at midlatitudes: Incoherent scatter radar observation at Millstone Hill, *Sci. China Tech. Sci*., 55, 1153–1160. doi:10.1007/s11431-012-4784-y, 2012..

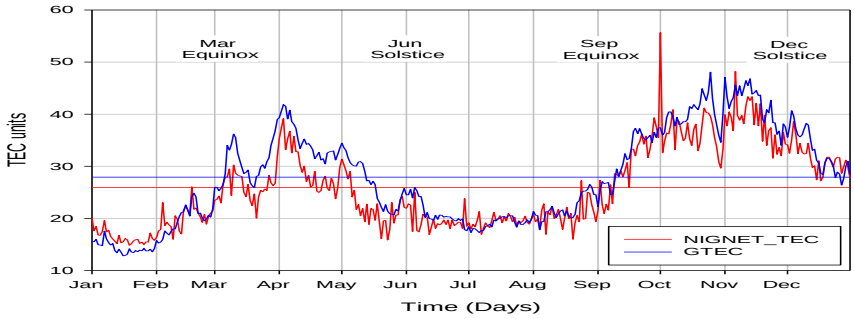
Zhang, S. R., Foster, J. C., Coster, A. J., and Erickson, P. J. (2011). East-West Coast differences in total electron contentover the continental US, *Geophysical Research Letters*, 38, L19101, doi:10.1029/2011GL049116.

APPENDICES

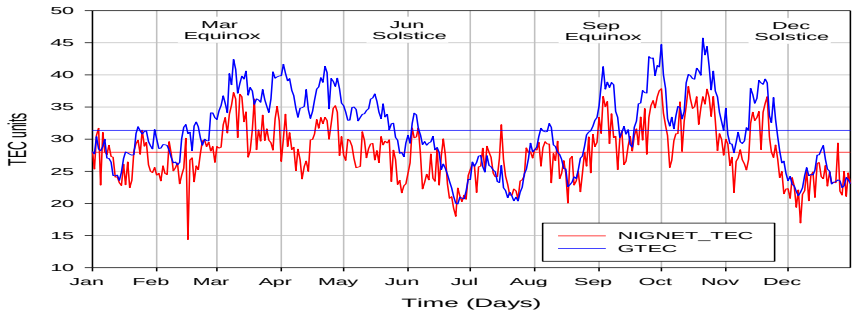
APPENDIX I: ANNUAL TEC TIME SERIES FOR THE NIGNET CORS



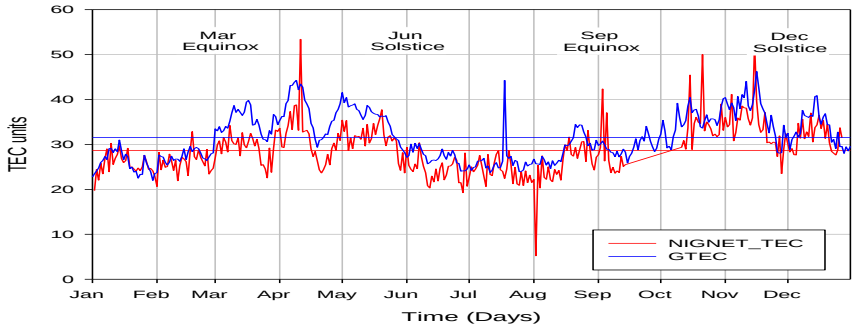
(a) Year 2010



(b) Year 2011

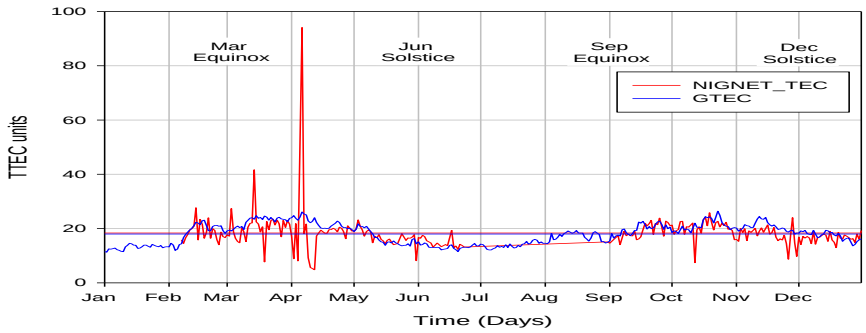


(c) Year 2012

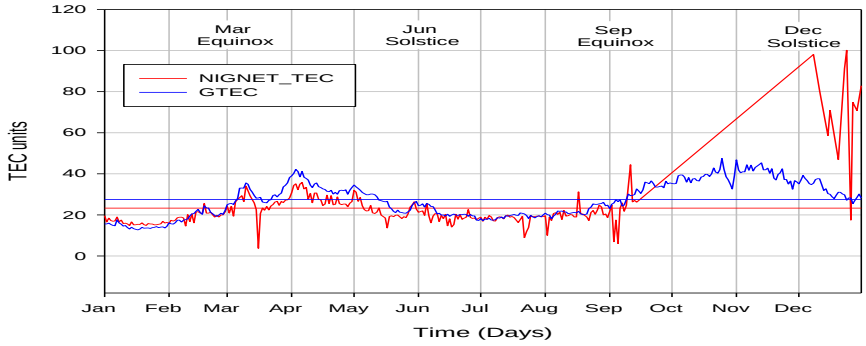


(d) Year 2013

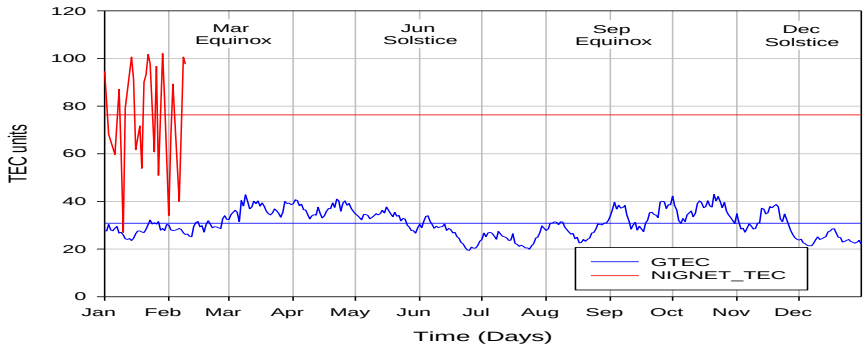
Annual TEC Time Series at BKFP NIGNET station 2010-2013



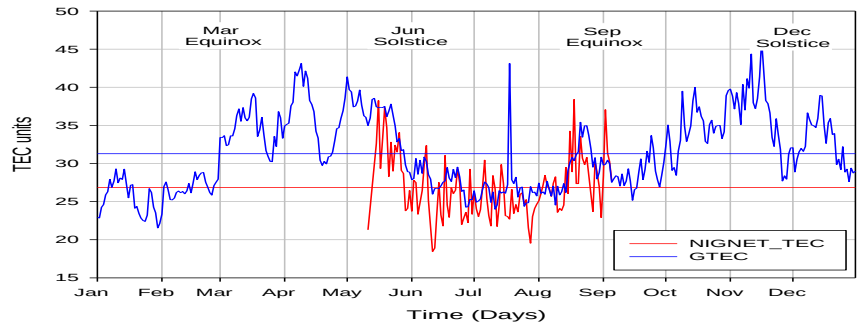
(a) Year 2010



(b) Year 2011

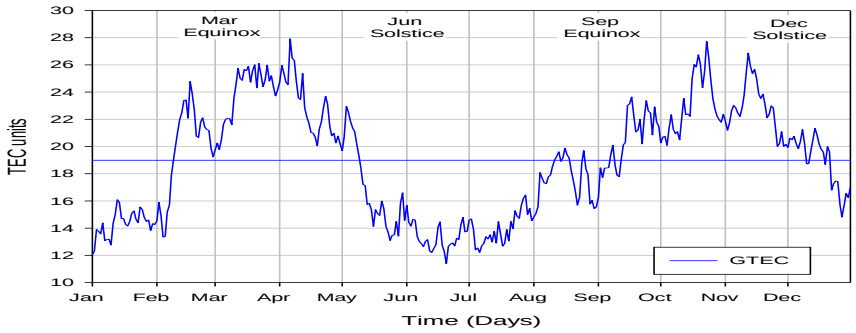


(c) Year 2012



(d) Year 2013

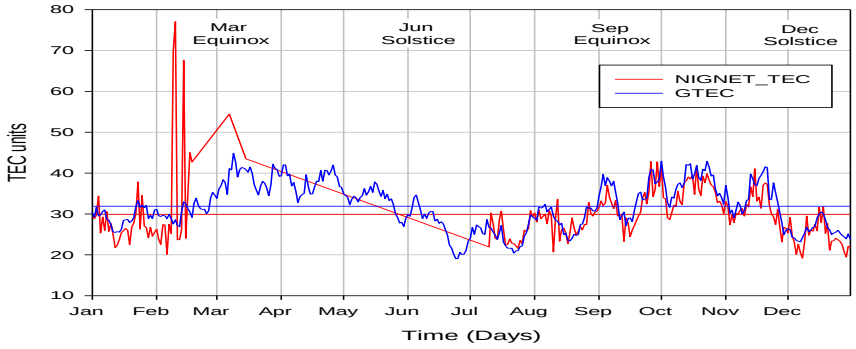
Annual TEC Time Series at CGGT NIGNET station 2010-2013



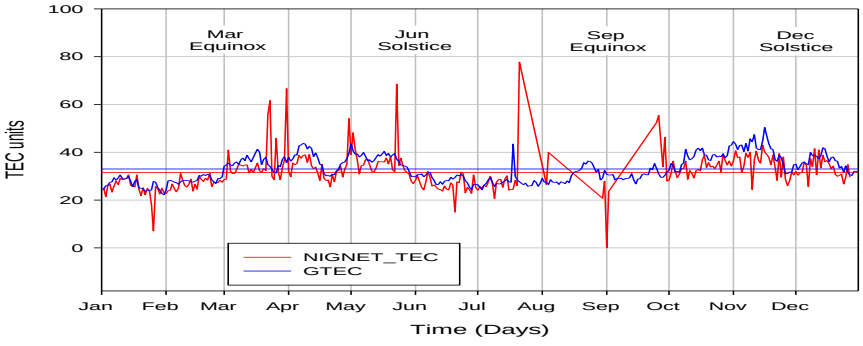
(a) Year 2010



(b) Year 2011

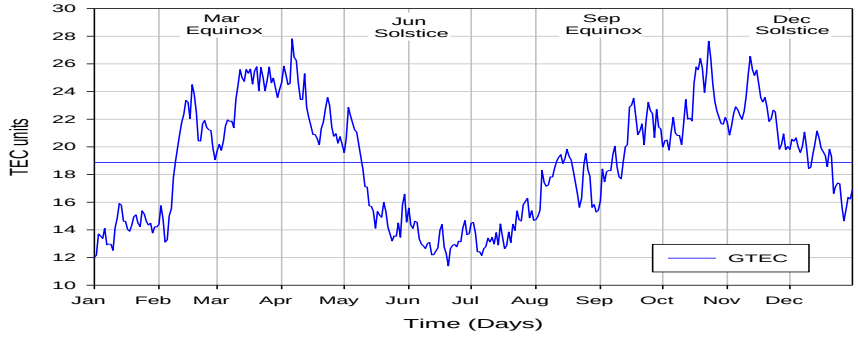


(c) Year 2012



(d) Year 2013

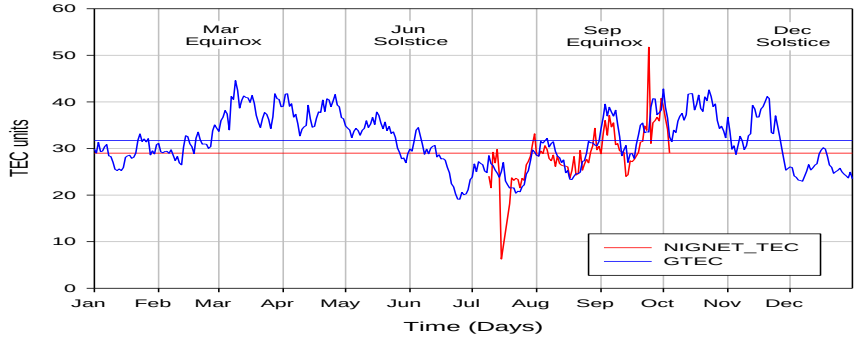
Annual TEC Time Series at CLBR NIGNET station 2010-2013



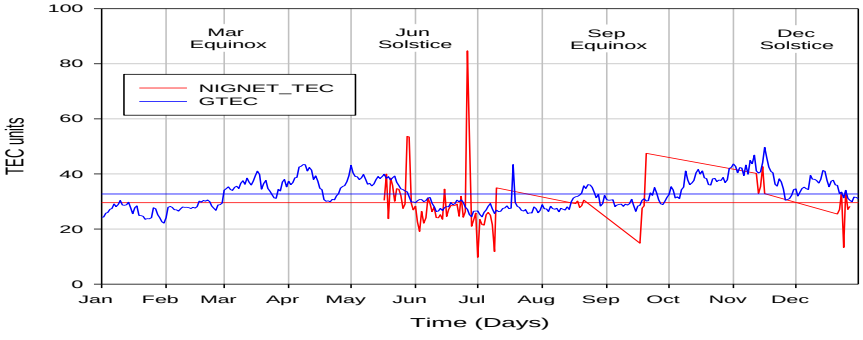
(a) Year 2010



(b) Year 2011

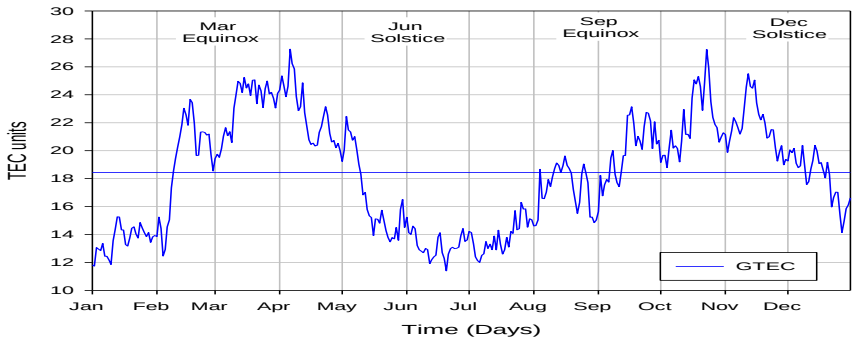


(c) Year 2012

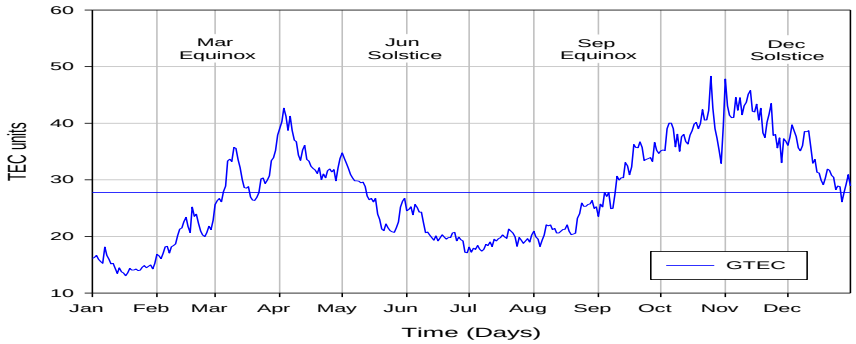


(d) Year 2013

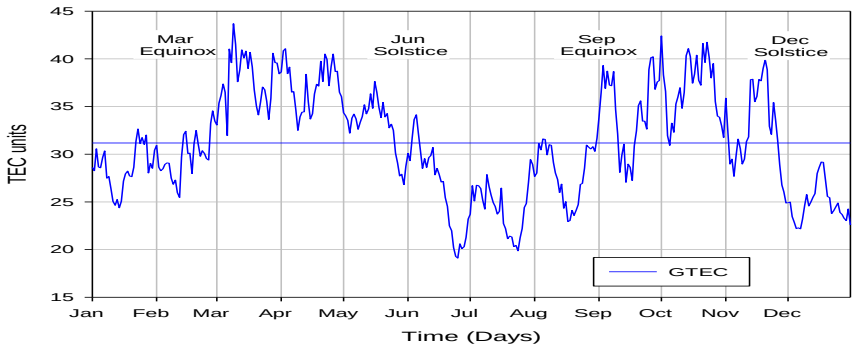
Annual TEC Time Series at FPNO NIGNET station 2010-2013



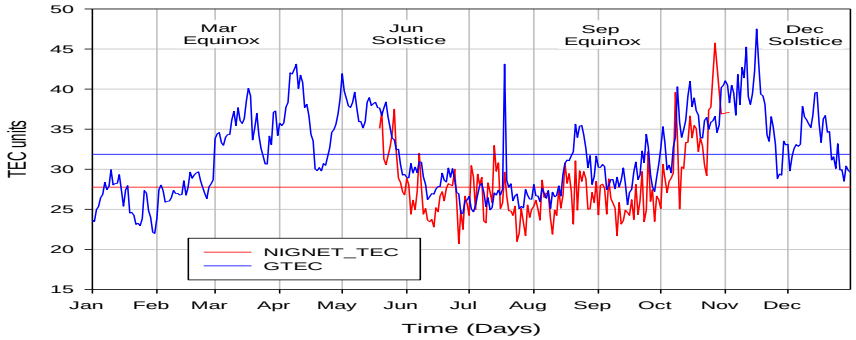
(a) Year 2010



(b) Year 2011

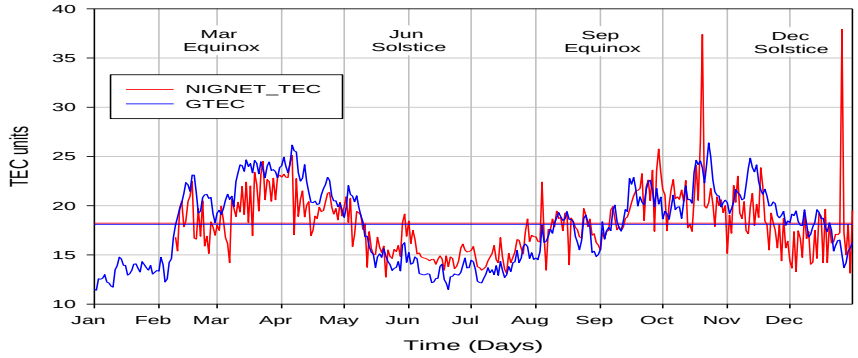


(c) Year 2012

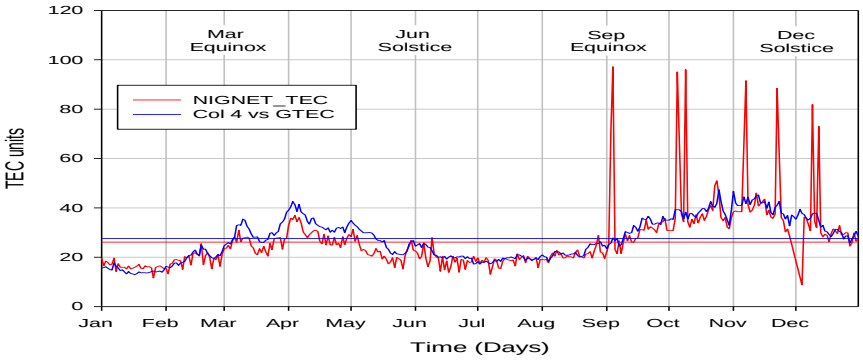


(d) Year 2013

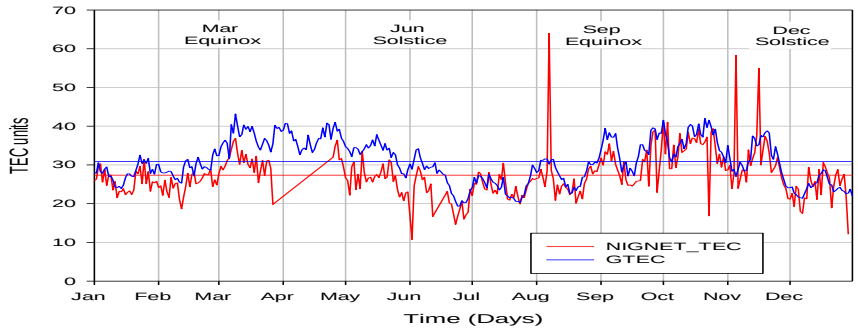
Annual TEC Time Series at FUTA NIGNET station 2010-2013



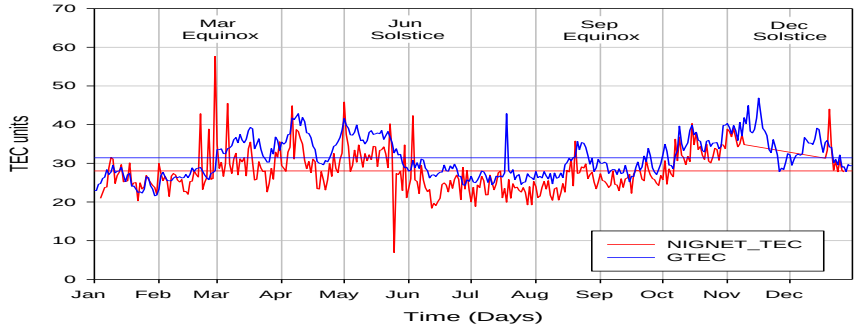
(a) Year 2010



(b) Year 2011

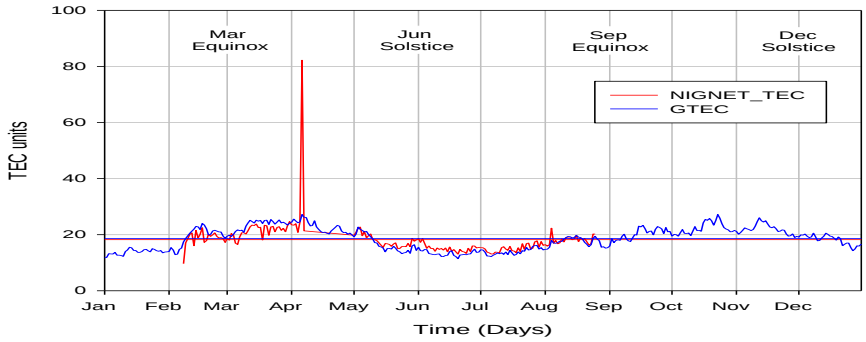


(c) Year 2012

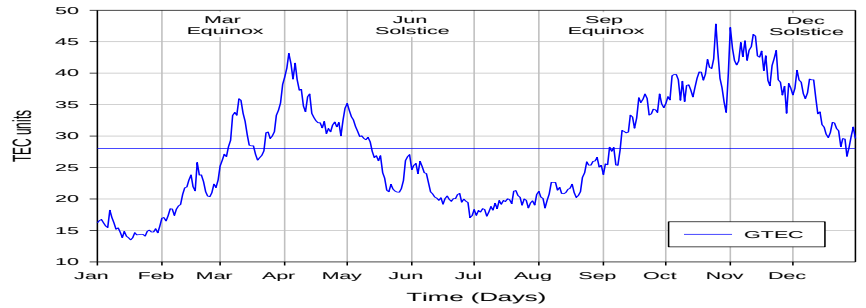


(d) Year 2013

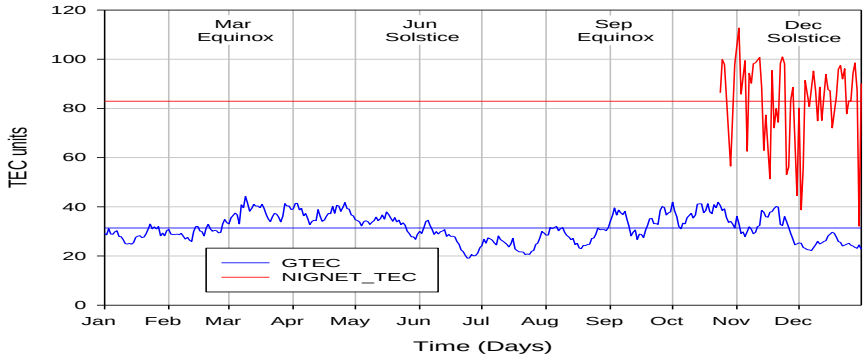
Annual TEC Time Series at FUTY NIGNET station 2010-2013



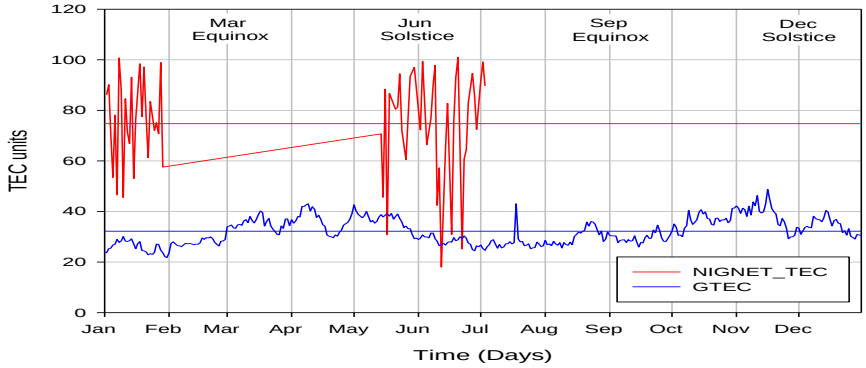
(a) Year 2010



(b) Year 2011

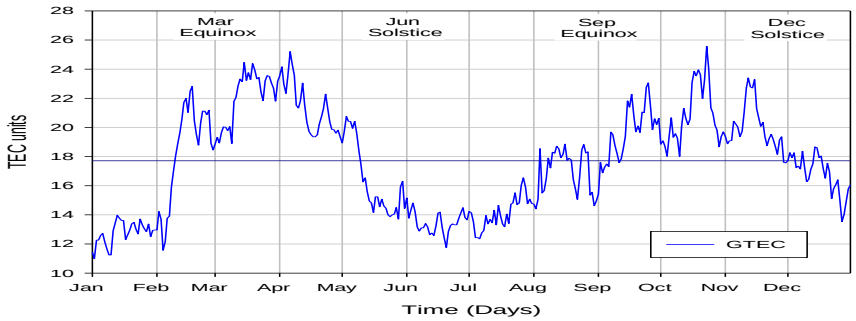


(c) Year 2012

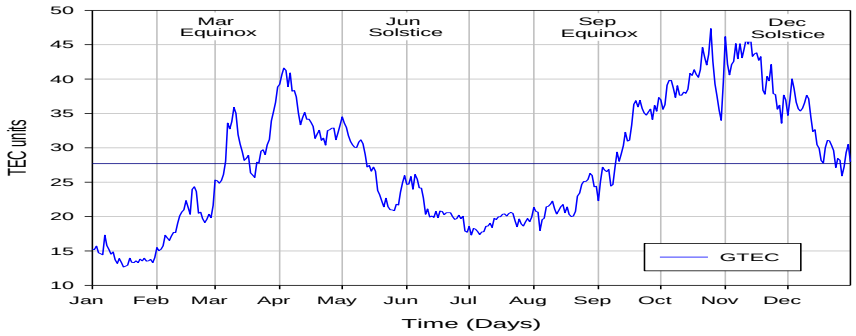


(d) Year 2013

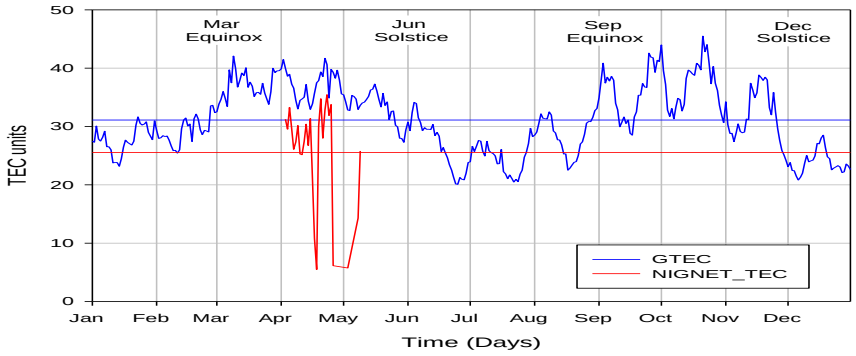
Annual TEC Time Series at GEMB NIGNET station 2010-2013



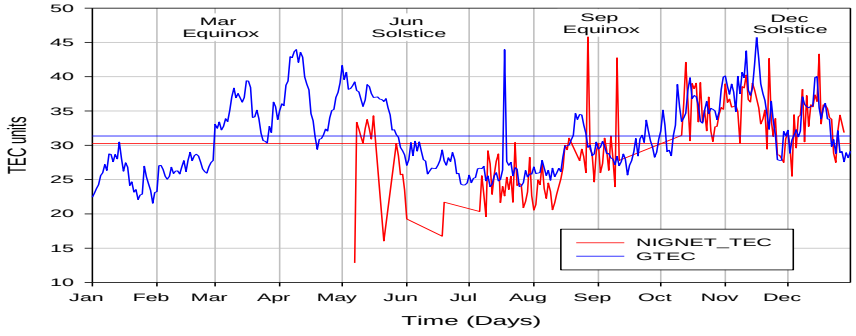
(a) Year 2010



(b) Year 2011

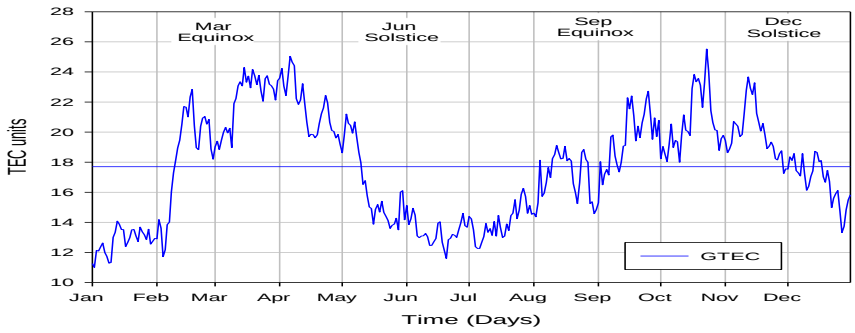


(c) Year 2012

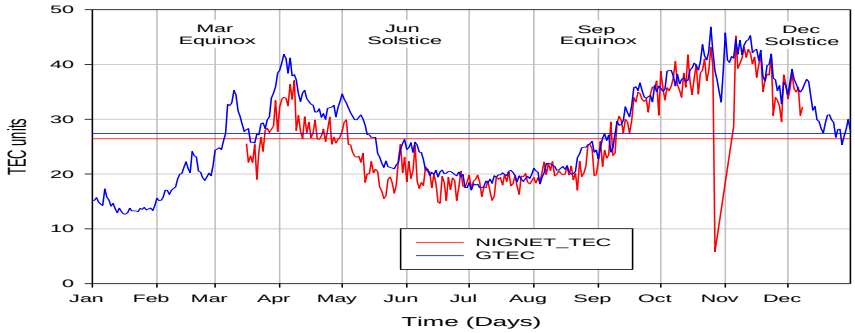


(d) Year 2013

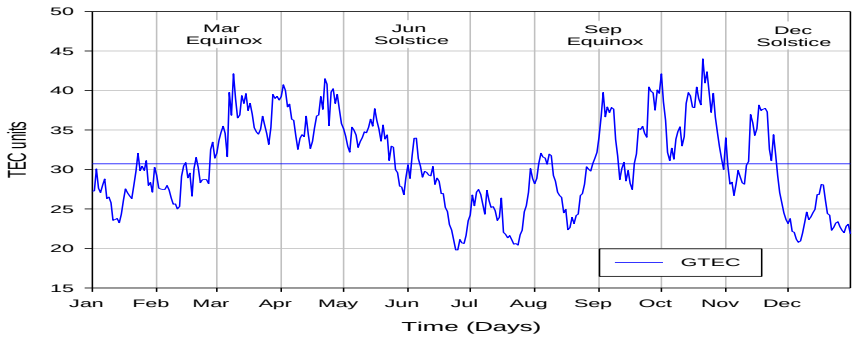
Annual TEC Time Series at HUKP NIGNET station 2010-2013



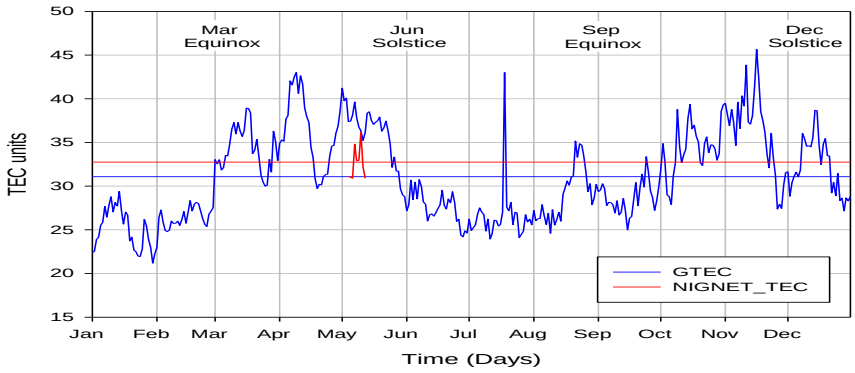
(a) Year 2010



(b) Year 2011

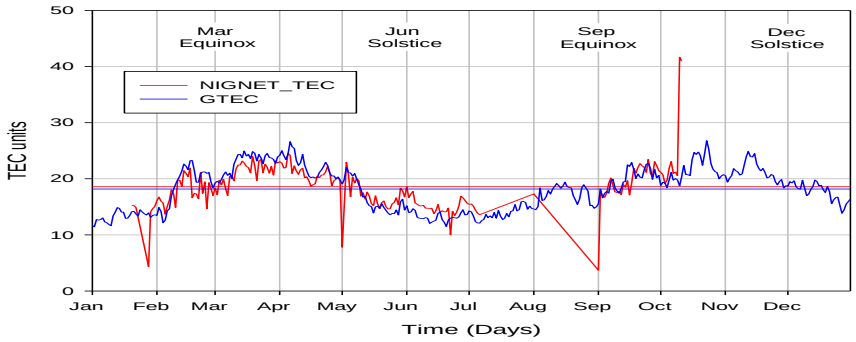


(c) Year 2012

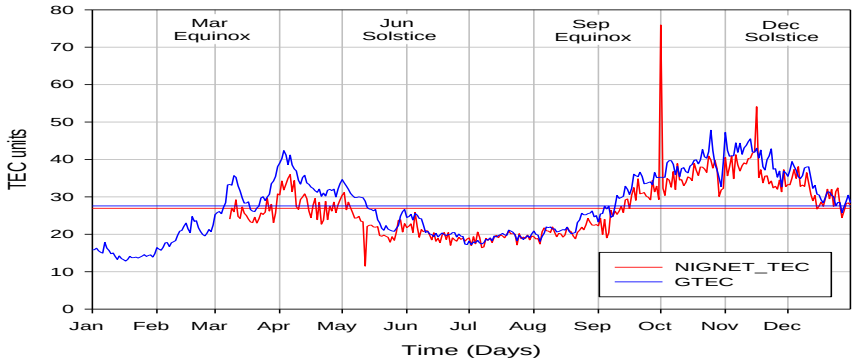


(d) Year 2013

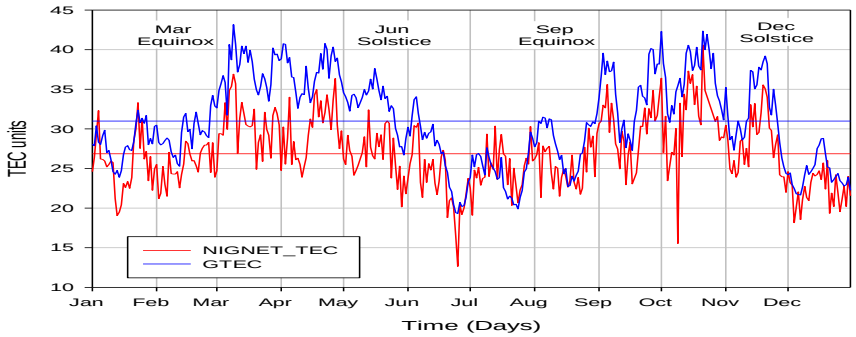
Annual TEC Time Series at MDGR NIGNET station 2010-2013



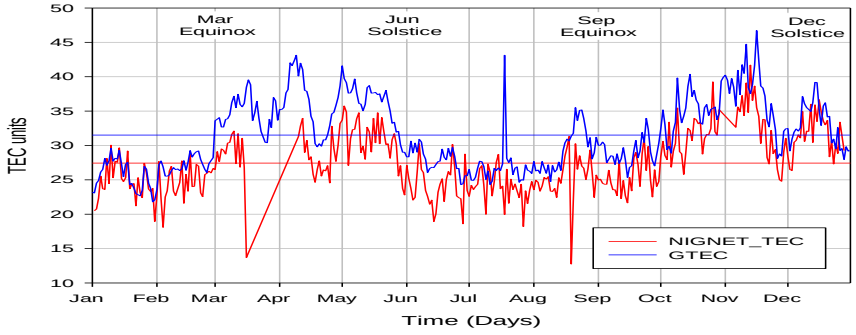
(a) Year 2010



(b) Year 2011

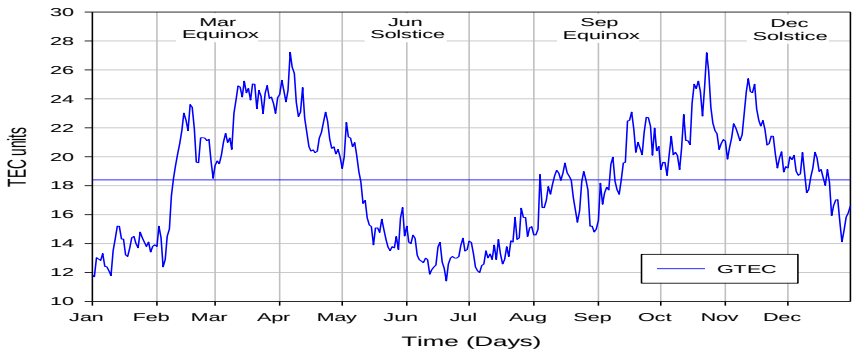


(c) Year 2012

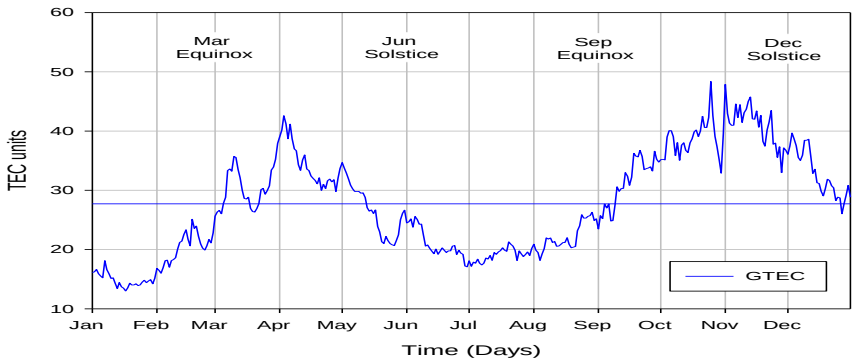


(d) Year 2013

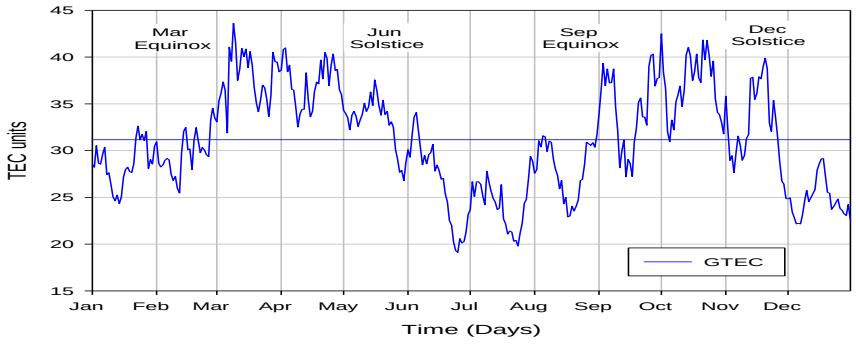
Annual TEC Time Series at OSGF NIGNET station 2010-2013



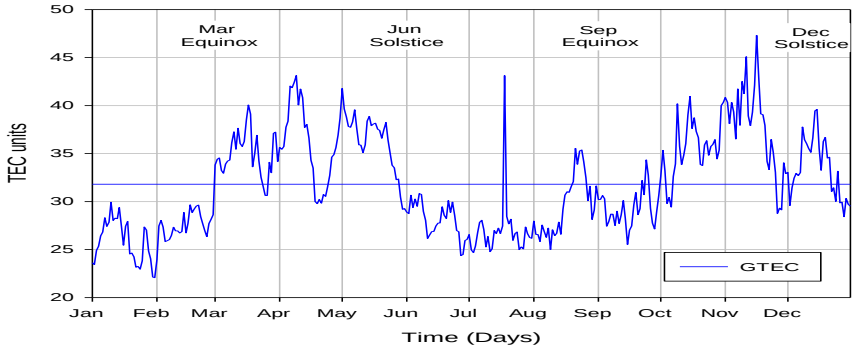
(a) Year 2010



(b) Year 2011

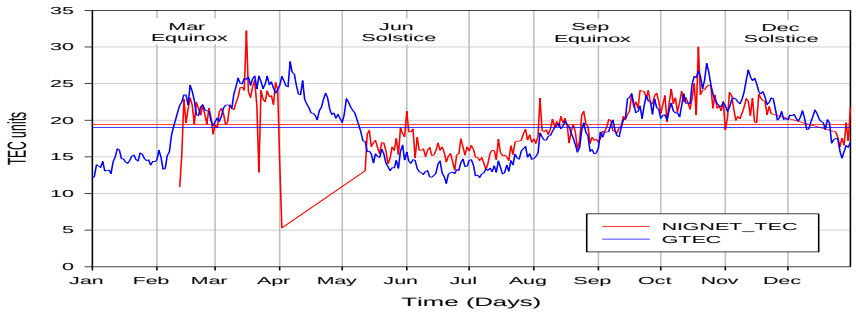


(c) Year 2012

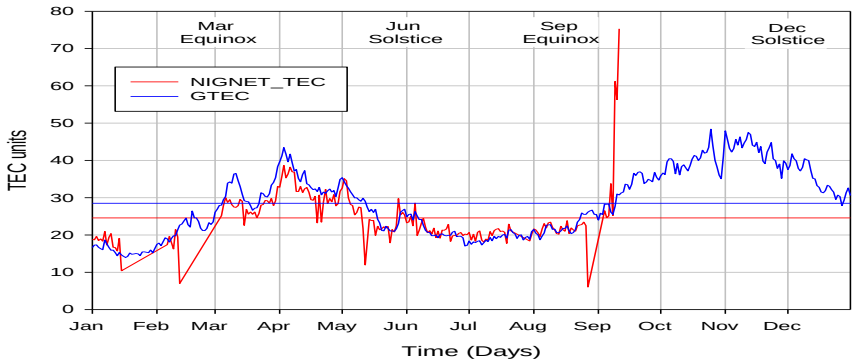


(d) Year 2013

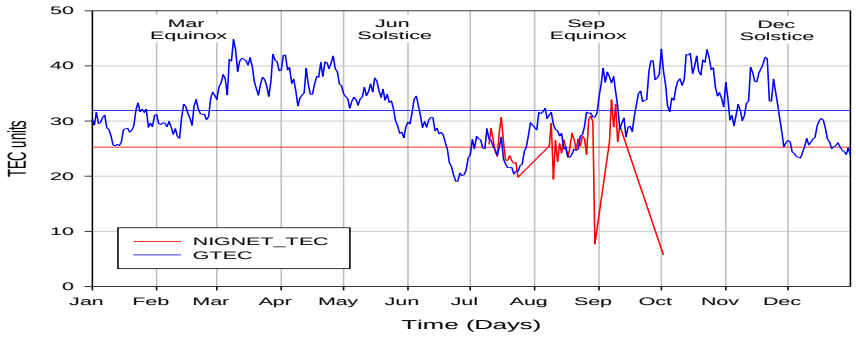
Annual TEC Time Series at RECT NIGNET station 2010-2013



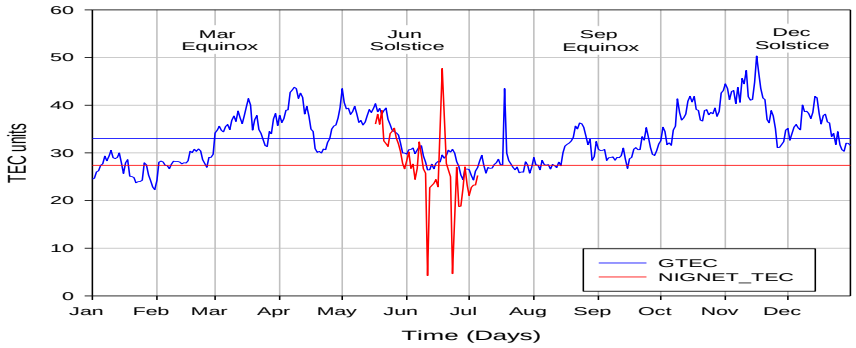
(a) Year 2010



(b) Year 2011

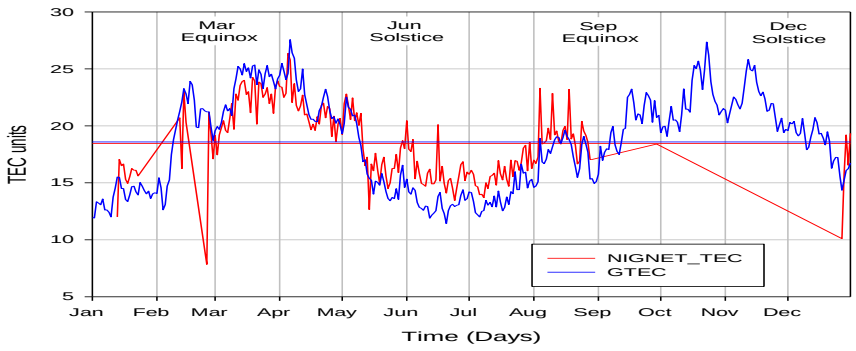


(c) Year 2012

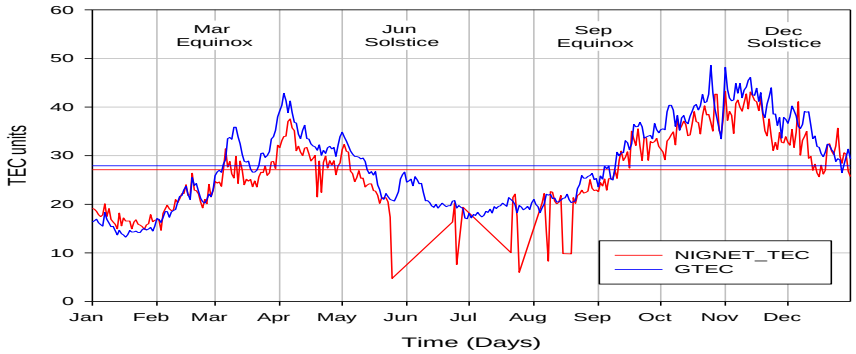


(d) Year 2013

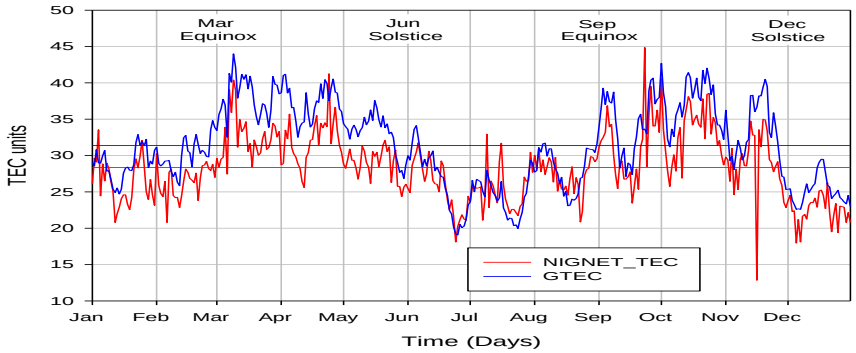
Annual TEC Time Series at RUST NIGNET station 2010-2013



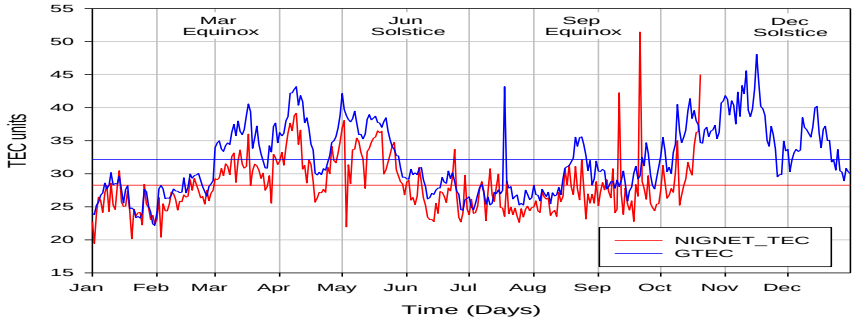
(a) Year 2010



(b) Year 2011

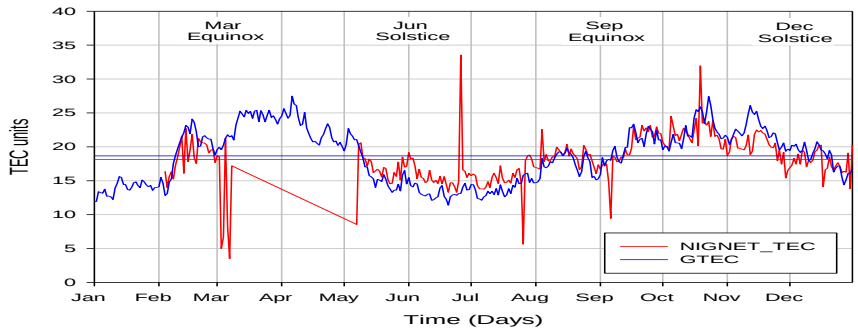


(c) Year 2012

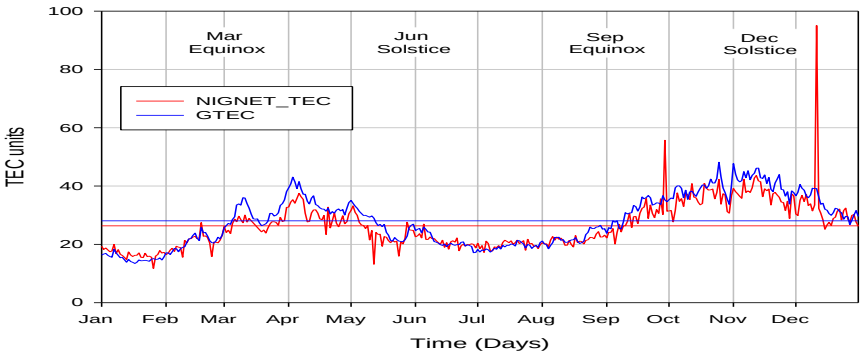


(d) Year 2013

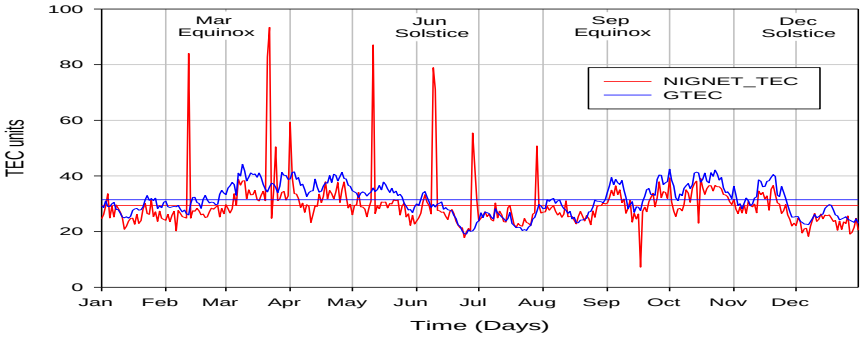
Annual TEC Time Series at ULAG NIGNET station 2010-2013



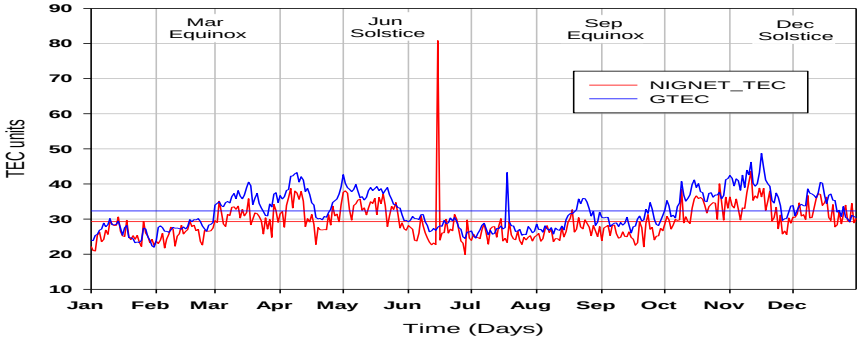
(a) Year 2010



(b) Year 2011



(c) Year 2012



(d) Year 2013

Annual TEC Time Series at UNEC NIGNET station 2010-2013

APPENDIX II: MONTHLY MEAN TEC AT THE NIGNET CORS

2010												
STN	JAN	FEB	MAR	APR	MAY	JUN	JUL	AUG	SEP	OCT	NOV	DEC
ABUZ	12.949	18.534	22.352	21.819	16.466	13.32	13.926	17.014	19.643	21.08	20.497	17.122
BKFP	12.95	18.56	22.256	21.475	16.378	13.407	14.113	16.942	19.712	21.149	20.362	17.087
CGGT	13.075	18.647	22.533	22.081	16.528	13.265	13.844	17.089	19.704	21.227	20.766	17.302
CLBR	14.274	19.787	23.871	23.002	16.877	13.347	13.964	17.624	20.5	23.066	22.881	18.913
FPNO	14.111	19.648	23.716	22.931	16.84	13.309	13.916	17.545	20.37	22.807	22.652	18.737
FUTA	13.595	19.19	23.163	22.613	16.697	13.218	13.817	17.281	19.986	22.013	21.832	18.104
FUTY	13.221	18.744	22.696	22.263	16.568	13.286	13.885	17.218	19.849	21.412	20.941	17.417
GEMB	13.787	19.303	23.327	22.752	16.756	13.321	13.925	17.466	20.222	22.311	21.97	18.203
HUKP	12.742	18.321	22.059	21.389	16.4	13.463	14.101	16.96	19.593	20.858	20.032	16.8
MDGR	12.739	18.262	22.118	21.639	16.422	13.362	13.972	17.029	19.549	20.706	20.031	16.746
OSGF	13.289	18.868	22.783	22.304	16.595	13.248	13.831	17.167	19.824	21.553	21.188	17.62
RECT	13.558	19.156	23.116	22.559	16.668	13.206	13.814	17.245	19.95	21.948	21.763	18.059
RUST	14.281	19.806	23.895	23.004	16.87	13.325	13.945	17.609	20.479	23.066	22.937	18.962
ULAG	13.789	19.375	23.383	22.706	16.71	13.207	13.84	17.33	20.083	22.276	22.171	18.383
UNEC	13.863	19.415	23.445	22.796	16.783	13.287	13.878	17.446	20.212	22.43	22.219	18.398
2011												
Stn	JAN	FEB	MAR	APR	MAY	JUN	JUL	AUG	SEP	OCT	NOV	DEC
ABUZ	14.24	19.533	29.969	34.612	26.569	21.201	19.044	22.014	31.16	38.914	40.883	40.883
BKFP	14.334	19.701	30.456	34.938	26.561	21.279	19.053	22.038	31.561	40.082	41.97	32.751
CGGT	14.334	19.641	29.891	34.512	26.577	21.144	19.047	22.059	31.062	38.505	40.599	32.088
CLBR	15.663	21.451	31.003	35.102	26.822	21.298	19.248	22.594	31.957	39.588	42.833	34.572
FPNO	15.466	21.17	30.833	34.944	26.751	21.236	19.205	22.481	31.784	39.322	42.364	34.147
FUTA	14.868	20.333	30.325	34.504	26.55	21.09	19.081	22.172	31.3	38.635	41.084	32.902
FUTY	14.501	19.848	29.885	34.555	26.697	21.208	19.103	22.2	31.14	38.466	40.75	32.364
GEMB	15.117	20.688	30.425	34.811	26.8	21.265	19.213	22.463	31.532	38.84	41.612	33.4
HUKP	14.095	19.387	30.052	34.868	26.662	21.401	19.111	22.04	31.359	39.575	41.415	32.18
MDGR	14.035	19.234	29.569	34.53	26.667	21.318	19.061	22.008	31	38.676	40.629	31.784
OSGF	14.552	19.925	30.08	34.525	26.572	21.12	19.064	22.113	31.162	38.556	40.782	32.406
RECT	14.831	20.278	30.312	34.462	26.514	21.061	19.055	22.127	31.276	38.654	41.053	32.848
RUST	15.664	21.447	31.024	35.066	26.778	21.259	19.22	22.543	31.948	39.614	42.851	34.595
ULAG	15.091	20.624	30.531	34.544	26.531	21.054	19.064	22.182	31.447	38.93	41.542	33.37
UNEC	15.182	20.777	30.566	34.79	26.711	21.204	19.177	22.388	31.56	38.953	41.732	33.536
2012												
STN	JAN	FEB	MAR	APR	MAY	JUN	JUL	AUG	SEP	OCT	NOV	DEC
ABUZ	27.84	29.193	37.063	37.145	33.112	26.612	24.402	28.168	35.084	36.892	31.939	23.971
BKFP	28.231	29.871	37.47	37.466	33.158	26.708	24.452	28.547	36.213	37.685	32.586	24.239
CGGT	27.883	29.099	37.091	37.085	33.09	26.545	24.399	28.013	34.564	36.644	31.862	24.047
CLBR	29.261	30.735	38.064	38.064	33.465	26.731	24.797	28.599	34.632	37.936	34.032	25.911
FPNO	29.074	30.494	38.569	37.846	33.379	26.671	24.681	28.438	34.544	37.701	33.7	25.64

STN	JAN	FEB	MAR	APR	MAY	JUN	JUL	AUG	SEP	OCT	NOV	DEC
FUTA	28.51	29.788	37.799	37.277	33.105	26.509	24.392	28.027	34.368	36.996	32.688	24.792
FUTY	28.011	29.124	37.234	37.164	33.177	26.583	24.549	28.057	34.253	36.637	31.954	24.201
GEMB	28.644	29.9	38.063	37.603	33.32	26.666	24.725	28.325	34.275	37.136	32.904	25.035
HUKP	27.69	29.245	36.988	37.317	33.283	26.837	24.544	28.52	35.861	37.28	32.015	23.82
MDGR	27.475	28.629	36.602	37.004	33.24	26.703	24.514	28.117	34.717	36.626	31.453	23.606
OSGF	28.141	29.388	37.393	37.171	33.089	26.528	24.4	28.026	34.502	36.776	32.184	24.346
RECT	28.506	29.785	37.757	37.231	33.063	26.48	24.348	27.997	34.422	37	32.667	24.753
RUST	29.287	30.774	38.829	38.023	33.437	26.698	24.738	28.558	34.659	37.991	34.095	25.948
ULAG	28.808	30.138	38.087	37.377	33.115	26.491	24.385	28.091	34.497	37.333	33.156	25.144
UNEC	28.767	28.157	38.193	36.399	33.292	25.77	24.608	28.281	33.303	37.313	32.08	25.206
2013												
STN	JAN	FEB	MAR	APR	MAY	JUN	JUL	AUG	SEP	OCT	NOV	DEC
ABUZ	25.4	26.833	34.569	36.368	35.976	27.547	26.46	29.041	28.953	34.624	36.657	32.651
BKFP	25.831	27.327	34.988	37.05	35.834	27.183	26.109	28.818	29.415	35.14	37.131	33.287
CGGT	25.347	26.811	34.518	36.035	36.043	27.759	26.681	29.209	28.823	34.616	36.711	32.615
CLBR	26.459	28.373	35.978	36.808	37.249	28.722	27.623	30.427	30.254	37.731	40.456	35.564
FPNO	26.303	28.177	35.745	36.604	37.055	28.632	27.508	30.259	30.027	37.228	39.85	35.039
FUTA	28.51	29.788	37.799	37.277	33.105	26.509	24.392	28.027	34.368	36.996	32.688	24.792
FUTY	25.338	26.871	34.596	35.884	36.174	27.929	26.902	29.447	28.838	34.903	37.113	32.866
GEMB	25.849	27.615	35.241	36.204	36.713	28.416	27.352	30.022	29.483	36.244	38.688	34.134
HUKP	25.395	26.792	34.66	36.95	36.072	27.387	26.283	28.928	29.219	34.773	36.723	32.783
MDGR	25.021	26.345	34.299	36.196	36.067	27.581	26.551	29.049	28.664	34.257	36.317	32.214
OSGF	25.543	27.102	34.722	36.049	36.164	27.923	26.818	29.389	29.004	35.007	37.178	32.969
RECT	25.816	27.502	34.984	36.043	36.295	28.132	26.984	29.594	29.251	35.525	37.83	33.424
RUST	26.504	28.427	36.002	36.809	37.236	28.723	27.603	30.406	30.292	37.778	40.512	35.582
ULAG	26.07	27.855	35.292	36.202	36.496	28.284	27.13	29.788	29.566	36.162	38.609	34.003
UNEC	26.023	27.811	35.385	36.34	36.788	28.467	27.348	30.029	29.653	36.461	38.931	34.306
2014												
Stn	JAN	FEB	MAR	APR	MAY	JUN						
ABUZ	30.571	42.515	48.835	46.298	35.934	26.858						
BKFP	31.204	43.054	50.476	46.867	35.827	26.748						
CGGT	30.501	42.457	48.084	46.093	35.984	26.867						
CLBR	32.631	44.825	49.797	48.419	37.193	27.36						
FPNO	32.32	44.748	49.284	47.946	37.04	27.306						
FUTA	31.235	43.336	47.942	46.531	36.442	27.072						
FUTY	30.625	42.606	47.893	46.248	36.06	26.869						
GEMB	31.609	43.79	48.508	47.241	36.655	27.169						
HUKP	30.667	42.697	50.276	46.893	35.982	26.954						
MDGR	30.098	42.126	48.625	46.146	35.833	26.817						
OSGF	30.806	42.797	48.013	46.264	36.166	26.95						
RECT	31.189	43.245	47.903	46.403	36.354	27.016						
RUST	32.715	45.245	49.793	48.392	37.198	27.344						

STN	JAN	FEB	MAR	APR	MAY	JUN						
ULAG	31.622	43.804	48.283	46.814	36.54	27.063						
UNEC	31.782	44.059	48.658	47.342	36.788	27.225						